Università degli Studi di Napoli "Federico II"

Facoltà di Ingegneria

Dottorato di Ricerca in "Ingegneria Aerospaziale, Navale e della Qualità" – XXVI Ciclo

**Settore scientifico disciplinare ING-IND/05:
Impianti e Sistemi Aerospaziali**

Exploiting Innovative Sensor Data Fusion Techniques for Sense and Avoid Units to be Installed on-board Unmanned Aerial Systems

Ing. Anna Elena Tirri

Tutors:

Ch.mo Prof. Ing. Antonio Moccia
Ch.mo Prof. Ing. Domenico Accardo

To my family

To the Love of my life

Abstract

Sense and Avoid Systems play an important role on-board Unmanned Aerial Vehicles in order to be allowed flying into civil Airspace. The key idea of these systems is to detect obstacles in the own trajectories, tracking the detected objects and execute a collision avoidance manoeuvre if the obstacle is closely approaching, thus becoming a collision threat. These functions can be achieved defining an adequate sensor setup, choosing a dynamic model that allows describing the target motion properly, identifying a suitable filtering methodologies given the non-linearities in the dynamic model.

This thesis deals with identification and test of innovative sensor data fusion techniques to be implemented in a fully autonomous system devoted to avoidance of non-cooperative intruders. In particular, sensors, hardware and software architectures are described, focusing the attention on the impact of an innovative filtering methodology, such as Particle Filter, on the performance of the developed tracking software with respect to assessed technique, such as Extended Kalman Filter.

The Particle Filter Obstacle Detect and Tracking system has been developed and tested in off-line simulations based on real data gathered during a flight test campaign within TECVOL project (carried out in collaboration with the Italian Aerospace Research Center).

In order to evaluate the effectiveness of the developed software for the assessment of a collision risk, an analysis has been carried out for the estimation of the Distance at Closest Point of Approach. Numerical results have shown that the Particle Filter algorithm is able to provide performance comparable to the Extended Kalman Filter ones and allows obtaining some improvements with respect to the EKF in terms of DCPA, thus reducing the delay in the collision detection.

KEYWORDS: Unmanned Aerial System, Sense and Avoid, Collision Detection, Particle Filter

Acknowledgements

…"If I have seen further it is by standing on the shoulders of giants"… (Isaac Newton)

A major research project like this is never the work of anyone alone. The contributions of many different people, in their different ways, have made this possible. I would like to extend my appreciation especially to the following people, to my "giants".

First of all, I would like to thank Prof. Antonio Moccia, my tutor, who made this thesis possible giving me the opportunity to discover a very interesting and appealing field.

I would like to express my sincere gratitude to my supervisor Prof. Domenico Accardo, who offered his continuous advice and encouragement throughout the course of this thesis. I thank him for the great effort he put into training me in the scientific field and for the efficient guidance.

A very special thanks goes to the researcher Giancarmine Fasano who always supported me during these three years with his advises, his passion for the research and with whom I shared also some bucolic experiences on Castel Volturno.

I am thankful to my colleagues Eliana, Valentina e Roberto; for the time spent together in laboratory made of laughter, joke and encouragement during the days.

I would like to thank all the Engineering Department, to all the splendid people who work there, who have became friends first of all and with whom I shared some convivial moments.

My special thanks to a person always with me during the most important steps of my life in the last recent years, for her support and presence even if not always physically. Thank you Mary, you are my sister!

My profound gratitude from my deep heart to my beloved family, parents and brother's family, and to my in-laws for their love and continuous support, for what they have done for me that makes me the person I am today, to my nephew, my little pest for his little and tender "Zia Anna"!

At last but not least, I would like express my immense gratitude to the most important person of my life, who shares with me the passion for aeronautical research, who helped me during the tough periods I went through with all his love, his sustain and his strength for both of us! *I love you Salvatore!*

Contents

Introduction

I.1   Unmanned Aerial Vehicles problem statement

The use of Unmanned Aircraft Systems has greatly increased in military domain over the last decade [1]. UAS provide several distinct operational capabilities and cost advantages compared to manned aircraft in most situations. In fact, the advantages of unmanned aerial vehicles is their ability to operate missions considered "dull, dirty and dangerous" for manned aircraft [2]. Inspired by military's experience, civil agencies have identified a large variety of missions that potentially could be performed by UASs with clearly benefits: surveying land and crops, aerial photography, communications and broadcast, monitoring forest fires and environmental conditions, and protecting critical infrastructures.

Several companies are developing unmanned aircraft with a great variety of sizes, speed, and manoeuvrability depending on the mission for which they will be used: from the EURO HAWK[TM] developed by Northrop Grumman[TM] in cooperation with German and EADS Deutschland GmbH (Figure 1) and Northrop Grumman's MQ-4C Triton (Figure 2) to Predator B and Reaper developed by General Atomics (Figure 3).

Figure 1. Northrop Grumman and EADS EURO HAWK^{TM}

Figure 2. Northrop Grumman's MQ-4C Triton

Figure 3. General Atomics Predator B and Reaper

Although there has been an increase in UAS operations in the military domain, the civil UAS market has not yet started significantly. Their use is limited due to the restricted admission in segregated areas of the airspace and inability to access the civil airspace in which manned aircraft operate.

Nowadays, worldwide agencies and organizations are hardly working to develop certifications and standards to enable unmanned aircraft integration in non-segregated airspace. In USA and Europe, regulatory agencies, such as Federal Aviation Administration and EUROCONTROL, are providing a set of issues to allow UAS flying in civilian, uncontrolled airspace. Also Japan and Australia are devolving a great effort to the identification of rules and regulations to guarantee a safe and efficient utilization of airspace by both manned and unmanned aircraft.

The general purpose is to introduce and integrate UAS into airspace in a consistent manner, to ensure global interoperability and regulatory compatibility with existing regulations. In particular, the ICAO guiding policy on UAS states [3]:

> *"A number of Civil Aviation Authorities (CAA) have adopted the policy that UAS must meet the equivalent levels of safety as manned aircraft...In general, UAS should be operated in accordance with the rule governing the flight of manned aircraft and meet equipment requirements applicable to the class of airspace within which they intend to operate...To safely integrate UAS in non-segregated airspace, the UAS must act and respond as manned aircraft do. Air Traffic, Airspace and Airport standards should not be significantly changed. The UAS must be able to comply with existing provisions to the greatest extent possible."*

Then, to gain full access to the Civil Airspace, UAS need to be able to bridge the gap from existing systems requiring accommodations to future systems that are able to obtain a standard airworthiness certificate. One of the most critical functional areas in this framework is the Sense and Avoid (SAA) capability. Research is underway on Airborne Sense and Avoid (ABSAA) concepts. In particular, it is aimed to the establishment of Sense and Avoid system definitions and performance levels, minimum Sense and Avoid information set required for collision avoidance manoeuvring and assessment of Sense and Avoid system multi-sensor and other technologies [4], [6]. The exploitation of new filtering technologies can provide to be a proficient solution for integration of UAS into Civil Airspace.

The thesis will focus on the analysis of innovative filtering methodologies in order to realize an Obstacle Detect and Tracking software for UAS Sense and Avoid system.

I.2   Sense and Avoid Technology

It is generally recognized that one prerequisite for the introduction of UAS into civil airspace is constituted by a Sense and Avoid system, whose main scope is the replacement of all those functions traditionally performed by onboard pilot.

Recent activity in WG-3's RTCA SC-203 has emphasized the development of a stable set of requirements for S&A. These draw heavily from the report of the Sense & Avoid Workshops [4], a series of meetings involving all the Department of Defense services, the FAA, the Joint UAS Center of Excellence, and several other experts in aircraft collision avoidance. One key result is that S&A needs to provide two main services:

a. A "self separation" service that would act when normal (e.g. Air Traffic Control) separation is lost, and could support earlier, gentler manoeuvres than those used for last-moment collision avoidance;

b. The collision avoidance service that attempts to protect a small "collision zone".

The requirements are further categorized by sub-functions, which are (see Figure 4):

1. **Detect** any of various types of hazards, such as traffic, terrain, or weather. At this step, it is merely an indication that something is there.

2. **Track** the motion of the detected object. This requires gaining sufficient confidence that the object is valid, and making a determination of its position and trajectory.

3. **Evaluate** each tracked object, first to decide if its track may be predicted with sufficient confidence and second, to test the track against criteria, which would indicate that a manoeuvre is needed.

4. **Prioritize** the tracked objects based on their track parameters and the tests performed during the evaluation step. In some implementations, this may help to deal with limited S&A system capacity, while in others prioritization might be combined with the evaluation or declaration steps.

5. **Declare** that the paths of own aircraft and the tracked object and the available avoidance time do indeed require manoeuvring to begin.

6. **Command** own aircraft to perform the chosen manoeuvre. Depending upon the implementation of the S&A, this might require communications to the aircraft, or if the manoeuvre determination was performed on-board, merely internal communication among the aircraft's subsystems.

7. **Execute** the commanded manoeuvre.

It should not be assumed that each of these sub-functions is performed only once. They typically will need to be repeated as long as the object can be seen. The first choice of manoeuvre may need to be modified, for reasons such as prediction errors, delays in manoeuvring, or adverse manoeuvres by the other aircraft. Therefore, the tracking and evaluation steps must keep assessing the effectiveness of the first choice.

(Not drawn to scale)
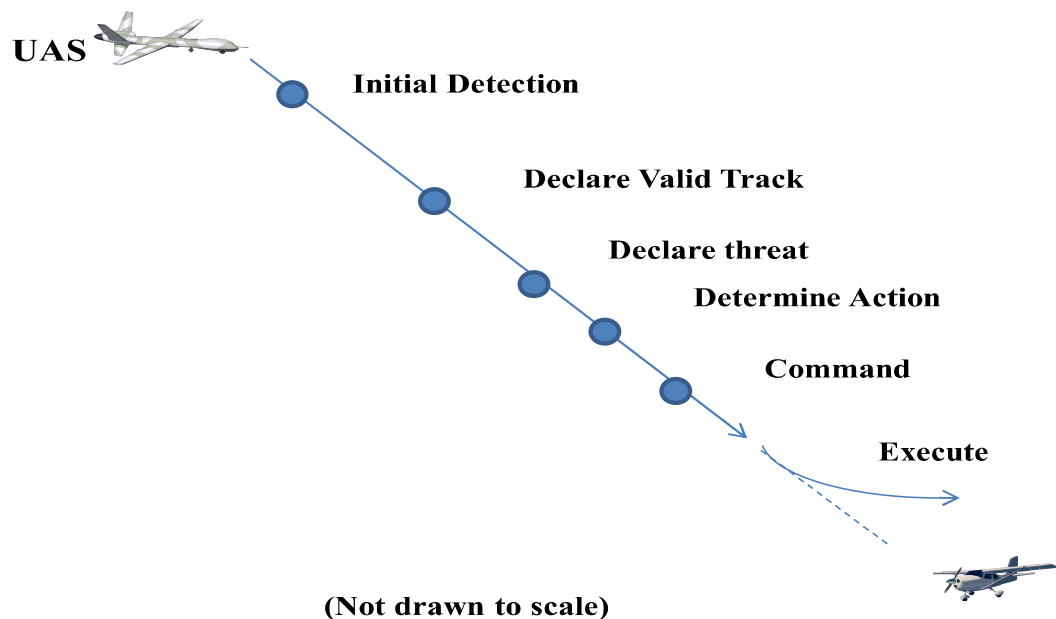
Figure 4. Sense and Avoid Timeline

It is worth pointing out that one of the main functions to be carried out by Sense and Avoid system concerns the traffic insertion and separation (very important task for the realization of sub-function 5 reported above) (Figure 5). In "normal" conditions, Air Navigation is mainly based on vertical and lateral separations:

- Vertical spacing greater than 500 feet (ft) or 150 m;
- Horizontal spacing greater than 0.5 Nautical Mile (NM) or 925 m.

One of the two conditions must be fulfilled. The vertical spacing is, by far, the most constraining one in terms of angular localization accuracy.

In Figure 5, the self separation and collision avoidance volume is reported. In particular, the Collision Volume threshold is a fixed distance based boundary; the Collision Avoidance threshold is a variable boundary that depends on time, distance, manoeuvrability, and other parameters.
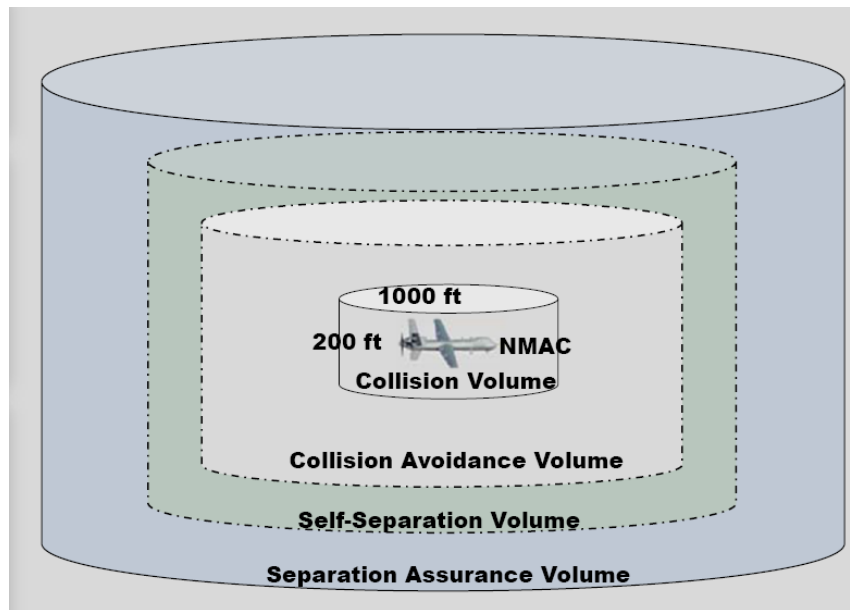
Figure 5. Self separation and collision avoidance function [5].

In the considered application, the system shall avoid collisions with other aircrafts considering a safety cylindrical area with a radius and a height both equal to 500 ft (150 m) defined around each aircraft. A collision or a quasi collision (air-miss) occurs if an aircraft enters in the safety area of another one.

I.3   Thesis objectives and outline

The main objective of this thesis is to develop and test an Obstacle Detection and Tracking System based on innovative filtering methodologies. The primary function of this system should consist of detecting obstacles in the own trajectory, tracking the detected object and execute a collision manoeuvre in case of a collision threat. Collision detection can be carried out estimating a fundamental parameter that is the Distance at Closest Point of Approach (DCPA). If this parameter is smaller than the safety boundary limit, meaning that the other aircraft is closely approaching, thus constituting a collision threat, an evasive manoeuvre has to be performed in time to avoid collision.

DCPA estimation is based on the evaluation of relative position and velocity estimates between two aircraft; an accurate estimate of these parameters can be obtained adopting a properly filtering procedure.

Since assessed methodologies can cause some loss of accuracy due to non-linearities, innovative techniques have been introduced and analyzed in order to overcome these

drawbacks and realize a suitable Obstacle Detection and Tracking algorithm for UAS Sense and Avoid units. All these activities have been analysed and they are reported in this thesis in accordance with the following outline.

Chapter 1 clarifies in more details the requirements mandated by civil aviation authorities for the realization of a reliable sense and avoid system in order to allow the integration of UAS into civil airspace. Then, the possible solutions in terms of sensors and architectures are described analyzing all the possible existing configurations based essentially on cooperative and non-cooperative systems. In parallel, the advantages and drawbacks of all systems are pointed out. The last part briefly shows the international experience and applications in UAS sense and avoid field.

An Airborne Obstacle Detection and Tracking system is presented in chapter 2. In particular, starting from the requirements prescribed by regulatory agencies, selected sensors within the framework of TECVOL project are described. Then, the hardware/software system configuration is reported and clarified together with the description of the basic elements and issues of a target tracking system.

An overview of the Kalman Filter is reported on chapter 3, in which drawbacks and shortcomings of this filter are also pointed out. A survey of all the possible filtering solutions able to overcome the KF restrictions is conducted in order to individuate the optimal solution stated the non-linearity of the considered applications. Thus, a Particle Filter algorithm is described and some solutions to resolve the most frequent algorithm limitations are provided.

Chapter 4 describes the radar-only tracking system. In the first part, the effects of tracking coordinates and dynamic model on PF performance are reported. Then, the different models are detailed in order to evaluate and identify the best configuration able to provide the most accurate state estimates, thus enhancing the estimation of the Distance at Closest Point of Approach. The influence of this choice on tracking coordinates is also demonstrated. Finally, the implementation issues for the realization of a software that had to preserve the characteristics of a quasi-real time system are pointed out.

In chapter 5, the results obtained from the different models are shown and a comparison between them is carried out in order to justify the choices made for the development of the obstacle tracking software showed in this work.

Finally, conclusions and further research are presented in the last chapter of this thesis.

Chapter 1

UAS Sense and Avoid

1.1 Integration of Unmanned Aerial Vehicles into Civil Airspace

Regulatory agencies require that Unmanned Aerial Systems must guarantee an *equivalent level of safety* compared to manned aircraft in order to be allowed flying into civil airspace. The intent of "see-and-avoid" is for pilots to use their sensors (eye) and other tools to find and maintain situational awareness of other traffic and to yield the right-of-way, in accordance with the rules, when there is a traffic conflict. The FAA did not provide a quantitative definition of see-and-avoid, largely due to the number of combinations of pilot vision, collision vectors, sky background, and aircraft schemes involved in seeing oncoming traffic. Subsequently, aeronautical regulatory agencies have detailed the significance of general guidelines in terms of technical issues [7], [8], and a series of enabling technologies

have been described. In order to realize these systems, the presence of different classes of UAS must be taken into account. In fact, UAS vary in size, speed, manoeuvrability, environmental conditions and airspace classes in which they are expected to fly. For example, mini UAS will likely fly in the G segment of airspace, whereas large UAS will be allowed to fly in the same classes of standard transport aircraft. As a consequence, different types of systems with different levels of performance must be adopted, and in some cases no additional onboard systems may be needed, as in some mini or micro UAS missions with the aircraft always in view of a ground observer.

In general, the surveillance function for separation assurance and collision avoidance can be performed by two fundamental methods: cooperative instruments, wherein an aircraft is equipped with a transponder to interrogate and/or broadcast information, and non-cooperative sensors, which are able to detect targets autonomously and represent the last level of safety against collision, as shown in Figure 6.
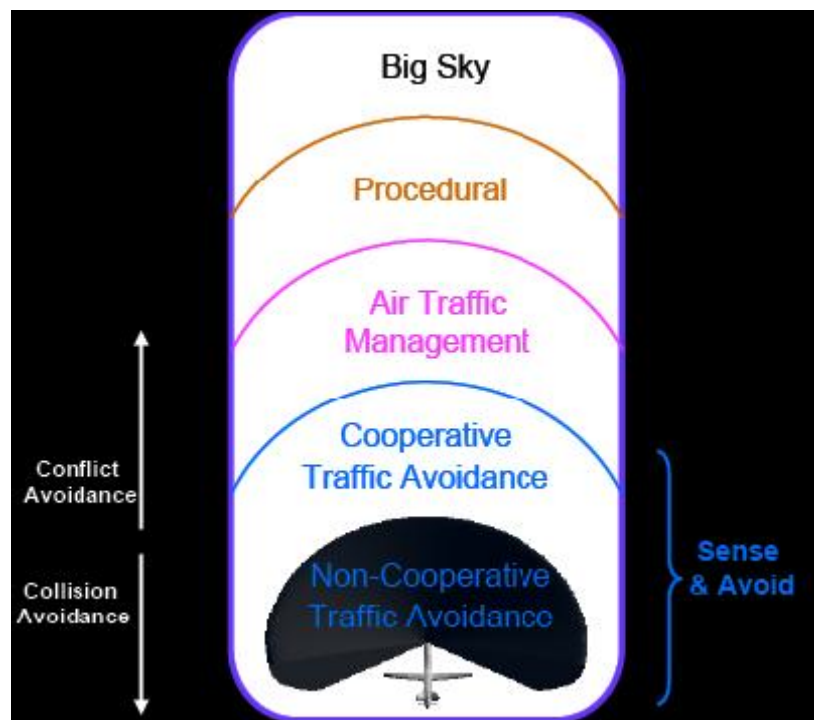
Figure 6. Flight safety levels

Cooperative systems are based on Traffic Alert and Collision Avoidance (TCAS) and Automatic Dependant Surveillance Broadcast (ADS-B). TCAS has a high grade of autonomy, since it is able to perform conflict detection and resolution by assigning proper avoidance manoeuvres in the vertical plane. It is worth noting that the choice of vertical avoidance manoeuvres is strictly dependent on the fact that TCAS range and altitude

precision is relatively high, while there is a large bearing angle noise from directional antenna construction. ADS-B is expected to provide an improvement of the separation assurance function, which is currently performed by controllers and based on measurements of surveillance radars. However, a non-cooperative collision avoidance capability still has to be required in order to avoid aircraft not equipped with ADS-B, or as a backup system in case of loss of data link. Consequently, the combination cooperative/non-cooperative system can be considered the best option for the realization of an autonomous obstacle detection system [9],[10],[11]. Recently, the General Atomics Aeronautical System, Inc. (GA-ASI) has successfully completed the first of several flight tests of a prototype Sense and Avoid system in which the entire system worked together as a "system of systems" to detect the various types of aircraft it might encounter in the air. This system was composed of radar, a transponder, and a traffic alert system.

Research studies are still being carried out to find out system requirements and sensing solutions. Lately, FAA has distributed a Roadmap for the integration of Unmanned Aerial Systems in the National Airspace (NAS) [12]. It aims at defining some guidelines, actions and considerations needed to enable UAS into NAS; this must be accomplished without reducing the existing capacity, decreasing safety, impacting current operators, or placing other airspace users or persons and property on the ground at increased risk. It is necessary to develop new or revised regulations/procedures and operational concepts, formulate standards, and promote technological development that will enable manned and unmanned aircraft to operate cohesively in the same airspace. Specific technology challenges is constituted by the critical "Sense and Avoid" functional areas that must assure both self-separation and collision avoidance capability. In particular, the roadmap outlines some goals and metrics to be followed to realize an independent SAA system but that is also compatible with other collision avoidance systems.

The trend is to consider different requirements and to develop a customized Obstacle DS&A system for each UAV category.

1.2 Sensing solutions and DS&A architectures

As stated above, the sensing solutions for the realization of a Sense and Avoid system for UAS are based on cooperative and non-cooperative systems that include both active and passive sensor systems. The most important cooperative system is the Traffic Alert and

Collision Avoidance System (TCAS) that is an airborne system used for detecting and tracking aircraft near the own aircraft. This system has been firstly introduced as a monitoring backup for air traffic controllers and pilots to prevent mid-air collision (MAC) if both operators failed to detect them [13], [14]. TCAS monitors the airspace surrounding the own aircraft by interrogating the transponder of the intruding aircraft. The interrogation reply enables TCAS to compute the following information about the intruder: range between the two aircraft; relative bearing to the intruder; altitude and vertical speed of the intruder if the latter is reporting altitude; closing rate between the two aircraft. Besides TCAS, Automatic Dependant Surveillance-Broadcast system (ADS-B) is also a cooperative technology [15]. ADS-B allows both pilots and ground-based stations to detect other similarly aircraft in the airspace with much more precision than has been possible. ADS-B is able to determine aircraft's precise position making use of satellite-based GPS. The aircraft's position and other information, such as altitude, speed, flight number, type of aircraft, and whether it's turning, climbing, or descending, are then converted to a digital code that is then broadcast, several times per second, via data link trough a universal access receiver. This system has several benefits with respect to TCAS system, such as: greater position accuracy with integrity; higher information updates rates; increased situational awareness to those who are equipped with; reduced voice communications and dependency on ATC for flight tracking and monitoring. The most important advantage of these systems is that they are established technologies and have proven to be reliable systems and most of them have been certified and approved for use. Despite these advantages, these cooperative technologies have some drawbacks, in fact they tend to be cost prohibitive for users and they only work when all aircraft that are sharing the airspace have them installed on-board and properly functioning. In addition, the degraded integrity of ADS-B compared to TCAS is due to the reliance of all data from an external device (either the GPS satellite or correspondent ADS-B transponders), thus it may be possible to create false signals that would be perceived as accurate. Different technologies that do not rely on other aircraft possessing cooperative systems are the non-cooperative technologies. These systems are comprised of radar, laser, electro-optical (EO), and infrared (IR). They can be divided in active and passive. The active systems transmit a signal to detect obstacles in the flight path, e.g. radar and laser, while passive system rely upon the detection of signals emanating from the obstacle themselves, e.g. EO and IR.

The radar is a system that generates, transmits and receives electro-magnetic waves. The phase difference of the return signal or the time of flight is then used to calculate intruder

range. Radars guarantee adequate detection range and all-time all-weather performance, but angular accuracy is unsatisfying and data rate is of order of 1 Hz. Radars operating at low frequencies (i.e. S band) are relatively unaffected by atmosphere, but are large in size and unable to provide required spatial resolution. Higher frequency radar (i.e. V band) is smaller in size and provides better resolution for given aperture size, but is more susceptible to atmospheric and weather effects [16]. At this end, Ka-band seems to be a good compromise between the two aforementioned solutions. Laser systems use eye-safe lasers operating similar to that of conventional radar systems. Laser scans of the immediate airspace are taken at regular intervals and processed through echo-analysis software. Obstacles in the flight path of the aircraft result in a warning, alerting operators or standardized avoidance software to the hazard. The benefits of this system rely on the nature of lasers themselves. In fact, the scan beams are of sufficient return power to detect even non-perpendicular surfaces at high resolution. Laser systems are highly configurable, allowing them to compensate for varying atmospheric conditions. Regarding the passive non-cooperative technologies, Electro-Optical does not need any information from an outside system, it can provide good azimuth and elevation information, but does not give a direct indication of range. EO has some peculiarities that make it suitable to be adopted onboard unmanned aerial vehicles, such as:

- fast scan rate (10 Hz or more);
- low cost;
- small size and weight;
- low electrical power consumption;
- and reduced sensitivity to rain.

However, EO sensors have also several disadvantages with respect to radars: no range-to-obstacle information is provided, detection range can be much shorter than radars causing the time-to-collision requirements not to be met, target detection performance is strongly dependant on background, large sensitivity to fog so the system is not all-time all-weather, and potentially high bandwidth requirement. Some drawbacks can be overcome utilizing an IR sensor. In fact, the IR can detect target temperature and rate of change of target temperature and this system does not require target to be illuminated so it can operate during night. An emerging approach that would negate the high bandwidth requirement of any active system is optical flow technology, which reports only when it detects an object

showing a lack of movement against the sky, instead of sending a continuous video stream to the ground controller. Imagery from one or more inexpensive optical sensors on the UAV is continuously compared to the last image by an onboard processor to detect minute changes in pixels, indicating traffic of potential interest.

In order to compensate the shortcomings of each single sensor configuration, a combination of systems seems to be the good compromise for the realization of a reliable S&A system. In fact, the integration of measurements from several sources is able to provide an increased S&A integrity. This solution has been adopted in TECVOL, in which a hierarchical configuration has been assumed. In particular, the radar is the main sensor that must perform initial detection and tracking, while EO sensors are used as auxiliary information sources to increase tracking accuracy and measurement rate (Figure 7).
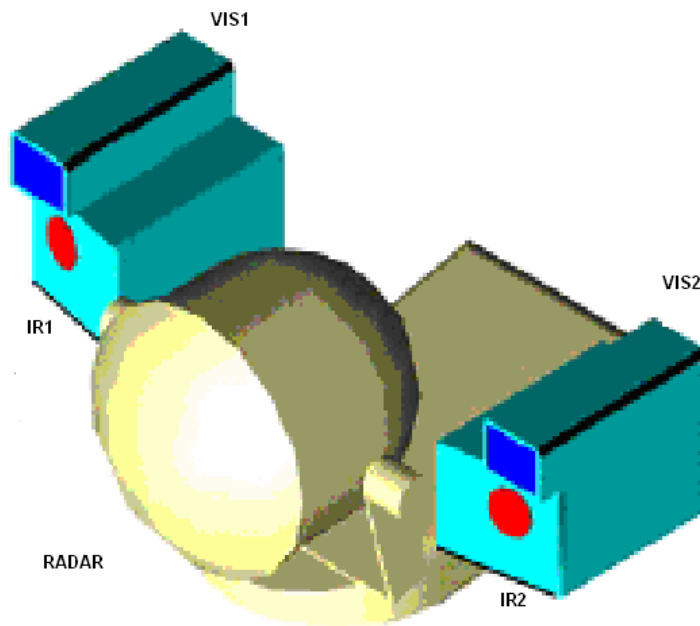
Figure 7. Sensor systems' layout

1.3 UAS S&A: international scenario

Sense and Avoid is a broad branch of research in the international panorama. It is demonstrated by the large amount of papers related to this argument [17], [18], [19], [20], [21], [22], [23], [24] and by the several projects carried out worldwide.

In particular, in the United States the Northrop Grumman has developed the MQ-4C Triton for real-time intelligence, surveillance and reconnaissance over vast ocean and coastal regions. It is a high-altitude UAS and has been built on elements of the Global Hawk but with some reinforcements with respect to it (Figure 8). The Triton is equipped with multi-function active sensor active electronically steered array radar and Electro-optical/infrared sensors; it has a 360-degree Field of Regard capacity.

Figure 8. Northrop Grumman MQ-4C Triton.

NASA's Dryden Flight Research Center has developed and tested the Ikhana that is a modified General Atomics Aeronautical Systems MQ-9 Predator B (Figure 9). In particular, the UAS has been utilized to test an aircraft tracking system based on ADS-B.

Figure 9. NASA's Dryden Flight Research Center Ikhana

Moreover, an experimental program has been conducted by Northrop Grumman-Integrated Systems, Calspan Corporation, Bihrle Applied Research, C2Projex, Defense Research Associates, and Air Force Research Laboratory (AFRL). The project aims at developing an SAA system initially consisting of an Electro-Optical (EO) sensors and a Traffic Collision Avoidance System (TCAS) for sensing non-cooperative and cooperative aircraft along with autonomous "avoid", or manoeuvring, logic. This system has been tested under the SAAFT (Sense and Avoid Flight Test) program [25]. Then, it has been continued under AFRL's multiple Intruder Autonomous Avoidance (MIAA) program, in which a radar was added as a second non-cooperative aircraft detection sensor and an ADS-B was added as a second cooperative aircraft detection sensor. The system was installed on a Calspan Learjet acting as a surrogate Global Hawk-like UAV (Figure 10).

Figure 10. Calspan Learjet for SAAFT program.

The MITRE Corporation's Center for Advanced Aviation System Development (MITRE/CAASD) is involved in many of the standards, architectural development, and sensor experimentations for sense and avoid, for both the sponsored work program and MITRE/CAASD's internally funded research. This research spans investigations of all the important aspects of the sense and avoidance problem, including ground-based and aircraft-based sensing systems, cooperative and non-cooperative sensing methods, and avoidance manoeuvres that involve pilot-in-the-loop and autonomous algorithms [26].

Chapter 2

Airborne Obstacle Detection and Tracking System

2.1 Sensing requirements

To safely operate UAS into Civil Airspace and to minimize the risk of mid-air collision, UAS system must be able to guarantee "*…an equivalent level of safety, comparable to see-and-avoid requirements for manned aircraft…*" both in controlled and uncontrolled airspace, as stated above. In order to satisfy the requirements, UAVs have to be endowed with two capabilities: a situational awareness capability (sense function) and a decision-making capability (avoid function).

Although the term "see-and-avoid" appeared in 14 CFR 91.113 "Right-of-Way rules: Except Weather Operations" [27] is not quantitative defined due to the number of combinations involved in seeing approaching traffic, a possible definition for Sense and Avoid system emerges from the system ability to provide situation awareness with adequate time to detect

conflict traffic and take appropriate action to avoid collision. This sense-and-avoid capability is described by addressing measures of surveillance, avoidance and system quality, such as [27]:

- Field-of-Regard extent;
- Range resolution;
- Angular resolution;
- Detection range;
- Time-To-Collision;
- System data rate.

In particular, flight regulations prescribe that any aircraft must detect traffic that might be a conflict when the safety bubble distance around the vehicle is less than 500 ft radius [28]. The standards also define the scanning volume within a collision threat is considered and the maximum relative speed between two aircraft (Table 1). In normal flight, it is generally possible to avoid the threat of an in-flight collision by scanning an area 60 degrees to the left and to the right of centered visual area and 10 degrees up and down from the flight vector [29]. In accordance with ICAO International standards, azimuth search area must be ranging between ± 110 degrees and no guidance is provided for the elevation angle. Indeed, it is commonly agreed that the sector that must be scanned equals the size of a typical cockpit window, i.e. ± 15 degrees in elevation and ±110 degrees in azimuth.

	Azimuth	Elevation
FAA P-8740-51: How to Avoid a Mid-Air Collision	+/- 60 degrees	+/- 10 degrees
International Standards, Rules of the Air, Section 3.2 (ICAO)	+/- 110 degrees	No guidance

Table 1. Traffic detection capability.

Regarding the aircraft speed, for flight below FL100, aircraft true air speed is limited to 250kts, i.e. the maximum relative speed for a frontal encounter is 500kts [30]. It is worth noting that collision threats largely occur in the vicinity of aerodrome, due to the large volume of aircraft and closer spacing compared with cruise flight.

In addition to the detection location, the range of the potential collision threat must also be considered. The system has to detect the aircraft in adequate time to process information, determine the conflict, and execute the manoeuvre according to the right-of-way rules. The minimum detect time is defined as the time from detection of an intruder until the completion of an evasive manoeuvre (function F1 through F6 in Figure 11) [31]. In other words, the system must provide sufficient time after intruder detection to perform all remaining collision avoidance functions resulting in successful execution of an avoidance manoeuvre if necessary.
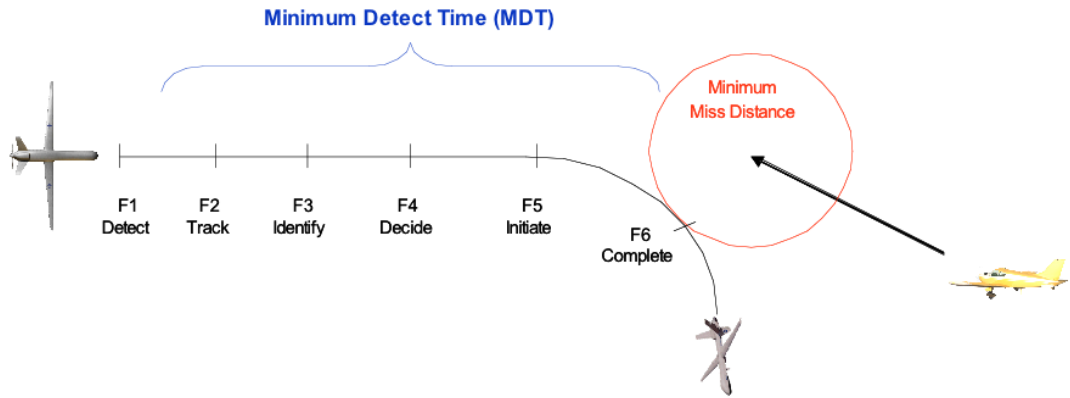
Figure 11. Minimum Detection Time definition

According to [32], applicable to high/medium altitude flight, the nominal time delay to avoid collision is equal 12.5 s that is considered the Time-To-Collision (TTC). These considerations can be applied even for Medium/Low altitude taking into account the unpredictable nature of environment and possible presence of obstacles visible only at a short distance. This value can be considered equal to about 20 s taking into account the latencies of the systems as well as the pilot's time of reaction.

Considering the above-mentioned requirements, the main feature of a sense and avoid system is its ability to calculate the DCPA. This value indicates the minimum distance between the own aircraft and intruder; it can be calculated from [9]:

$$\overline{d}_{AB} = \frac{\overline{r} \cdot \overline{V}_{AB}}{\left\| \overline{V}_{AB} \right\|^2} \overline{V}_{AB} - \overline{r} \tag{1}$$

where $\overline{d}_{AB}$ is the *minimum separation distance* (whose norm is the DCPA) [33], $\overline{V}_{AB} = \overline{V}_A - \overline{V}_B$ is the relative speed vector ($V_A - V_B$) between the intruder (aircraft A) and the

ownship (aircraft B), and *r* is the relative position between the aircraft (see Figure 12). If the intruder is modelled as a spherical object with radius R, it can be demonstrated [9] that assuming constant velocity vectors, V_A and V_B respectively, the two aircraft are headed for collision if and only if the following conditions are satisfied:

$$\left\| \overline{d}_{AB} \right\| \leq R \ \text{ and } \ \dot{r} < 0 \tag{2}$$

These values are a measure of the collision risk; if these conditions are satisfied, a Near Mid Air Collision threat is considered.
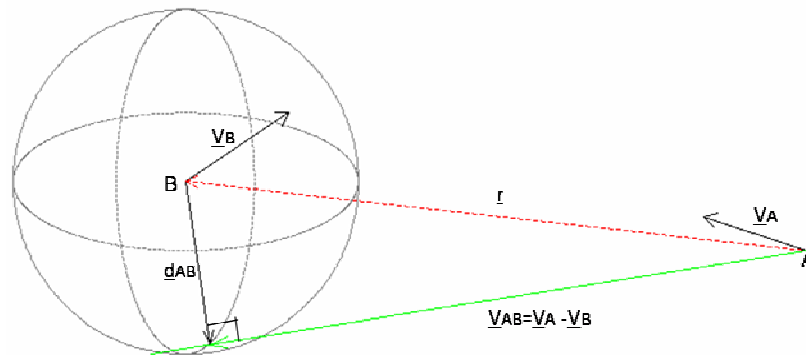
Figure 12. Definition of *minimum separation distance* vector $\overline{d}_{AB}$

2.2   TECVOL overall system description

The research activity at the basis of this thesis has been conducted by means of experimental data gathered during a flight test campaign realized in the framework of TECVOL project. The project was carried out by the Italian Aerospace Research Center (CIRA) in which the University of Naples "Federico II" was in charge of developing and testing the anti-collision sensing system.

The prototypical sensing system was installed onboard a Very Light Aircraft named FLARE (Flying Laboratory for Aeronautical REsearch) that can be optionally piloted. It was a customized version of TECNAM^{TM} P92 (Figure 13).

Figure 13. FLARE experimental aircraft.

The onboard system included:

   – Airborne Ka-band pulse radar;

   – Electro-optical sensors;

   – A set of navigation sensors (Attitude and Heading Reference Systems, Laser Altimeter, Standalone GPS, and Air Data Sensor);

   – Flight Control Computer (FCC);

   – Obstacle Detection and Identification unit (ODID).

In particular, ODID is the obstacle sensing part of the overall system, which comprises a pulsed Ka-band radar, four EO sensors, a CPU devoted to image processing (IP-CPU), a CPU devoted to real-time tracking (RTT-CPU) by sensor data fusion. Thus, the second unit provides autonomous navigation and flight control by a set of navigation sensors (Attitude and Heading Reference System (AHRS), Laser Altimeter, Standalone GPS, Air Data Sensors). Moreover it comprises a Guidance Navigation and Control (GNC) Computer capable of processing obstacle dynamics and UAV navigation data in real-time to generate escape trajectories and the relevant commands for servos. In Figure 14, the ODID setup onboard FLARE is shown.

Figure 14. ODID unit

Several different geometries were considered during the flight tests. Some were carried out with FLARE aircraft piloted by the safety pilot, while other tests were executed with FLARE flying in autonomous mode. In order to test the adopted sensing setup and perform the autonomous collision avoidance tests, the latter mode was the one adopted. In particular, two types of manoeuvres were tested:

- Tail chase tests with FLARE pursuing the intruder. These tests allowed gathering a large quantity of sensor data with smooth relative dynamics;
- Frontal and near-frontal encounters, which are the most significant from the application point of view. In these tests, slight altitude differences were commanded between aircraft for safety reasons, with the intruder at higher altitude than FLARE in most cases. During tests, realistic collision geometries were performed in which small distances at closest point of approach were reached.

The tests were performed considering different weather/illumination conditions in order to verify the capability of the developed system to detect and track the intruder in different operating conditions.

2.3   Sensing sensors and hardware architecture

The prototypical sensing system installed onboard FLARE was based on an integrated radar/electro-optical configuration. The main reason for selecting a multi-sensor architecture was that the integration of heterogeneous information sources could compensate single sensor failings.

The selected radar for autonomous collision avoidance is the AI-130TM OASys™ (Obstacle Awareness System) model produced by Amphitech™. It is a pulsed radar operating with a carrier at 35 GHz (Figure 15). The selected frequency provides a good compromise between antenna dimensions, angular accuracy and sensitivity to rain and fog.

Figure 15. Amphitec OASys Radar

In the assigned hierarchical sensors architecture, radar is the main sensor, as already stated before. This choice depends on its capability of working all-time all-weather and of providing a direct range-to-obstacle measure.

EO sensors are used as auxiliary information sources in order to increase accuracy and data rate. They are constituted of visible and InfraRed cameras. In particular, the two visible cameras are installed parallel to the aircraft longitudinal axis and work with 1280x960 resolution; they are two Marlin™ cameras produced by Allied Vision Technologies™ with a field of view (FOV) of 49.8° x 38.9° (Figure 16). Conversely, IR sensors have a resolution of 320x240 pixels and are set slightly eccentric in order to cover the same field of view (FOV) of the visible cameras; they are two FLIR™ thermal cameras with a FOV of 24° x 18° (Figure 17).

Figure 16. Visible Cameras

Figure 17. Infra Red cameras

The whole DS&A system hardware architecture is made up of two separate processing units, which implement different functions with different operating systems (OSs) (Figure 18). The Real Time Computer is based on a deterministic OS. It is directly connected with the radar sensor via an Ethernet link and the TCP/IP protocol, performs tracking and exchange data with the Guidance, Navigation and Control (GNC) system by a deterministic data bus, which is the Controller Area Network (CAN) bus. The EO sensors are connected via a Firewire link to the Image Processing Computer, based on a conventional OS, which has to process the visible and infrared images to find estimates of intruders' position and shape. The two computers exchange data by an Ethernet connection.
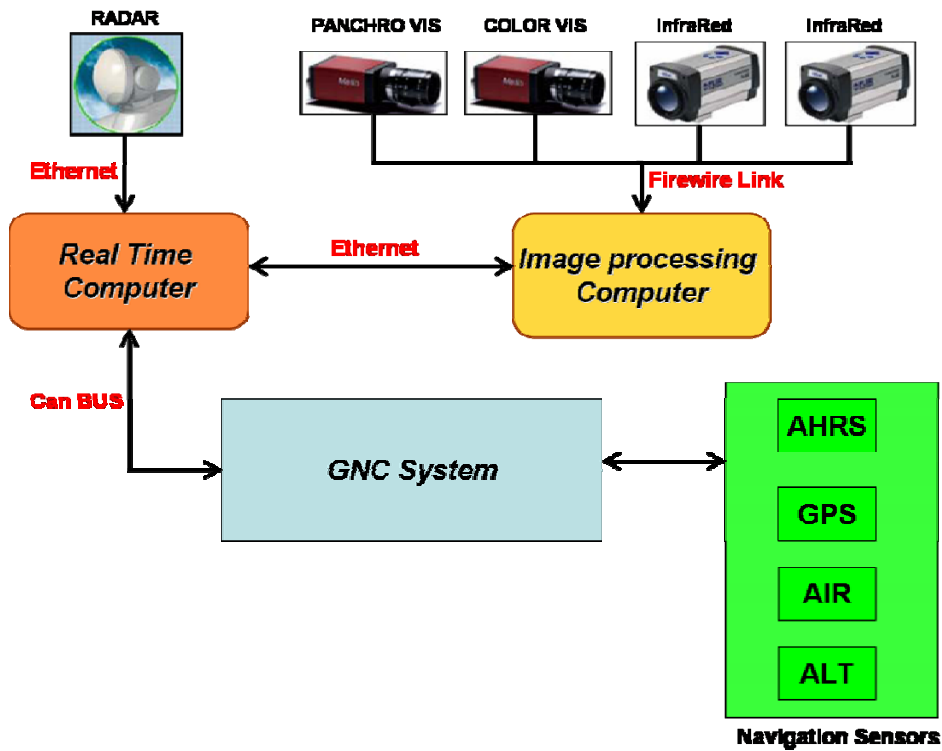
Figure 18. DS&A hardware architecture

2.4 Target Tracking Issues

A critical feature of a Sense and Avoid system is the ability to track target in the flight path in order to establish whether it may be a possible threat and, in case this happens, execute subsequently the right manoeuvre to avoid collision. Thus, the purpose of tracking system is to keep track of detected and identified target.

The basic elements of a target tracking systems are shown in Figure 19 [34].
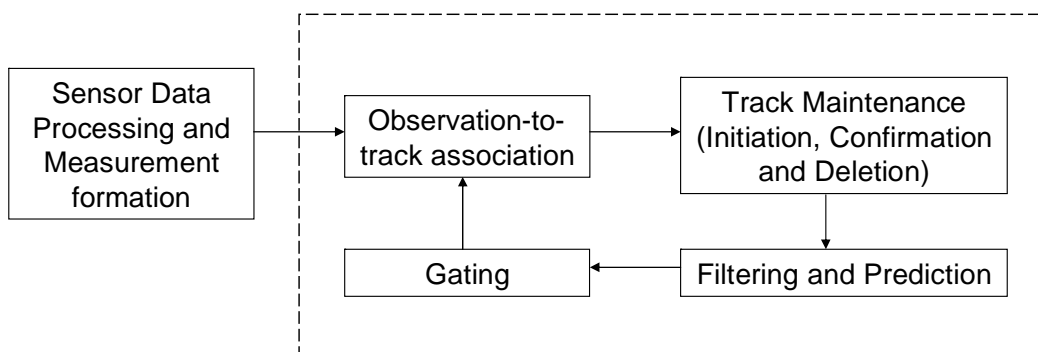
Figure 19. Basic element of a target tracking system

The inputs to the algorithm are sensor measurements, which represent objects of interest, false alarms, and clutter. Thus, the critical issues in target tracking are addressed to data association, gating operations and to the definition of target dynamic model able to describe the target path properly.

In order to continuously tracking a target, the system must be able to determine which target in the measurement data belongs to each track, i.e. the measurements need to be associated to the right track in some way. In fact, due to the presence of clutter and/or other object in the search volume, the system could associate the wrong information to an approaching target causing, in this way, a collision between the planes. The first operation is then the *data association*. There are different methods to solve the data association problem: the Target-Oriented approach, the Track-Oriented approach, and the Multiple Hypothesis approach [35], [36], [37], and [38]. The algorithms that use the first approach are the Nearest Neighbor algorithm and the Probabilistic Data Association. This approach is based on a priori knowledge of the number of targets and requires separate track initiation modules. The Track-Oriented approach treats each track individually, for that the number of targets is not required to be known. The Multiple Hypothesis approach is measurement-oriented and uses probabilistic methods to evaluate all association hypotheses and requires elaborate management schemes to limit the growth of the hypothesis.

The last method, Multiple Hypothesis approach, is the most implemented one when multiple objects have to be tracked. In the case a measurement passes the gates of more than one track, all of those track update hypotheses are maintained until later measurements arrive to solve the situation. This approach is computationally heavy because it requires the maintenance of several tracks if they are not properly eliminated when incorrect. It is clear that data association processes need the storage of large quantities of data to perform observations-to-track pairing.

To reduce the high computational load that these methods require, the *gating* process can be performed. In fact, gating decreases the required amount of calculations and helps preventing incorrect associations when there are no valid observations of the object.

This method provides a limit beyond which the measurements are excluded. Usually, this limit is set equal to three standard deviations from the predicted mean. This limit is called *association gate*. In literature, several gating techniques exist that allow building a volume in the state space around the predicted estimate, where valid observations are likely to fall.

In case of linear Gaussian systems, the ellipsoidal gating technique is considered the best solution [39]. The validation gate is typically an ellipsoid described at any time by a gate

center point (the predicted measurement) and a gate volume. The gate limit is set equal a probability threshold that can be obtained from tables of the chi-square distribution and is usually kept constant for any given application. Other techniques can be applied in the gating process, such as rectangular gating, centralized gating, and model-based gating [34].

After the association phase, track status has to be properly handled. In particular, tracks can be divided into three categories: one-plot (single observation not associated to any existing track), tentative (at least two observations, but confirmation logic still required), firm (confirmed track). Tracks not updated within a reasonable interval are deleted.

Finally, the filtering and prediction phase allows for combination of track prediction and sensor measurements, and produce new track prediction. It is usually performed using Kalman filtering even if, in most highly non-linear problems, innovative methodologies are preferred, as it will be shown later.

Another tracking issue is constituted by the choice of the dynamic model needed to describe the targets trajectories. In fact, the primary objective of a target tracking is to estimate the state trajectories of a target. In particular, they extract useful information on the target's state from measurement data.

Different target dynamic models have been developed over the years and the most important ones can be found in [40]. The target motion is described by the evolution of the target state with respect to time. An important issue in target tracking concerns the uncertainty of the motion model caused by a lack of information about the control input of the target, the function that describes the variation of the target state and noises affecting the evolution of the model.

Some of these models have been analyzed and developed in this thesis in order to identify the optimal one in view of the application. They will be described later.

Chapter 3

Beyond Kalman Filter solutions: advanced filters

In many target tracking problems, the filtering phase can be considered the most insidious aspect. Whenever the state of a system must be estimated from noisy sensor information, some kind of state estimator is employed to fuse together the data from different sensors to produce an accurate estimate of the true system state. When the system dynamics and observation models are linear, the state estimates may be computed using the Kalman Filter. However, in most applications of interest the system dynamics and observation equations are nonlinear and suitable extensions to the Kalman filter have been sought. The optimal solution to the nonlinear filtering problems requires that a complete description of the conditional probability density is maintained. Unfortunately, this exact description requires a potentially unlimited number of parameters and a number of suboptimal approximations have been proposed [41], [42], [43].

These methods usually employ awkward analytical approximations to probability distributions, derivatives of the state transitions and observation equations, or Monte Carlo methods which require the use of many thousands of point to approximate the conditional

density. In many high-dimensioned applications these methods are rarely practical. For these reasons, the most widely used filter is the Extended Kalman Filter (EKF) that closely resembles a Kalman Filter except that each linear step is replaced by its linearised equivalent.

The Extended Kalman Filter has been developed within TECVOL project; it has demonstrated good capabilities in tracking intruders and has shown good performance compared to systems used as reference, such as Global Positioning System.

Although the EKF is conceptually simple it has, in practice, some drawbacks, this is the main reason for the introduction of new filtering methodologies. Before exploiting the new filters and their performance in detect and tracking field, a brief overview of the Kalman filter and its drawbacks are presented in the following sections.

3.1 Kalman Filter overview: drawbacks and limitations

In target tracking applications, the most popular methods for updating target positions include variations of the Kalman filter for state estimation based on sensor measurements [44], [45], [46]. During the years, it had become a very popular filtering technique for estimating and resolving redundant errors involved in tracing the targets [47], [48], [49].

The Kalman Filter is essentially based on two groups of equations: the "Time Update Equations" and "Measurement Update equations", as reported in Figure 20 in discrete time form. The time update equations can be thought of as "predictor" equations, while the measurement update equations can be thought of as "corrector" equations.

It is in general based on a few assumptions: the system state evolves according to a known linear equation driven by a known input and an additive process noise, which is zero-mean white (uncorrelated in time) with known covariance matrix $Q(k)$. Moreover, measurements are a known function of the state with an additive measurement noise, which is again zero-mean white with known covariance $R(k)$. Required initial parameters are the initial state with its uncertainty (that is, its covariance). System and measurement noise are assumed to be uncorrelated.
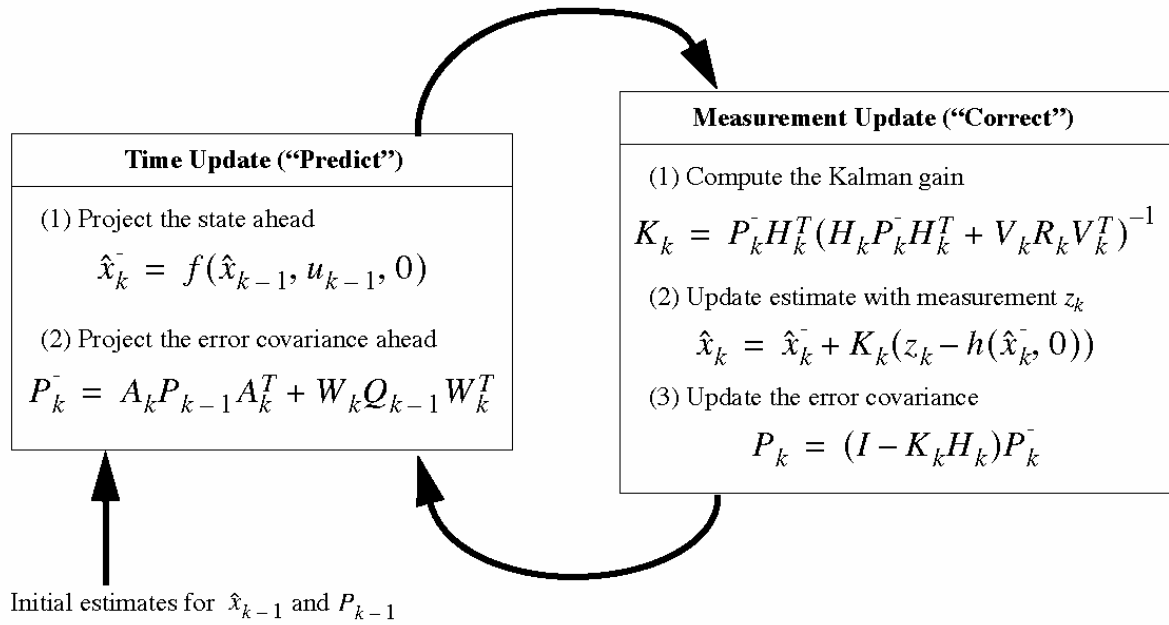
Figure 20. Kalman Filter scheme

As stated above, in most nonlinear target tracking problems, the Extended Kalman Filter results to be the optimal filter. The EKF gives an approximation of the optimal target state estimate. The non-linearities of the system dynamics are approximated by a linearized version of the non-linear system model around the last state estimate so that the traditional linear equations of Kalman filter can be applied.

However, the use of the EKF has a series of drawbacks:

- Linearization can produce highly unstable filter performance if the timestep intervals are not sufficiently small.
- The derivation of the Jacobian matrices is nontrivial in most applications and often lead to significant implementation difficulties.
- Sufficiently small timestep intervals usually imply high computational overhead as the number of calculations demanded for the generation of the Jacobian and the prediction of state estimate and covariance are large.

In the EKF, the state distribution is approximated by a Gaussian Random Variable (GRV), which is then propagated analytically through the first-order linearization of the nonlinear system. As such, the EKF can be viewed as providing "first-order" approximations to the optimal terms. These approximations can introduce large errors in the true posterior mean and covariance of the transformed (Gaussian) random variable; this may lead to suboptimal

performance and sometimes divergence of the filter. In addition, the EKF requires not only a precise system model but also the statistical property of the noise has to be properly modelled in order to achieve accurate performance. Model uncertainty and incomplete statistical information are often encountered in real applications and make it difficult to precisely estimate the system states, leading to very large estimation errors.

In order to take into account possible nonlinearity of the target motion model and the presence of non-Gaussian system noises, innovative methodologies must be considered. Different advanced techniques are present in literature, such as: Unscented Kalman Filter [50], Interval Analysis [51], H-Infinity Filter [52], and Particle Filter [53]. These techniques are analyzed in more details in the following sections. In all cases, the main interest is in an accurate estimate of the state space propagated through a dynamical system, represented by:

$$\begin{cases} x_{k+1} = f(x_k, u_k, v_k) \\ y_{k+1} = g(x_{k+1}, w_{k+1}) \end{cases} \tag{3}$$

3.2   Unscented Kalman Filter

The Unscented Kalman Filter represents the state distribution by a GRV in the same manner as the EKF, but now this distribution is specified using a minimal set of chosen sample points that completely captures the mean and covariance of the GRV. These samples capture the posterior mean and covariance accurately to the third order for any nonlinearity when propagated through the true nonlinear system [50]. The UKF is an extension of the Unscented Transformation to the recursive estimation of the state space redefined as the concatenation of the original state x_k and noise variables: $x_k^a = \left[x_k^T v_k^T n_k^T\right]^T$. To better understand the UKF procedure, the unscented transformation is explained at first.

Unscented Transformation

The UT is a method for calculating the statistics of a random variable, which undergoes a nonlinear transformation [42]. Consider propagating a random variable x (dimension L) through a nonlinear function, $y = f(x)$. Assume x has a mean $\bar{x}$ and a covariance P_x. To

calculate the statistics of y, we form a matrix $\mathcal{X}$ of 2L+1 sigma vectors $\mathcal{X}_i$ according to the following:

$$
\begin{aligned}
\mathcal{X}_0 &= \overline{x} \\
\mathcal{X}_i &= \overline{x} + \left(\sqrt{(L+\lambda)P_x}\right)_i \quad i = 1,...,L \\
\mathcal{X}_i &= \overline{x} - \left(\sqrt{(L+\lambda)P_x}\right)_{i-L} \quad i = L+1,...,2L
\end{aligned}
\tag{4}
$$

where $\lambda = \alpha^2(L+\kappa) - L$ is a scaling parameter. The constant α determines the spread of the sigma points around $\overline{x}$ and is usually set to a small positive value (e.g., $1 \leq \alpha \leq 1e-4$). The constant κ is a secondary scaling parameter which is usually set to 0 or 3-L, and β is used to incorporate prior knowledge of the distribution of x (for Gaussian distributions, $\beta = 2$ is optimal). $\left(\sqrt{(L+\lambda)P_x}\right)_i$ is the ith column of the matrix square root. These sigma vectors are propagated through the nonlinear function,

$$
y_i = f(\mathcal{X}_i) \quad i = 0,...,L
\tag{5}
$$

and the mean and covariance for y are approximated using a weighted sample mean and covariance of the posterior sigma points,

$$
\overline{y} \approx \sum_{i=0}^{2L} W_i^{(m)} y_i
\tag{6}
$$

$$
P_y \approx \sum_{i=0}^{2L} W_i^{(c)} \{y_i - \overline{y}\}\{y_i - \overline{y}\}^T
\tag{7}
$$

with weights W_i given by:

$$
\begin{aligned}
W_0^{(m)} &= \lambda/(L+\lambda) \\
W_0^{(c)} &= \lambda/(L+\lambda) + (1-\alpha^2+\beta) \\
W_i^{(m)} &= W_i^{(c)} = 1/\{2(L+\lambda)\} \quad i = 1,...,2L
\end{aligned}
\tag{8}
$$

Now, in the UKF, the UT sigma point selection scheme is applied to the new augmented state vector x_k^a, defined before, to calculate the corresponding sigma matrix, χ_k^a. All the UKF equations are reported in Table 2.

The advantage of this filter over the EKF is that no explicit calculations of Jacobians or Hessians are necessary to implement this algorithm. In [54], the potential of UKF is outlined; in fact, the UKF shows a better level of accuracy than the EKF at a comparable level of complexity in state-estimation, and parameter estimation domains. The advantages of the UKF rely on its ability to predict the state of the system more accurately than EKF and it is much less difficult to implement.

Initialize with:

$$\hat{x}_0 = E[x_0] \tag{9}$$

$$P_0 = E\left[(x_0 - \hat{x}_0)(x_0 - \hat{x}_0)^T\right] \tag{10}$$

$$\hat{x}_0^a = E[x^a] = \begin{bmatrix}\hat{x}_0^T & 0 & 0\end{bmatrix}^T \tag{11}$$

$$P_0^a = E\left[(x_0^a - \hat{x}_0^a)(x_0^a - \hat{x}_0^a)^T\right] = \begin{vmatrix} P_0 & 0 & 0 \\ 0 & R^v & 0 \\ 0 & 0 & R^n \end{vmatrix} \tag{12}$$

For $k \in \{1,...,\infty\}$,

Calculate sigma points:

$$\chi_{k-1}^a = \begin{bmatrix}\hat{x}_{k-1}^a & \hat{x}_{k-1}^a + \gamma\sqrt{P_{k-1}^a} & \hat{x}_{k-1}^a - \gamma\sqrt{P_{k-1}^a}\end{bmatrix} \tag{13}$$

Time update:

$$\chi_{k|k-1}^x = F\begin{bmatrix}\chi_{k-1}^x & u_{k-1} & \chi_{k-1}^v\end{bmatrix} \tag{14}$$

$$\hat{x}_k^- = \sum_{i=0}^{2L} W_i^{(m)}\chi_{i,k|k-1}^x \tag{15}$$

$$P_k^- = \sum_{i=0}^{2L} W_i^{(c)}\left[\chi_{i,k|k-1}^x - \hat{x}_k^-\right]\left[\chi_{i,k|k-1}^x - \hat{x}_k^-\right]^T \tag{16}$$

$$y_{k|k-1} = H\begin{bmatrix}\chi_{k|k-1}^x, \chi_{k-1}^n\end{bmatrix} \tag{17}$$

$$\hat{y}_k^- = \sum_{i=0}^{2L} W_i^{(m)}y_{i,k|k-1} \tag{18}$$

Measurement update equations:

$$P_{\tilde{y}_k\tilde{y}_k} = \sum_{i=0}^{2L} W_i^{(c)}\left[y_{i,k|k-1} - \hat{y}_k^-\right]\left[y_{i,k|k-1} - \hat{y}_k^-\right]^T \tag{19}$$

$$P_{x_k y_k} = \sum_{i=0}^{2L} W_i^{(c)} \left[\chi_{i,k|k-1} - \hat{x}_k^- \right] \left[y_{i,k|k-1} - \hat{y}_k^- \right]^T \tag{20}$$

$$\kappa_k = P_{x_k y_k} P_{\tilde{y}_k \tilde{y}_k}^{-1} \tag{21}$$

$$\hat{x}_k = \hat{x}_k^- + \kappa_k \left(y_k - \hat{y}_k^- \right) \tag{22}$$

$$P_k = P_k^- + \kappa_k P_{\tilde{y}_k \tilde{y}_k} \kappa_k^T \tag{23}$$

Where, $x^a = \begin{bmatrix} x^T & v^T & n^T \end{bmatrix}^T$, $\chi^a = \begin{bmatrix} \left(\chi^x \right)^T & \left(\chi^v \right)^T & \left(\chi^n \right)^T \end{bmatrix}$,

$\gamma = \sqrt{(L + \lambda)}$, $\lambda =$ composite scaling parameter, $L =$ dimension of augmented state, $R^v =$ process noise cov., $R^n =$ measurement noise cov., $W_i =$ weights as calculated in Eq.8.

Table 2. Unscented Kalman Filter Equations.

3.3   Interval Analysis

Interval analysis is basically about guaranteed numerical methods for approximating sets. Guaranteed means that outer (and sometimes inner) approximations of the sets of interest are obtained, which can (at least in principle), be made as precise as desired. Thus interval computation is a special case of computation on sets, and set theory provides the foundations for interval analysis [55].

Usually, interval analysis is used to model quantities, which vary around a central value within certain bounds. A real interval, denoted $[x]$, is defined as a closed and connected subset of R: $[x] = [\underline{x}, \overline{x}] = \{ x \in R / \underline{x} \le x \le \overline{x} \}$, where $\underline{x}$ and $\overline{x}$ are the minimal and maximal bound of $[x]$. A box $[x]$ of R^{n_x} is defined as a Cartesian product of n_x intervals:

$$[x] = [x_1] \times [x_2] \times ... \times [x_{n_x}] = x_{i=1}^{n_x} [x_i].$$

In general, the image of a box $[x]$ by a function f may have any shape. It may have a non-convex shape or even a disconnected shape if f is discontinuous as shown in Figure 21. Whatever the shape of $f([x])$, an inclusion function $[f]$ defined as:

$$\forall [x] \in R^n, f([x]) \subset [f]([x]) \tag{24}$$

makes it possible to compute a box contain $f([x])$. This function should be calculated such that the box enclosing the image set is optimal. As suggested by Figure 21, $[f]([x])$ may offer a very pessimistic vision of $f([x])$. Different algorithms exist to reduce the size of boxes enclosing $f([x])$ [56].

In state estimation, knowing the state x at time $k-1$, the problem consists in deriving the state vector x_k from the input vector u_k and the measurement vector y_k using the system model in Equation (3) and only the interval knowledge of data.

The main steps to follow for the implementation of an interval filter are presented below:

- Initialization step: at time step $k=0$, a state box $[x_k]$ can be constructed in a limited region of the state space.

- Prediction step: the state box $[x_k]$ is updated using the evolution model of system (3) and the input data thanks to interval tool. Firstly, a box $[u_k]$ around input data using a prior knowledge on sensors noise can be constructed. Then the predicted state box $[x_{k+1}]$ is computed as follows: $[x_{k+1}] = [f]([x_k], [u_k], [v_k])$. Since an inclusion function $[f]$ is used in this step then one may obtained a non-optimized solution of $[x_{k+1}]$. For this reason a contracting algorithm, such as Waltz algorithm, is used in the next step in order to contracting $[x]$.

- Correction step: this step consists in reducing the size of the predicted state box $[x_{k+1}]$ using Waltz algorithm and measurement vector y_{k+1}. This is done by as follows:

  - From sensor data one can construct a box $[y_{k+1}]$ around the measurement y_{k+1} using a prior knowledge of sensor noise.

  - Measurement prediction: the measurement predicting box $[\tilde{y}_{k+1}]$ is computed using the observation equation of system (3) thanks to interval tools: $[y_{k+1}] = [h]([x_{k+1}], [w_{k+1}])$.

  - Innovation computing: the innovation should indicate the proximity between the real and the predicted values. Thus, in the bounded error framework, it can be evaluated as the intersection between the two boxes: $[I_{k+1}] = [y_{k+1}] \cap [\tilde{y}_{k+1}]$.

- • Contraction: the Waltz algorithm is then computing taking into account the intersection box. The output of this algorithm is the contracted state box $[x_{k+1}]$.

$$\mathbf{f}([\mathbf{x}])$$

$$[\mathbf{f}]([\mathbf{x}])$$

$$[\mathbf{f}]^*([\mathbf{x}])$$
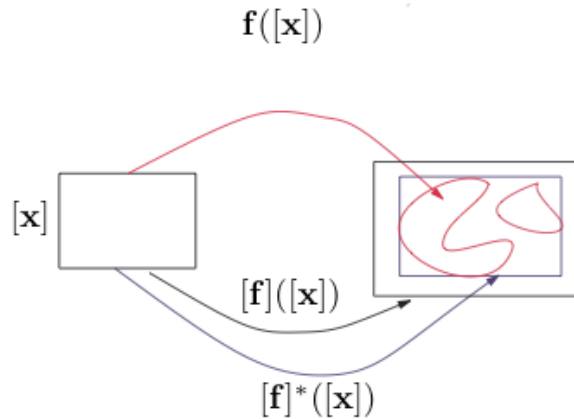
Figure 21. f([x]) is the image of [x] by f, [f]([x]) is a pessimistic inclusion function of f([x]) and [f]*([x]) is the optimal inclusion function of f ([x]).

The Interval Analysis has been employed to solve problems with uncertainty parameters [51]; this approach is used to represent constant numbers and their uncertainties. The interval analysis allows obtaining the solution of certain problems that cannot be solved by non-interval methods. This filter models the uncertainty sources bounded by intervals as it happens in [56]. In this work, an interval-based model is tested; it has been demonstrated that the model has few tuning parameters and the results show that the model always converge even when there are only few consistent measures.

The main disadvantage of this method is its exponential complexity with the number of interval variables. Choosing a contractor method properly, it is possible to decrease or eliminate the need to split boxes into sub boxes, thereby playing an essential role in keeping the dimensionality problems under control.

3.4   H-Infinity Filter

The H-Infinity Filters can be used to estimate system states that cannot be observed directly. It acts like Kalman Filters. The advantage of this filter relies on its robustness in case of unpredictable noise sources. In Kalman filters, the process and measurement noises must have zero mean at each time instant, in addition, the standard deviation of the noise

processes have to be known. In case these assumptions are not satisfied, the Kalman filter does not provide a good state estimate. The solution is the adoption of an H-Infinity filter, also called minimax filter. This filter does not make any assumption about the noise, and it minimizes the worst-case estimation error [52]. Several studies on the nonlinear robust filter have been accomplished in [57], [58], [59], [60].

Unlike the Kalman Filter, which is interested the estimation of the system state x_k, the H-Infinity filter concerns the linear combination of x_k:

$$z_k = L_k x_k \tag{25}$$

The output L_k matrix is selected by the user according to the different applications.

The H-Infinity filter computes the estimated state $\hat{z}_k$ based on the measurement Y_k, where $Y_k = \{y_k, 0 \le k \le N-1\}$, and evaluates the estimation error by a performance measure, which can be regarded as an energy gain:

$$J = \frac{\displaystyle\sum_{k=0}^{N-1} \left\| z_k - \hat{z}_k \right\|_{Q_k}^2}{\left\| x_0 - \hat{x}_0 \right\|_{P_0^{-1}}^2 + \displaystyle\sum_{k=0}^{N-1} \left(\left\| w_k \right\|_{W_k^{-1}}^2 + \left\| v_k \right\|_{V_k^{-1}}^2 \right)} \tag{26}$$

where N is the size of the measurement history, Q_k, P_0, W_k, V_k are the weighting matrices for the estimation error, the initial conditions, the process noise and the measurement noise. Moreover, $Q_k \ge 0$, $P_0^{-1} > 0$, $W_k > 0$, $V_k > 0$ and $\left((x_0 - \hat{x}_0), w_k, v_k \right) \ne 0$. The notation $\left\| x_k \right\|_{Q_k}^2$ is defined as $\left\| x_k \right\|_{Q_k}^2 = x_k^T Q_k x_k$. The denominator of J can be considered as the energy of the unknown disturbances, and the numerator is the energy of the estimation error. The $H\infty$ filter aims to provide a uniformly small estimation error $e_k = z_k - \hat{z}_k$ for any $w_k, v_k \in l_2$ and $x_0 \in R^n$, such that the energy gain J is bounded by a prescribed value:

$$\sup J < \frac{1}{\gamma} \tag{27}$$

where **sup** denotes the supremum and $\frac{1}{\gamma}$ is the noise attenuation level. This condition keeps the robustness of the $H\infty$ filter, because the estimation energy gain is limited by $\frac{1}{\gamma}$ no matter what the bounded energy disturbances are. To solve this optimal estimation $\hat{z}$ due to the bounded energy gain J, the $H\infty$ filter can be interpreted as a *minimax* problem [61]:

$$\min_{\hat{z}_k} \max_{(w_k,v_k,x_0)} J = -\frac{1}{2\gamma}\|x_0 - \hat{x}_0\|_{P_0^{-1}}^2 + \frac{1}{2}\sum_{k=0}^{N-1}\left[\|z_k - \hat{z}_k\|_{Q_k}^2 - \frac{1}{\gamma}\left(\|w_k\|_{W_k^{-1}}^2 + \|v_k\|_{V_k^{-1}}^2\right)\right] \tag{28}$$

where the estimation value $\hat{z}_k$ plays against the bounded energy disturbances w_k and v_k. Many strategies have been proposed for solving this *minimax* problem [62]. A linear quadratic game approach does not require checking the positive definiteness and inertia of the Riccati difference equations for every step, but is implemented through recursive updating the filter gain H_k, the solution P_k of the Riccati difference equation, and the state estimation $\hat{x}_k$ [61]. The updating equations are given as follows:

$$\overline{Q}_k = L_k^T Q_k L_k \tag{29}$$

$$S_k = \left(I - \gamma\overline{Q}_k P_k + C_k^T V_k^{-1} C_k P_k\right)^{-1} \tag{30}$$

$$P_{k+1} = A_k P_k S_k A_k^T + B_k W_k B_k^T \tag{31}$$

$$H_k = A_k P_k S_k C_k^T V_k^{-1} \tag{32}$$

$$\hat{x}_{k+1} = A_k \hat{x}_k + H_k\left(y_k - C_k \hat{x}_k\right) \tag{33}$$

where $P_0 = p_0$ and $P_k > 0$, I is the identity matrix.

Apparently, these recursive equations have a similar form as the classic Kalman filter. Although it is not necessary to know the statistics of noises w_k and v_k in the $H\infty$ filter, it should be better tuning the weight matrices Q_k, P_0, W_k, V_k carefully, because these values determine the estimation error in the performance criterion (Equation 26). The weight matrices W_k, V_k can be chosen according to the experience about the noise. For example, if the noise w is smaller than v, W_k should be smaller than V_k. P_0 is based on the initial estimation error. If the confidence about the initial estimation $\hat{Z}_0$ is high, P_0 should be small. Similarly, if there is a particular interest in having precise estimations of some

elements in the state, or some elements having bigger magnitude in their physical definition, the corresponding elements in the matrix Q_k can be set larger than others. As the performance criterion, γ cannot be very large, because otherwise some eigenvalues of the matrix P may have magnitudes more than one. These eigenvalues prevent a proper derivation of the $H\infty$ filter equations, so that the $H\infty$ filter problem has no solution.

Definitively, a robust $H\infty$ filter does not require a priori knowledge about the statistical properties of the system and measurement noise, but only depends on the assumption of finite noise power. The recursive equations of this filter are very similar to those of the Kalman filter, so the $H\infty$ has relatively low computation cost in the implementation and adapts to the real estimation problem.

3.5   Particle Filter Method

Particle Filter technique, well known as Sequential Importance Sampling (SIS), is a Monte Carlo method, in particular it is a technique for implementing a recursive Bayesian filter by Monte Carlo simulations. The key idea is to represent the required posterior density function by a set of random samples with associated weights and to compute estimates based on these samples and weights. As the number of particles becomes very large, the SIS filter approaches the optimal Bayesian estimates since the Monte Carlo characteristics are very close to the posterior probability density function (pdf).

In particular, the Particle filter is based on the recursive generation of random measures that approximate the distribution of unknowns (Monte Carlo integration). The random measures are composed of particles (samples) drawn from relevant distributions and of importance weights of the particles. These random measures allow for the computation of all sorts of estimates of the unknown. As new observation become available, the particles and the weights are propagated following the concept of sequential importance sampling [53], [63], [64], [65].

A pseudo-code description of the SIS algorithm is reported in Table 3.

The particle filter algorithm is essentially based on three important procedures: generation of particles, computation of particle weights and resampling. The first step suggests generating the particles from an importance density $q(x_k \mid x_{k-1}^i, z_k)$. In the second step, the weights are

evaluated on the basis of the importance density, the joint posterior density $p(x_k^i \mid z_k)$ and the state transition probability $p(x_k^i \mid x_{k-1}^i)$. The weights are then normalized.

The most critical step on the development of the PF algorithm is the choice of a good proposal distribution since it is essential to the efficiency of importance sampling [66].

$$\left[\{x_k^i, w_k^i\}_{i=1}^N\right] = PF\left[\{x_{k-1}^i, w_{k-1}^i\}_{i=1}^N, z_k\right]$$

- For i=1:N
  - Draw $x_k^i \approx q(x_k \mid x_{k-1}^i, z_k)$
  - Evaluate the importance weights up to a normalizing constant:

  $$\widetilde{w}_k^i = w_{k-1}^i \frac{p(z_k \mid x_k^i) p(x_k^i \mid x_{k-1}^i)}{q(x_k^i \mid x_{k-1}^i, z_k)}$$

- End For
- Calculate total weight: $t = SUM\left[\{\widetilde{w}_k^i\}_{i=1}^N\right]$
- For i=1:N
  - Normalize $w_k^i = t^{-1} \widetilde{w}_k^i$
- End For

Table 3. Particle Filter Algorithm

However, in high-dimensional space it becomes very difficult to find a good proposal distribution. A possible solution is to construct the proposal distribution considering the possibility to perform the importance sampling in a recursively way.

The advantage of the SIS algorithm is that it doesn't rely on a Markov chain process in which the state of the system depend only on the previous state without caring about the process; instead, several i.i.d. samples are generated and updated to create an importance sampler, thus improving the efficiency of the system. The drawback is that the importance weights may have large variances causing a loss of accuracy in the state estimates. The variance of the weights can increase over time causing so the degeneracy of the particles. This is unfavourable from the application point of view since a great computational effort is devoted to the update of the weight coefficients. In order to avoid this phenomenon, a resampling scheme must be considered. Different resampling algorithms have been introduced: residual resampling, systematic resampling, stratified resampling, and multinomial resampling [67]. In the following sub-sections, the degeneracy phenomenon

and the resampling procedures will be discussed in more details. They are the basis for the generation of the Sampling Importance Resampling Particle filter algorithm implemented in the Obstacle Detection and Tracking software that is the focus of this thesis.

3.5.1 Degeneracy phenomenon

A common problem with the SIS particle filter is the degeneracy phenomenon in which, after a few iterations, all but one particle will have negligible weight. This phenomenon is very likely to happen since the variance of the importance weights has been demonstrated [65] to increase over time. This degeneracy implies that a great computational effort is devoted to updating particles whose contribution to the approximation of the posterior filtered density is almost zero. A measure of the degeneracy phenomenon is the effective samples size N_{eff} [68], defined as:

$$N_{eff} = \frac{N_s}{1 + Var\left(w_k^{*i}\right)} \tag{34}$$

where w_k^{*i} is defined as the "true weight". This cannot be evaluated exactly, but an estimate of N_{eff} can be obtained by:

$$\hat{N}_{eff} = \frac{1}{\sum_{i=1}^{N_s}\left(w_k^i\right)^2} \tag{35}$$

where w_k^i is a normalized weight. The effective sample size is smaller than the number of particles N_s but small N_{eff} indicates severe degeneracy. Then, this problem is an undesirable effect in particle filters; to reduce this effect one solution could be the explosion of the number of particles but it is highly impractical. One of the most adopted solutions is the introduction of the resampling procedure.

3.5.2 Resampling Procedures

Resempling is a technique used to reduce the effect of the degeneracy phenomenon, as stated before. It is a critical operation in particle filtering because with time, a small number of weights dominate the remaining weights, thereby leading to poor approximation of the posterior density and consequently to inferior estimates. With resampling, the particles with large weights are replicated and the ones with negligible weights are removed. After this step, the new particles will be more concentrated in domains of higher posterior probability, which entails improved estimates. Several resampling procedures can be adopted to prevent the particles to collapse. The most important and the most considered for particle filter applications are: multinomial resampling, stratified resampling, residual resampling and systematic resampling. They will be explained below.

Multinomial Resampling

This procedure is based on the following scheme:

- Produce a uniform distribution u ~ U(0, 1), construct a cumulative distribution function for importance weights, calculate $s_i = \sum_{j=1}^{i} \widetilde{w}_k^j$;

- Find s_i: $s_{i-1} \leq u < s_i$, the particle with index i is chosen;

- Given $\left\{ x_k^i, w_k^i \right\}$, for $j=1,\ldots, N_p$ generate new samples x_k^j by duplicating x_k^i according to the associated $\widetilde{w}_k^i$;

- Reset $w_k^i = 1/N_p$

Multinomial resampling uniformly generates N_p new independent particles from the old particle set. Each particle is replicated N_i times (N_i can be zero), namely each x_k^i produces N_i children. In this case, $\sum_{i=1}^{N_p} N_i = N_p$, $E[N_i] = N_p \widetilde{W}_k^i$, $Var[N_i] = N_p \widetilde{W}_k^i \left(1 - \widetilde{W}_k^i\right)$.

Residual Resampling

The two-step selection procedure is as follows:

- For each for $i=1,\ldots, N_p$, retain $k_i = \lfloor N_p \widetilde{W}_k^i \rfloor$ copies of x_n^i;

- Let $N_r = N_p - k_1 - \ldots - k_{N_p}$, obtain N_r i.i.d. draws from $\{x_n^i\}$ with probabilities proportional to $N_p \widetilde{W}_k^i - k_i \, (i = 1,\ldots,N_p)$;

- Reset $w_k^i = 1/N_p$.

Residual resampling procedure is computationally cheaper than the conventional SIR and achieves a lower sampler variance, and it doesn't introduce additional bias. Every particle in residual resampling is replicated.

Systematic Resampling

The procedure proceeds as follows: u ~ U(0, 1)

- $u \sim U(0,1)/N_p$; $j = 1$; $l= 0$; $i = 0$;

- do while $u < 1$

  - if $l > u$ then

    - $u = u + 1/Np$; output x_k^i

  - else

    - pick k in $\{j, \cdots, N_p\}$

    - $i = x^{(k)}$, $l = l + W^{(k)}$

    - switch $(x^{(k)}, W^{(k)})$ with $(x^{(k)}, W^{(j)})$

    - $j = j + 1$

  - end if

- end do

The systematic resampling treats the weights as continuous random variables in the interval $(0, 1)$, which are randomly ordered. The number of grid points $u + k/N_p$ in each interval is counted. Every particle is replicated and the new particle set is chosen to minimize $Var[N_i] = E[(N_i - E[N_i])^2]$. The complexity of systematic resampling is $O(N_p)$.

Stratified Resampling

Stratified resampling is based on ideas used in survey sampling and consists in:

- pre-partitioning the $(0, 1)$ interval into n disjoint sets, $(0,1] = (0,1/n]...[(\{n-1\}/n,1]$;
- The independent uniforms U_i distributions are then drawn independently in each of these sub-intervals: $U^i = U((\{i-1\}/n, i/n])$, where $U([a, b])$ denotes the uniform distribution on the interval $[a, b]$.
- use the inversion method as in multinomial resampling.

It is easily checked that, as was the case for residual sampling, the difference between the duplication count N_p and its target value $N_p W_k^i$ is less than one in absolute value (for all i).

3.6 Sampling Importance Resampling Particle Filter (SIR) for Intruder Detection

In the developed Obstacle Tracking software, the Particle Filter model is based on a Sampling Importance Resampling algorithm [53]. It is constituted by three main steps:

1. generation of particles;
2. calculation of the weights associated to the particles;
3. resampling procedure.

A generic scheme of a Particle filter algorithm with importance sampling and resampling is reported in Figure 22.

Then, the state space is propagated through a non-linear dynamic equation. The algorithm is initialized generating the particles from a multivariate normal distribution with mean equal to the first radar measurements and specified standard deviation values. In particular, the uncertainties have been estimated on the basis of obstacle dynamic behaviour. Choosing a

large initial uncertainty on obstacle position allows letting a good number of particles representing the state in important or high likelihood regions.

Consequently, radar measurements have a non-negligible importance in the track initialization phase.
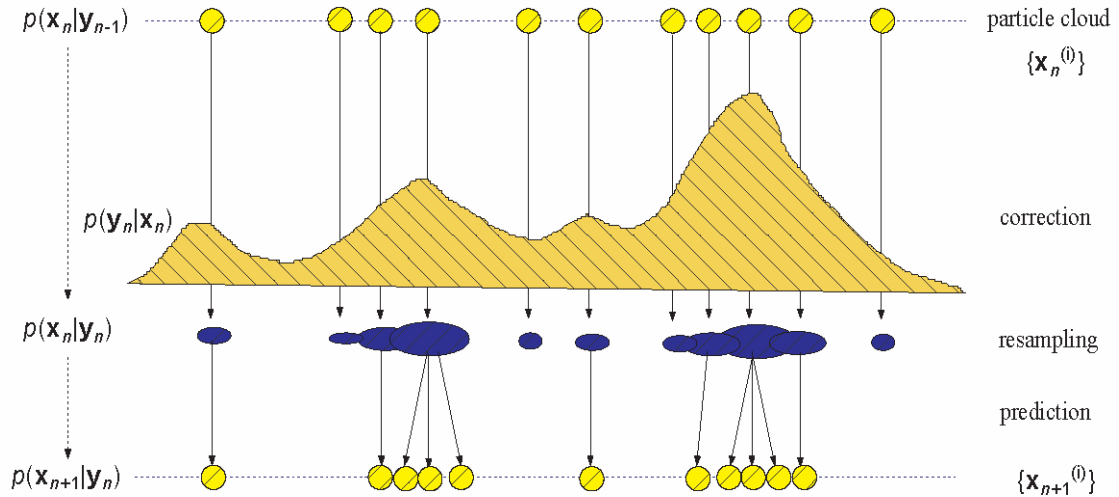
Figure 22. A generic particle filter scheme.

At the first step, all the particles are generated with the same weight. Then, these weights are updated as soon as a new measurement arrives. In the software the resampling procedure is based on a Systematic Resampling Scheme [53] which is performed at each time step and not only when the number of particles with non-negligible weight falls below a threshold value. The resampling phase enables a great quantity of particles to survive during the propagation of the state space, thus avoiding the degeneracy phenomenon.

The distribution function is modified on the basis of the new modified weights. Finally, the prediction step is executed; it exploits the system model to predict the state distribution function from one measurement time to another one. Since the state is subject to a process noise modelled as an independent and identically distributed process noise sequence, the prediction step translates, deforms, and spreads the state distribution.

The software outputs based on range, azimuth, elevation and their first time derivatives are then calculated on the basis of the state estimates weighted on all particles.

In Figure 23 a Particle Filtering scheme is reported in order to better clarify how the developed software has been conceived. The scheme exploits the main steps of the algorithm: initialization, prediction, filtering and resampling. In particular, the filtering phase is based on weights update obtained considering measurement prediction, sensor outputs and measurement covariance matrix R.

PF Initialization

Generation of Particles x_k^i
and Weights w_k^i

State at k+1

Transition to $k+1$

$$x_{k+1}^i = f\left(x_k^i\right) + n_k$$

Measurement at $k+1$

$$z_{k+1}^i = H\left(x_{k+1}^i\right) + v_{k+1}$$

Estimate at k+1

Prediction at $k+1$

$$\hat{x}_{(k+1|k)}^i = f\left(\hat{x}_{(k|k)}^i\right) + n_k$$

Measurement prediction at $k+1$

$$\hat{z}_{(k+1|k)}^i = H\left(\hat{x}_{(k+1|k)}^i\right) + v_k$$

Weights Update at $k+1$

$$w_{k+1}^i = w_k^i \exp^{-\frac{1}{2}\left(\left(z_{k+1}^i - \hat{z}_{(k+1|k)}^i\right)' R^{-1}\left(z_{k+1}^i - \hat{z}_{(k+1|k)}\right)\right)}$$

Resampling

$$\hat{x}_{(k+1|k+1)}^i = resampling\left(\hat{x}_{(k+1|k)}^i, w_{k+1}^i\right)$$
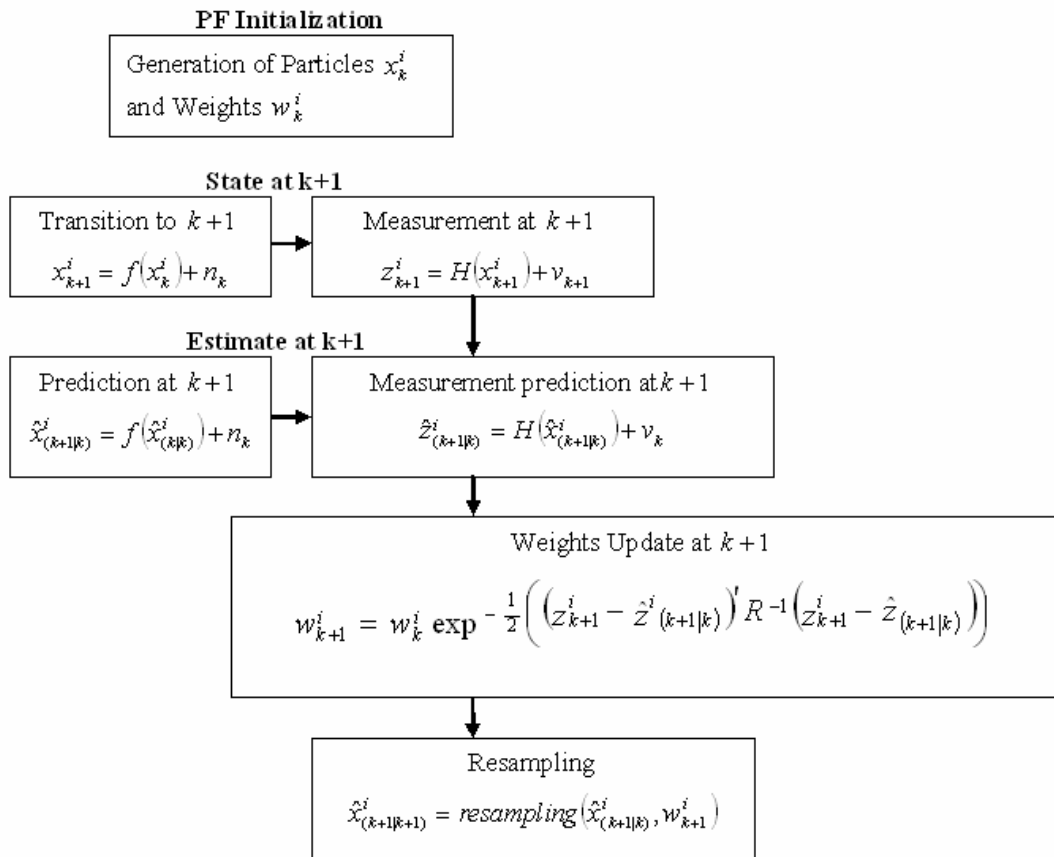
Figure 23. SIR Particle Filter algorithm

Chapter 4

Radar-only tracking algorithm design

4.1   Tracking Aspects for Intruder State Estimation

Tracking is based on fusion of information from different sensors in order to autonomously reach required situational awareness for the UAV. Basically, tracking functions are based on:

- o Association of measurements gathered in different scans/frames to the same intruder;
- o Measurement of obstacle kinematics in order to identify a potential collision;
- o Increase measurement rate with respect to sensor raw data;
- o Elimination of false alarms and clutter returns.

Since the system is completely autonomous, it is mandatory to have reliable estimates not only of intruders' positions, but also of their motion, since this latter information is needed by the collision avoidance logic to decide whether or not it is necessary to perform an evasive manoeuvre. Then, the adoption of a dynamic model able to describe the targets motion properly as well as the choice of tracking coordinates is a very important point. During the research activity three different dynamic models have been analyzed and implemented in order to evaluate the performance of the developed software and establish the best configuration able to provide the most accurate state estimates among them. In particular, the first model has been implemented in Cartesian coordinates whilst the other ones in spherical reference systems. This choice was based on the necessity to compare the algorithms behaviour since the spherical coordinates are also the coordinates of the sensors output. In the following sections, firstly a briefly overview on the choice of tracking coordinates is shown, and then the dynamic models are described. Finally, the most relevant results of the developed models are presented and analyzed in order to demonstrate the impact of coordinates systems and dynamic models on the filter accuracy.

4.1.1 Effect of tracking coordinates and dynamic model on Particle Filter performance

One of the most important problems related to airborne tracking is the choice of coordinate systems [34], [38], [47], [70], [71]. In fact, it is possible to operate in Cartesian or in Spherical coordinates. This choice impacts on the definition of the dynamic model for tracking applications. The coordinates systems have both some advantages and drawbacks. Before going on the details of the analysis, it is worth pointing out that, in order to compare the results of the developed algorithm with the EKF performance, the selection of the reference systems in which operate was dictated by previous considerations on collision avoidance logic and software developed during TECVOL project. In particular, the tracker outputs consisted of estimated range, azimuth and elevation in Body reference Frame (BRF) and their first order time derivatives. The same estimates had also to be provided in a locally level reference frame: North-East-Down (NED) system.

The BRF can be assumed with axes along longitudinal, lateral and vertical aircraft axes and origin in the aircraft centre of mass, or in the inertial navigation unit if more convenient. The NED has the same origin of BRF, while its axes can be considered non rotating for aircraft

platforms. It is worth noting that, due to the sensors' layout on FLARE, there is a vertical separation of the order of 1 m between obstacle detection sensors and aircraft AHRS (which is located in close proximity to aircraft centre of mass). This generates a parallax effect in tracking estimates both in BRF and in NED. This effect can certainly be neglected in tracking algorithm development and simulation; it has to be taken into account only for real time functioning since it can give some angular errors.

Tracking in BRF or in NED is somewhat similar; in fact, the advantage of body coordinates is that the measurement conversion in NED is avoided during tracking phase, thus eliminating the effect of errors in attitude angles measurements, however tracking in NED has the advantage of discarding attitude dynamics for the computation of relative motion, which instead has to be taken into account when tracking in BRF system. Moreover, in the latter case, latencies in navigation data acquisition and reception by the tracker could impact on tracking performance. For this application, the NED was considered the tracking reference frame.

As stated above, different models exist in tracking application, which differ in the choice of the state variables coordinates: Cartesian or Spherical.

Cartesian coordinates are useful in the prediction phase when in absence of intruder aggressive manoeuvres the relative dynamics can be considered linear. In this case, the state vector is composed of the three components in NED of the obstacle position, their first time derivatives that are the obstacle velocities and also the second time derivatives that are the obstacle accelerations. With this assumption the measurement equation is non linear since both radar and eventually electro-optical sensors measurement outputs are in spherical coordinates. An approach can be based on considering the sensor measurements converted in Cartesian coordinates. The alternative is to track directly in spherical coordinates obtaining then a linear measurement equation even if these coordinates are not the sensor coordinates since it is supposed that tracking is performed in NED in any case. It is worth pointing out that the choice of spherical coordinates can require the estimation of high order derivatives of angles even when non-manoeuvring dynamics are considered; in this case the relative dynamics are affected by the so called "pseudo-accelerations" [47]. These aspects can be resolved adopting filters that can easily handle non-linear dynamics as for example Particle Filter that is the scope of this thesis.

The most important features of spherical filters is that, under reasonable assumptions (essentially, elevation angle must be sufficiently small) it is possible to decouple the filters for range, azimuth and elevation, obtaining a lighter algorithm from the computational point

of view. In any case, range and angle filters have to exchange their estimates for range and angle extrapolation.

A detailed description of spherical filters is reported in [38]. Briefly, the range filter includes range, range rate and range acceleration in the vector state. The angle filters are derived by projection in the RHV reference frame, which is a target-dependant reference frame with one axis along the range vector, and the other two axes perpendicular to the range vector and in the horizontal and vertical plane, respectively (Figure 24).

RHV reference frame also allows defining the angle filters. In fact, the state components are not the stabilized angles with their time derivatives, but, in the case of stabilized azimuth for example

$$\overline{x}_\varphi = \begin{bmatrix} \varphi \\ v_H \\ a_H \end{bmatrix} \tag{36}$$

where v_H and a_H are, respectively, the relative velocity component perpendicular to the line of sight along the H axis of the RHV reference frame, and the horizontal relative acceleration. Analysing the structure of spherical filters, it comes out that some information must be exchanged among range and angle filters in order to propagate system dynamics. In fact, as it will be shown in the following section on dynamic models, range filter transition matrix contains target angular rate perpendicular to its line of sight (ωp), which can be estimated on the basis of angle filters.

The advantages of the spherical filters relies on the fact that the three filters require computational effort based on inversion of 3x3 matrix separately instead of 9x9 matrix as in other cases.

In the following sections, different dynamic models will be shown in which Cartesian coordinates first and spherical coordinates then have been implemented in order to evaluate their impact on PF algorithm performance.
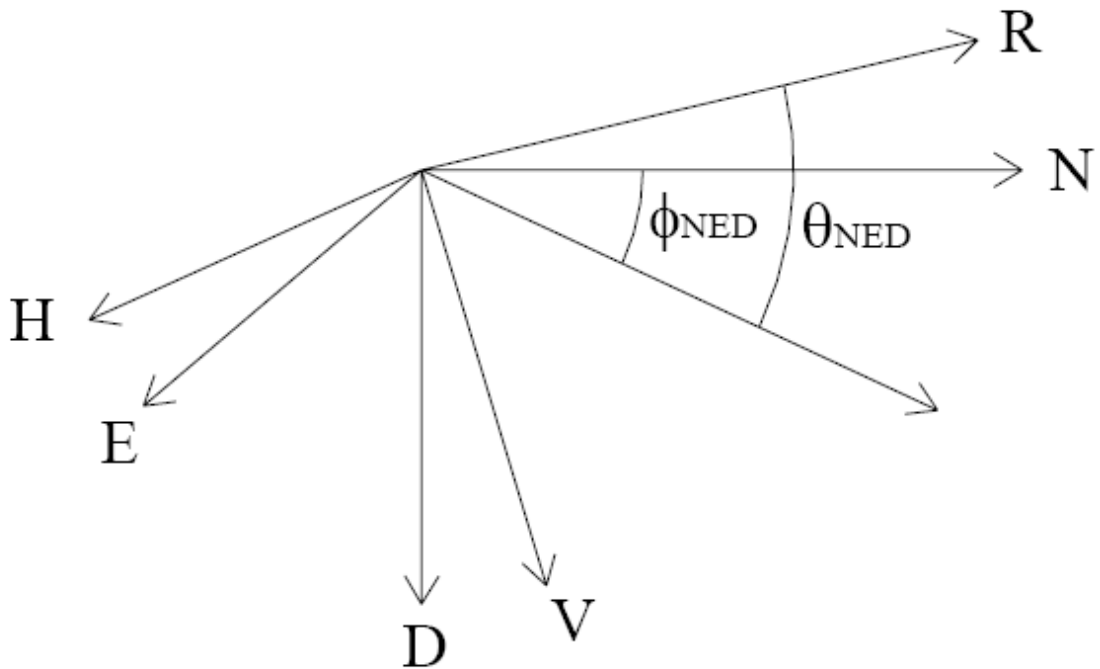
Figure 24. RHV Reference Frame.

4.1.2 Obstacle dynamic model: Singer Model

The most used models for random target motion are based on target acceleration. One of the most common among them is the Singer acceleration model [69]. It assumes that the target acceleration evolves in terms of a correlated noise process, so that, considering a one dimensional case with a scalar coordinate , acceleration auto-correlation function is given by

$$r_{\ddot{x}}(\tau) = E\{\ddot{x}(t)\ddot{x}(t+\tau)\} = \sigma_m^2 e^{-(\mu\tau)} \tag{37}$$

where

σ_m^2 is the acceleration instantaneous variance; μ is the inverse of target acceleration time constant.

σ_m and μ represent the input parameters for the model: σ_m is connected to the range of accelerations that can be foreseen for the target and can be determined for example on the basis of a ternary-uniform mixture [70], while μ is connected to how fast target dynamics

changes so that the time constant can be considered as a manoeuvre time duration. In continuous terms, the dynamic model is in the form

$$
\begin{bmatrix} \dot{x} \\ \ddot{x} \\ \dddot{x} \end{bmatrix} = \begin{bmatrix} 0 & 1 & 0 \\ 0 & 0 & 1 \\ 0 & 0 & -\mu \end{bmatrix} \begin{bmatrix} x \\ \dot{x} \\ \ddot{x} \end{bmatrix} + \begin{bmatrix} 0 \\ 0 \\ 1 \end{bmatrix} w(t) = A \begin{bmatrix} x \\ \dot{x} \\ \ddot{x} \end{bmatrix} + Bw(t)
\tag{38}
$$

where w(t) is a white zero-mean Gaussian process with variance σ_m^2. In discrete terms (considering a sampling interval equal to T), target acceleration is a first order Markov process of the form

$$
a(k+1)\rho_m a(k) + \sqrt{1 - \rho_m^2} \sigma_m r(k)
\tag{39}
$$

Where $\rho_m = \exp(-\mu T)$ and r(k) is a zero-mean unit-standard deviation Gaussian random variable. The resulting transition matrix is

$$
\Phi(k+1|k) = \begin{bmatrix} 1 & T & \dfrac{\left(e^{-\mu T} - 1 + \mu T\right)}{\mu^2} \\ 0 & 1 & \dfrac{\left(1 - e^{-\mu T}\right)}{\mu} \\ 0 & 0 & e^{-\mu T} \end{bmatrix}
\tag{40}
$$

while the exact solution for the system noise covariance matrix Q is given by

$$
Q = 2\sigma_m^2 \mu \begin{bmatrix} q_{11} & q_{12} & q_{13} \\ q_{12} & q_{22} & q_{23} \\ q_{13} & q_{23} & q_{33} \end{bmatrix}
\tag{41}
$$

where

$$q_{11} = \frac{1}{2\mu^5}\left[1 - e^{-2\mu T} + 2\mu T + \frac{2\mu^3 T^3}{3} - 2\mu^2 T^2 - 4\mu T e^{-\mu T}\right]$$

$$q_{12} = \frac{1}{2\mu^4}\left[e^{-2\mu T} + 1 - 2e^{-\mu T} + 2\mu T e^{-\mu T} - 2\mu T + \mu^2 T^2\right]$$

$$q_{13} = \frac{1}{2\mu^3}\left[1 - e^{-2\mu T} - 2\mu T e^{-\mu T}\right]$$

$$q_{22} = \frac{1}{2\mu^3}\left[4e^{-\mu T} - 3 - e^{-2\mu T} - 2\mu T\right]$$

$$q_{23} = \frac{1}{2\mu^2}\left[e^{-2\mu T} + 1 - 2e^{-\mu T}\right]$$

$$q_{33} = \frac{1}{2\mu}\left[1 - 2e^{-2\mu T}\right]$$

(42)

As it results from previous equations, the model is flexible in that it allows taking into account different dynamic environments by properly adjusting σ_m and μ. Singer acceleration model can assume some forms of interest on the basis of the ratio between sampling time and manoeuvre time constant. In particular, if sampling interval is much less that manoeuvre time, then acceleration is essentially seen as a constant with its derivative being a white noise process. This is known as constant acceleration model [70] and Q matrix takes the limit form

$$\lim_{\mu T \to 0} Q = 2\sigma_m^2 \mu \begin{bmatrix} \dfrac{T^5}{20} & \dfrac{T^4}{8} & \dfrac{T^3}{6} \\ \dfrac{T^4}{8} & \dfrac{T^3}{3} & \dfrac{T^2}{2} \\ \dfrac{T^3}{6} & \dfrac{T^2}{2} & T \end{bmatrix}$$

(43)

When sampling interval is much larger that manoeuvre time, the acceleration is seen itself as white noise: the resulting model is known as constant velocity model [70] and its Q matrix is

$$\lim_{\mu T \to \infty} Q = 2\sigma_m^2 \mu \begin{bmatrix} \dfrac{2T^3}{3\mu} & \dfrac{T^2}{\mu} & \dfrac{1}{\mu^2} \\ \dfrac{T^2}{\mu} & \dfrac{2T}{\mu} & \dfrac{1}{\mu} \\ \dfrac{1}{\mu^2} & \dfrac{1}{\mu} & 1 \end{bmatrix}$$

(44)

These limiting cases put into evidence how Singer model allows covering a wide range of dynamic environments, as a function of design choices. On the other hand, model success relies on the accuracy of these choices.

The deterministic input vector $\bar{u}$ contains the UAV acceleration components in NED reference frame (Eq.45):

$$\bar{u}(k) = \begin{bmatrix} -\frac{1}{2}T^2 a_N \\ Ta_N \\ 0 \\ -\frac{1}{2}T^2 a_E \\ Ta_E \\ 0 \\ -\frac{1}{2}T^2 a_D \\ Ta_D \\ 0 \end{bmatrix} \tag{45}$$

w(t) is a white zero-mean Gaussian process noise.

Usually, the measurement equation is in the form (Eq.46):

$$\bar{y}(k) = H\bar{x}(k) + \bar{w}(k) \tag{46}$$

with

$$H = \begin{bmatrix} 1 & 0 & 0 & 0 & 0 & 0 & 0 & 0 & 0 \\ 0 & 0 & 0 & 1 & 0 & 0 & 0 & 0 & 0 \\ 0 & 0 & 0 & 0 & 0 & 0 & 1 & 0 & 0 \end{bmatrix} \tag{47}$$

while the measurements covariance matrix is

$$R = \begin{bmatrix} R_a^{xx} & R_a^{xy} & R_a^{xz} \\ R_a^{xy} & R_a^{yy} & R_a^{yz} \\ R_a^{xz} & R_a^{yz} & R_a^{zz} \end{bmatrix} \tag{48}$$

These matrices depend on measurement values and so R has to be calculated as new measurements arrive.

In the Cartesian PF algorithm the measurement equation is non-linear and it is expressed by Eq.49 in terms of obstacle coordinates in NED reference frame:

$$y = \begin{bmatrix} \sqrt{x_{NED}^2 + y_{NED}^2 + z_{NED}^2} \\ \arctan\left(\dfrac{y_{NED}}{x_{NED}}\right) \\ -\arcsin\left(\dfrac{z_{NED}}{\sqrt{x_{NED}^2 + y_{NED}^2 + z_{NED}^2}}\right) \end{bmatrix} + \overline{w} \qquad (49)$$

In this case, R is constant and assigned off-line on the basis of sensors specifications.

The Singer model can be applied also when the state variables are not limited to only one variable; in addition, the model can be formulated taking into account the coordinate system that better suits the problem in consideration.

4.1.3 Nearly Constant Acceleration model for Spherical Particle filter

Since the hardware sensing setup installed on-board the aircraft was composed of radar and electro-optical sensors whose outputs are in spherical coordinates, it was decided to evaluate the performance of the filter also in spherical coordinates. This choice was based on the fact that the statistics of the errors are likely to be similar to the characteristics of the sensor outputs so that the target state estimates are expected to be more accurate than those in Cartesian coordinates. Different target dynamic models in spherical coordinates have been tested; in particular, the nearly constant acceleration model was able to provide more accurate estimates than the Singer model in Cartesian coordinates. In the case of spherical reference system, the target state is propagated through a non-linear dynamic equation and a linear measurement equation since the state variables are in spherical coordinates, i.e. sensor measurements output. In the following, the state and measurement equations are described in more details.

The constant acceleration model is a particular case of the Wiener-process acceleration model [70] that assumes the acceleration as a Wiener process, i.e. the acceleration is a process with independent increments. In this case, the acceleration derivative $\dot{a}(t)$ is an independent (white noise) process $w(t)$: $\dot{a}(t) = w(t)$.

The corresponding state-space representation is (Eq.50):

$$
\begin{bmatrix} \dot{x} \\ \ddot{x} \\ \dddot{x} \end{bmatrix} = \begin{bmatrix} 0 & 1 & 0 \\ 0 & 0 & 1 \\ 0 & 0 & 0 \end{bmatrix} \begin{bmatrix} x \\ \dot{x} \\ \ddot{x} \end{bmatrix} + \begin{bmatrix} 0 \\ 0 \\ 1 \end{bmatrix} w(t)
\tag{50}
$$

In discrete time, the target dynamic is described by the following representation (Eq.51):

$$
x_{k+1} = \Phi x_k + w_k
\tag{51}
$$

where the state $x(t)$ is comprised of nine components that are the obstacle positions and their first and second time derivatives in spherical coordinates. For this reason, the transition matrix is different for the range, azimuth, and elevation variables (taking into account the explanation provided before on the choice of coordinate system); in particular, they can be expressed as (Eq. 52-53-54):

$$
\Phi_R = \begin{bmatrix} 1 + \omega_p^2 \dfrac{T^2}{2} & T & \dfrac{T^2}{2} \\ \omega_p^2 T & 1 + \omega_p^2 \dfrac{T^2}{2} & T \\ 0 & 0 & 1 \end{bmatrix}
\tag{52}
$$

where Φ_R is the transition matrix for estimating the range and its first and second time derivatives. ω_p is the angular rate of the rotating coordinate frame that has one axis along the line of sight of the sensor relative to the inertial frame (NED).

In order to estimate the angles and their derivatives, the transition matrices are Φ_H and Φ_V:

$$\Phi_H = \begin{bmatrix} 1 & \dfrac{T}{R_H}\left(1-\dfrac{TV_R}{2R}\right) & \dfrac{T^2}{2R_H} \\ 0 & 1-\dfrac{TV_R}{R}\left(1-\dfrac{TV_R}{2R}\right) & T\left(1-\dfrac{TV_R}{2R}\right) \\ 0 & 0 & 1 \end{bmatrix} \qquad (53)$$

where R is the range estimate obtained from the range filter, V_R is the range rate and $R_H = R\cos\varepsilon$ in which ε is the elevation angle.

$$\Phi_V = \begin{bmatrix} 1 & \dfrac{T}{R}\left(\dfrac{TV_R}{2R}-1\right) & -\dfrac{T^2}{2R} \\ 0 & 1-\dfrac{TV_R}{R}\left(1-\dfrac{TV_R}{2R}\right) & T\left(1-\dfrac{TV_R}{2R}\right) \\ 0 & 0 & 1 \end{bmatrix} \qquad (54)$$

In the developed model, the process noise can be expressed as (Eq.55):

$$Q = \text{cov}(w_k) = S_w Q_3 \qquad Q_3 = \begin{bmatrix} \dfrac{T^5}{20} & \dfrac{T^4}{8} & \dfrac{T^3}{6} \\ \dfrac{T^4}{8} & \dfrac{T^3}{3} & \dfrac{T^2}{2} \\ \dfrac{T^3}{6} & \dfrac{T^2}{2} & T \end{bmatrix} \qquad (55)$$

The term S_w is the power spectral density, not the variance, of the continuous-time white noise.

In case of Spherical Particle Filter, the measurement equation is linear and it is in the form (Eq. 56):

$$\bar{y}(k) = H\bar{x}(k) + \bar{v}(k) \qquad (56)$$

where H is the observation matrix expressed by (Eq.57):

$$H = \begin{bmatrix} 1 & 0 & 0 & 0 & 0 & 0 & 0 & 0 & 0 \\ 0 & 0 & 0 & 1 & 0 & 0 & 0 & 0 & 0 \\ 0 & 0 & 0 & 0 & 0 & 0 & 1 & 0 & 0 \end{bmatrix} \tag{57}$$

and $\bar{v}(k)$ is the observation process noise.

The derivation of the measurement covariance matrix is straightforward and its values depend on the sensor specifications.

4.2   Nearly Constant Velocity model: obstacle dynamic improvement

In this section a variation of the target dynamic has been considered and implemented in the Obstacle Detection and Tracking software based on Spherical Particle filter. The principal aim of this choice relied on the possibility of obtaining some improvements in terms of algorithm performance and specifically in the estimation of Distance at Closest Point of Approach with respect to the previous developed models. In particular, considering the scenario in which the data were gathered, a less sophisticated model based on a nearly constant velocity model [70] was chosen to describe the target trajectory. In this case, the following equations have been applied where the target state is propagated through a non-linear dynamic equation since the state variables are in spherical coordinates, thus closer to sensor measurements outputs.

The state vector is comprised of obstacle position in terms of range, azimuth and elevation in North-East-Down reference frame, and their first time derivatives. Hereinafter, the obstacle dynamic model is reported for the sake of clarity.

The target state vector in spherical coordinates is defined as:

$$x = \left[r, \dot{r}, \vartheta, \dot{\vartheta}, \phi, \dot{\phi} \right] \tag{58}$$

where r is the range, ϑ is the azimuth, ϕ is the elevation angle, and $\dot{r}, \dot{\vartheta}, \dot{\phi}$ are their first time derivatives.

In order to evaluate the velocity components, let us consider:

$$v = \begin{bmatrix} v_r \\ v_\vartheta \\ v_\phi \end{bmatrix} = \begin{bmatrix} \dot{r} \\ r\dot{\vartheta}\cos\phi \\ r\dot{\phi} \end{bmatrix} \tag{59}$$

where the velocity vector has been defined as $v = \begin{bmatrix} v_r, v_\vartheta, v_\phi \end{bmatrix}$ for the sake of simplicity.

For a spherical constant-velocity dynamic model representing the object motion, it is assumed that $\dot{v}_r = \dot{v}_\vartheta = \dot{v}_\phi = 0$. Taking the time derivative of each component in (59) yields:

$$\dot{v}_r = \ddot{r} = 0 \tag{60}$$

$$\dot{v}_\vartheta = \dot{r}\dot{\vartheta}\cos\varphi + r\ddot{\vartheta}\cos\varphi - r\dot{\vartheta}\dot{\varphi}\sin\varphi = 0 \tag{61}$$

$$\dot{v}_\phi = \dot{r}\dot{\varphi} + r\ddot{\varphi} = 0 \tag{62}$$

Rearranging the above expressions in terms of angular velocities and considering discrete-time domain with sampling time *T*, the components of the dynamic motion equation are given by:

$$r_n = r_{n-1} + T\dot{r}_{n-1} \tag{63}$$

$$\dot{r}_n = \dot{r}_{n-1} \tag{64}$$

$$\vartheta_n = \vartheta_{n-1} + T\dot{\vartheta}_{n-1}\left[1 + \frac{T}{2r_{n-1}}\left(r_{n-1}\dot{\phi}_{n-1}tg\,\phi_{n-1} - \dot{r}_{n-1}\right)\right] \tag{65}$$

$$\dot{\vartheta}_n = \dot{\vartheta}_{n-1}\left[1 + T\left(\dot{\phi}_{n-1}tg\,\phi_{n-1} - \frac{\dot{r}_{n-1}}{r_{n-1}}\right)\right] \tag{67}$$

$$\phi_n = \phi_{n-1} + T\dot{\phi}_{n-1}\left[1 - \frac{T}{2r_{n-1}}\dot{r}_{n-1}\right] \tag{68}$$

$$\dot{\phi}_n = \dot{\phi}_{n-1}\left[1 - \frac{T}{2r_{n-1}}\dot{r}_{n-1}\right] \tag{69}$$

The non-linear dynamic motion equation for the spherical state vector can be written as:

$$x_n = f(x_{n-1}) + n_{n-1} \tag{70}$$

with the zero-mean Gaussian dynamic acceleration noise distribution

$$n_n \sim N(0, Q_\rho) \tag{71}$$

The components of $f(x_{n-1})$ are given by the non-linear equations (63)-(69) and the process noise matrix is:

$$Q_\rho = \begin{vmatrix} q_r Q_1 & 0_2 & 0_2 \\ 0_2 & q_h Q_1 & 0_2 \\ 0_2 & 0_2 & q_v Q_1 \end{vmatrix} \tag{72}$$

with:

$$Q_1 = \begin{bmatrix} \dfrac{T^3}{3} & \dfrac{T^2}{2} \\ \dfrac{T^2}{2} & T \end{bmatrix} \tag{73}$$

where q_r, q_h and q_v must be set depending on the target manoeuvres [72].

Since the model is in spherical coordinates, the measurement equation is linear and it can be expressed as:

$$y_n = Hy_n + w_n \tag{74}$$

with

$$H = \begin{bmatrix} 1 & 0 & 0 & 0 & 0 & 0 \\ 0 & 0 & 1 & 0 & 0 & 0 \\ 0 & 0 & 0 & 0 & 1 & 0 \end{bmatrix} \tag{75}$$

and w_n is the observation noise which is considered to be independent zero-mean Gaussian noise defined by:

$$w_n \sim N(0, R_n) \tag{76}$$

where R_n is the measurement covariance matrix, as stated above.

The developed Obstacle Detection and Tracking software provides also an estimate of the Distance at Closest Point of Approach (see Equation (1)). Since the particles are characterized by own positions and velocities and given the non-linear dependencies between $\bar{r}$, $\bar{V}$ and DCPA, the latter is calculated for each particle. In this way, in order to avoid further approximations due to the evaluation of this distance from position and velocity mean values, DCPA has been calculated as mean value of the different distances evaluated as:

$$DCPA_n = \left| \frac{\bar{r} \cdot \bar{V}}{\left\| \bar{V} \right\|^2} \bar{V} - \bar{r} \right| \tag{77}$$

This is a form of "deep integration" of a collision detection sensor since an estimate of the level of collision threat is determined by means of the same data fusion algorithm. This is an additional advantage of using PF rather than EKF, since the need of linearized models in EKF does not allow estimating DCPA by the filter itself.

The three models described above have been implemented in the Obstacle Detection and Tracking software; their performance will be shown in the next section and compared in order to evaluate which of them is able to provide more accurate performance in terms of state variables estimates and in terms of DCPA, i.e. assessment of collision risk. Before entering in the details of the results, some considerations about the implementation issues for the realization of quasi-real time software will be presented.

4.3   Implementation issues for quasi-real time software

In general, the tracking software allows effective fusion of information provided by different sensors, such as radar and inertial unit; moreover it performs the gating/association functions in order to associate at the same intruder measurements gathered in different scans and to eliminate false alarms and clutter returns. In fact, the inputs to the algorithm are sensor measurements, which represent in general object of interest, false alarm and clutter. In this case, most of the clutter return will likely come from ground echoes. Track/measurement association is carried out using ellipsoidal gating and a centralized statistic [34]; in particular, this statistic has been considered:

$$\xi = \left[\underline{y} - \hat{y} \right]' \left[R + HPH' \right]^{-1} \left[\underline{y} - \hat{y} \right]$$

(78)

Where P is the predicted state estimation covariance matrix at time of detection, and $\hat{y}$ is predicted measurement at time of detection on the basis of predicted state and measurement equation.

This is a normalized distance between measurement and prediction. Normalization is made on the basis of measurement and prediction uncertainties (that is, covariance). This is a very intuitive principle: the more the track and the measurement are believed to be accurate, the more the measurement-to-track distance will be expected to be small. This also implies that an excessively optimistic covariance estimate (both for state and measurement) can be dangerous and can definitely lead to track deletion. The statistic ζ is distributed as a chi-squared normal variable with a number of degrees of freedom that equals the dimension of the measurement vector. Thus, in the considered system (radar measurement) n=3. The upper limit for the statistic can be defined to yield a given (low) probability of rejecting the correct measurement when present. Assuming for example this probability equal to 0.01, from chi-square tables the gate limit is 11.34. This limit establishes in the state space an ellipsoidal region, hence the definition of ellipsoidal gating.

As for association, it is kept at a very simple level; in fact it will be based on nearest neighbour logic.

Other important points are related to the sensor latency and the proper inclusion of aircraft navigation measurements. Thus, proper data registration techniques have been considered as a pre-requisite for the developed algorithm [73]. Regarding time registration, the radar sends its measurements at the end of each pass with a maximum latency of the order of 1 s. Since the tracker works at 10 Hz, in the developed system a measurement is assigned a time stamp, which is the nearest time on the tracker 0.1 s scale. Since the radar delay is typically larger than the 0.1 s scale, it is likely that a measurement relative to time 1 t arrives when the state has already been propagated to a later time n t. In this case, the state and covariance must be updated at time 1 t. Also, the gating and association processes have to be performed with values of state and covariance at time 1 t. Then, the problem is how to produce updated parameters from measurement at time 1 t.

In order to perform gating, association and track updating, the solution is to keep in memory a sliding window where navigation and track data are stored. The considered time window dimensions correspond to the largest possible radar data latency. Given that, state and covariance at time 1 t have to be known and stored. In the developed PF tracker, the key idea is to consider all the variables at time 1 t, to perform the filtering step taking into account the radar measurement at that time, and then updating the state (and covariance) until time n t by means of a Monte Carlo approach.

Chapter 5

Results

5.1   Flight Testing Strategy

During the flight campaign with FLARE, several different tests were carried out in order to gather data from both radar and electro-optical sensors and to estimate the performance of the developed hardware/software system. Besides, the most important outcome of these tests was the possibility to evaluate some of the effects that are present in real time environment but cannot be easily modelled in numerical simulation and/or in laboratory test facilities.

These effects are essentially based on vibration and electromagnetic interferences, the presence of ground clutter and background for both radar and electro-optical sensors, the effects of illumination conditions and changes on the acquisition process and images performed by EO sensor.

Flight tests were performed by exploiting the following configuration of test facilities:

- FLARE aircraft piloted by human pilot or by the autonomous flight control system with the fully installed and functional setup described in the previous sections;
- A piloted VLA aircraft in the same class of FLARE equipped with GPS;
- A Ground Control Station (GCS) for real-time flight coordination and test monitoring [74];
- A full-duplex data-link between FLARE and GCS. This data- link allowed GCS operators to send commands to initiate or terminate tests and to receive synthetic filter output and navigation measurements. Indeed, no workload was assigned to human pilot in terms of sensor unit management in flight;
- A downlink between intruder and GCS. This data-link was used for flight monitoring.

In particular, the first tests were performed for the radar acceptance, for which the entire architecture described in the previous sections was properly installed on board FLARE, except for the EO sensors. The radar was remotely commanded from the ground station, by means of the radio link, the CAN bus and the real time computer. A proper ground/on board software was developed for these flights. Different tests allowed validating the different operating modes for the radar, ant to evaluate detection range for a VLA intruder.

As for sense and avoid flight tests, they were divided in two main categories: obstacle detection and tracking flight performance assessment combined autonomous collision avoidance.

During the tests autonomous anti-collision logic was not engaged, since the focus was set on sensor system development and performance estimation. Two types of manoeuvres were basically executed during flight experiments:

1. Chasing tests with FLARE pursuing the intruder (Figure 25.a). These tests were performed in order to estimate tracking performance for long time duration with negligible miss detection rate. Moreover, chasing phases can be effectively used to estimate residual radar misalignment with respect to AHRS thanks to the large number of intruder detections, smooth relative dynamics, and consequent small impact of latencies. For this reason, the two aircraft started their routes from the closest point that is compatible with safe flight and they continued their straight

flight increasing the relative distance. This condition was achieved by assigning a small speed excess to intruder aircraft;

2. Quasi-frontal encounters (Figure 25.b). These tests were performed to estimate detection and tracking performance in real scenarios. The two aircraft started the test from furthest points within the data-link coverage area. They followed quasi-collision trajectories on parallel routes or on routes that formed a small angle. Different relative flight level configurations were assigned to the aircraft depending on the expected ground clutter level.

(a)

(b)
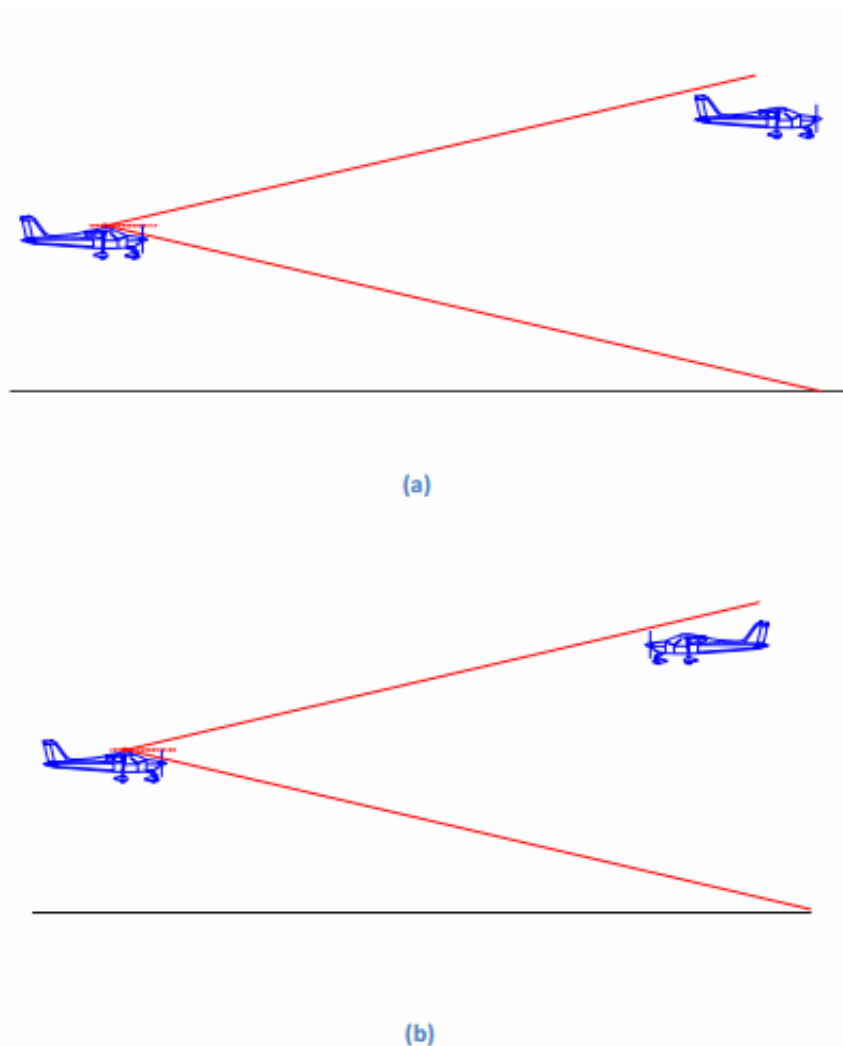
Figure 25. Obstacle detection and tracking flight tests.

5.2   Particle Filter algorithms outputs

In this section the developed obstacle detection and tracking results based on Particle Filter technique are presented and discussed. The Particle Filter algorithm has been implemented in off-line simulations based on real data gathered during the flight test campaign performed by means of FLARE and on software that replicates ad hoc the real time tracking module described in the previous sections. Furthermore, radar only tracking configuration has been considered since the primarily interest was on the impact of the particle filtering in obstacle tracking performance and on the comparison between several dynamic model in Cartesian and/or Spherical reference system in order to point out the main differences between the algorithms behaviour. The analysis allowed choosing the best configuration able to provide the most accurate estimates of the software outputs comparable to EKF performance. In the following sections the results obtained implementing the different dynamic models will be shown; then a comparable analysis is performed to justify the final adopted configuration.

5.2.1 Singer model results

In this section, the particle filter algorithm results based on singer model will be shown. The model has been developed in Cartesian coordinates; the state vector is comprised of 9 components that are the obstacle positions, velocity and accelerations in NED reference frame; however the outputs of the software are only base on range, azimuth, elevation and their first time derivatives. Considering these coordinates, the dynamic model in stabilized NED coordinates is linear while the measurement equation is non-linear since the radar outputs are in spherical coordinates.

The considered flight segment has duration of about 30 s, which correspond to an initial range of about 160 m, in which the UAV follows the intruder (chasing flight). In Figure 26, it can be noticed that after a very few seconds a firm track is generated on the basis of radar measurements. The Cartesian PF is able to track the intruder trajectory without loss of track; this derives from radar range accuracy and the absence of intruder manoeuvres.
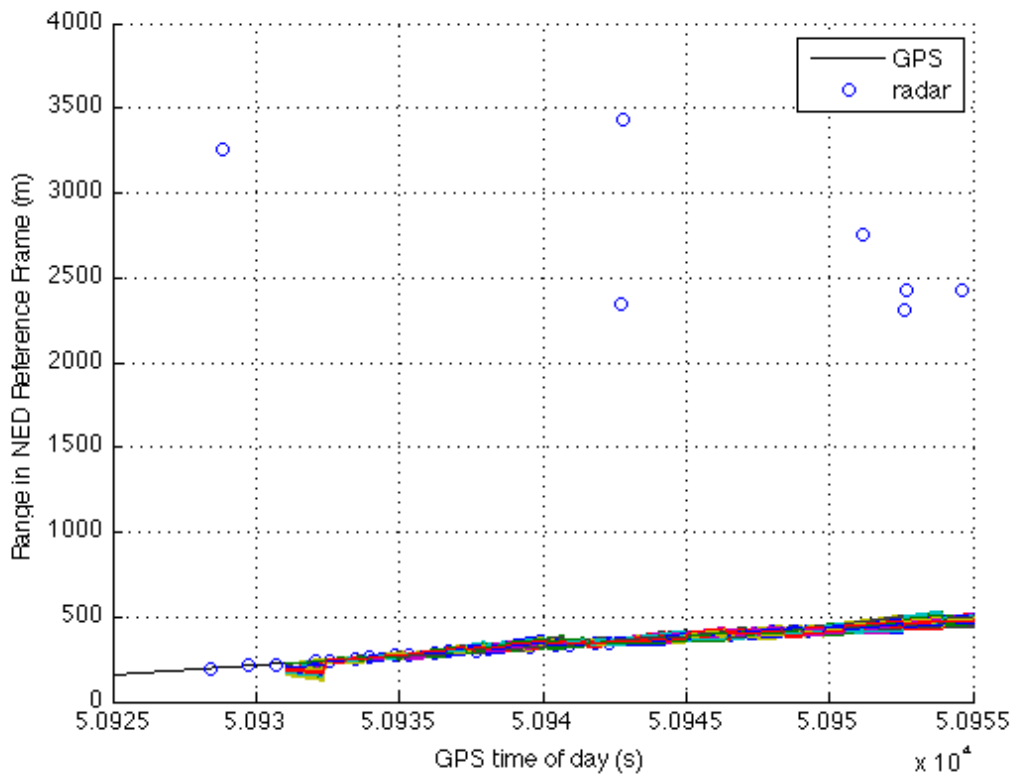
Figure 26. Range as estimated by GPS, by radar, and by radar-only Cartesian PF tracker as function of GPS time of the day.

In the angular estimates diagrams (Figure 27-Figure 28), the particles take very few seconds before to track the target angular dynamics as accurate as the GPS reference measurements. In addition, the effect of the resampling procedure on the particle pattern can be noticed.

The range rate and angular rates are reported in Figure 29, Figure 30 and Figure 31. These parameters are not directly provided by the sensor but they are very important parameters. In fact, the collision detection performances can be determined on the basis of the angular rates in terms of estimated value of the distance at closest point of approach.
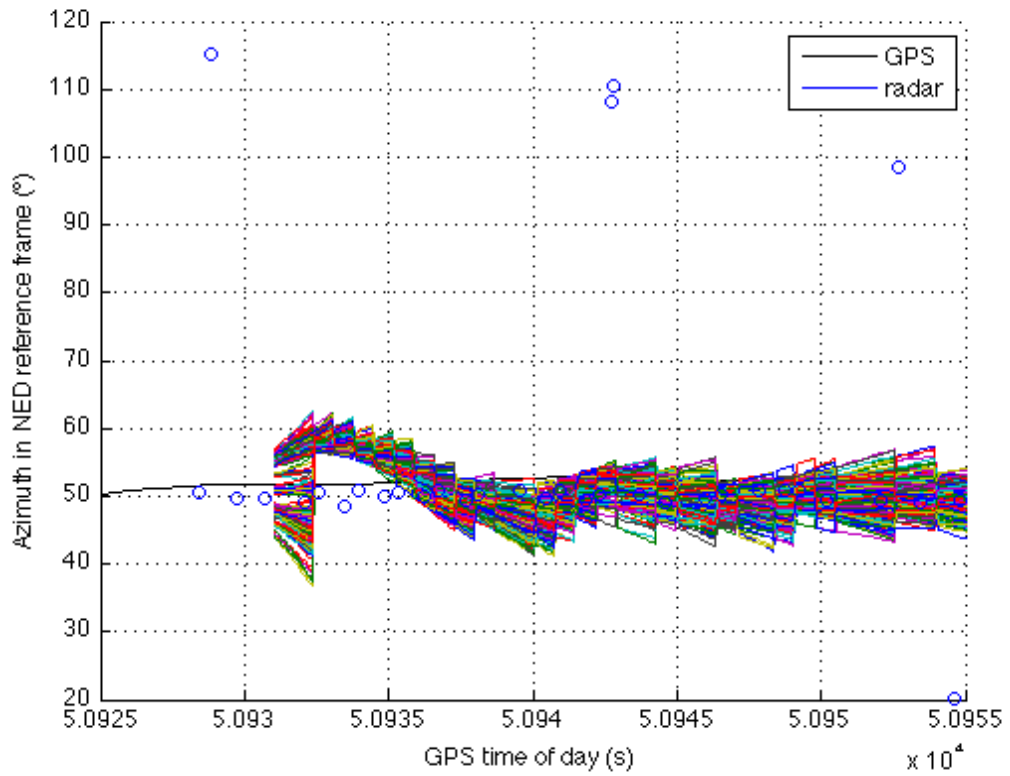
Figure 27. Azimuth in NED reference frame as estimated by GPS, by radar, and by radar-only Cartesian PF tracker as function of GPS time of the day.
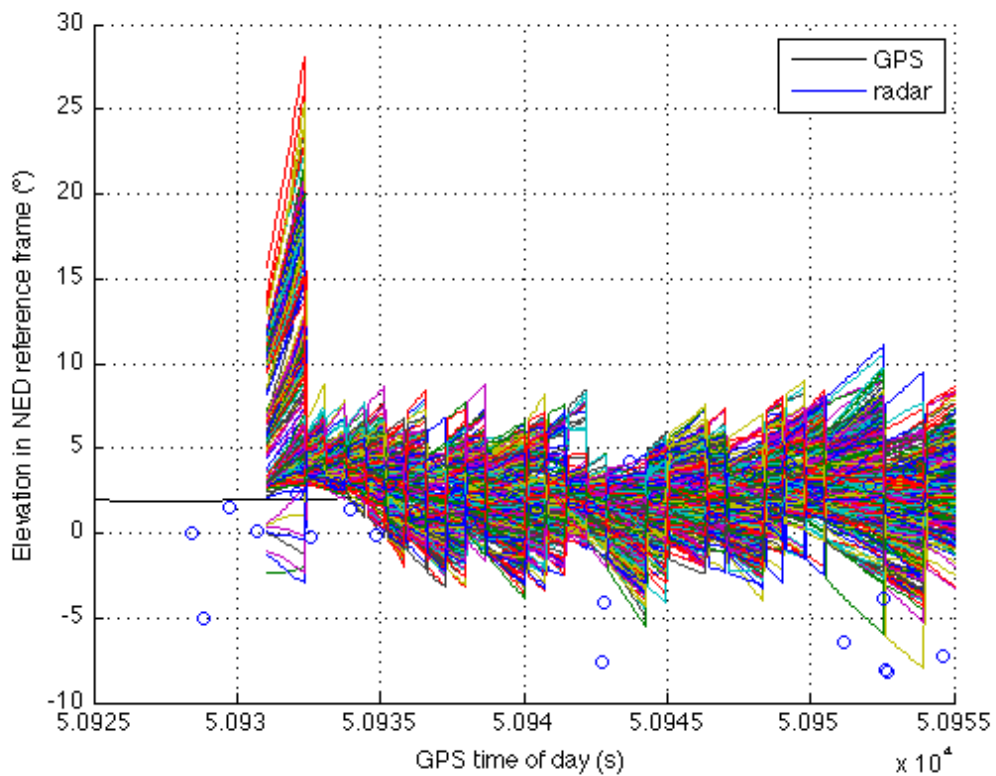
Figure 28. Elevation in NED reference frame as estimated by GPS, by radar, and by radar-only Cartesian PF tracker as function of GPS time of the day.
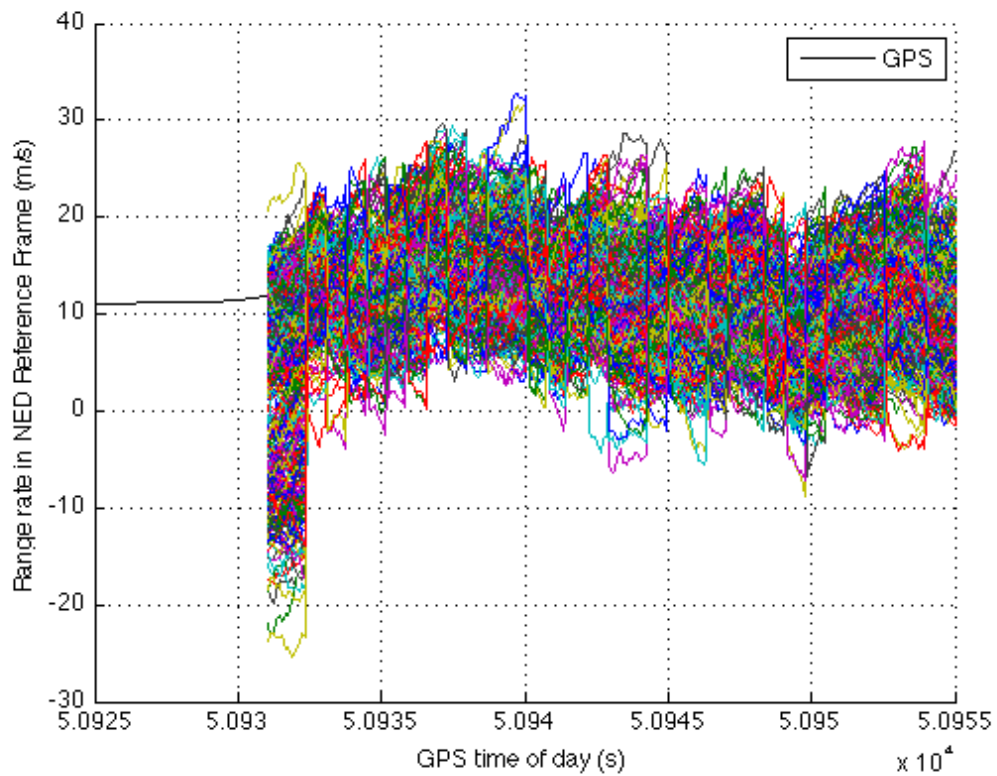
Figure 29. Range rate in NED reference frame as estimated by GPS, and by radar-only Cartesian PF tracker as function of GPS time of the day.
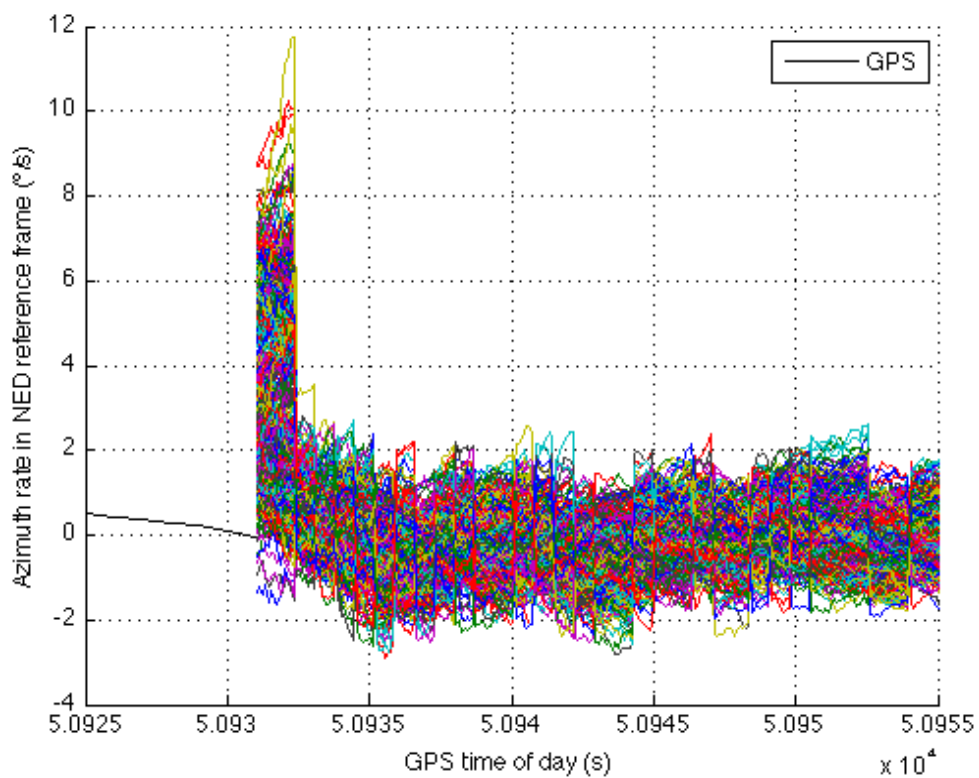
Figure 30. Azimuth rate in NED reference frame as estimated by GPS, and by radar-only Cartesian PF tracker as function of GPS time of the day.
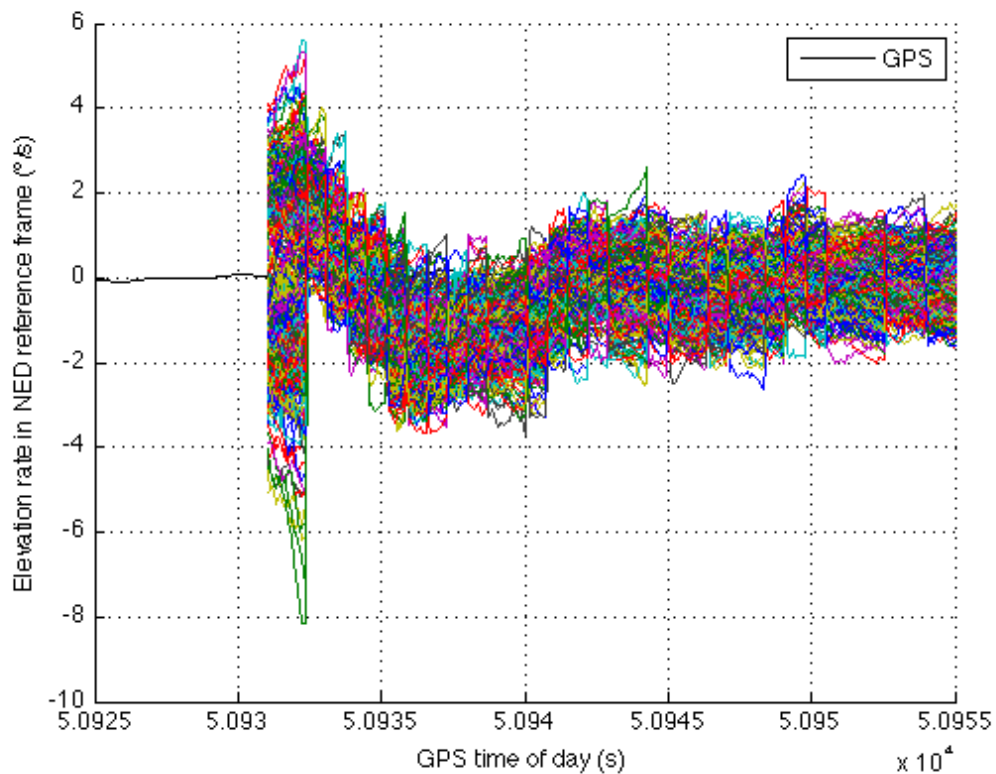
Figure 31. Elevation rate in NED reference frame as estimated by GPS, and by radar-only Cartesian PF tracker as function of GPS time of the day.

5.2.2 Nearly constant acceleration model

Once analysed the performance of Particle Filter in Cartesian coordinates, in order to evaluate the capability of PF to be suitable for several problems even highly non-linear, the software was also developed in spherical coordinates. The target dynamic model is based on a nearly constant acceleration model with a linear measurement equation and non-linear dynamic. The simulations are based on 100 Monte Carlo runs; even in this case the number of particles has been chosen equal to 500. The flight configuration was based on a chasing geometry and a frontal encounter configuration.

Chasing geometry

In this scenario a flight segment of about 30 s in a chasing geometry is considered. Figure 32 shows the Spherical PF range estimate in NED; the software is able to track the intruder with a high level of accuracy.
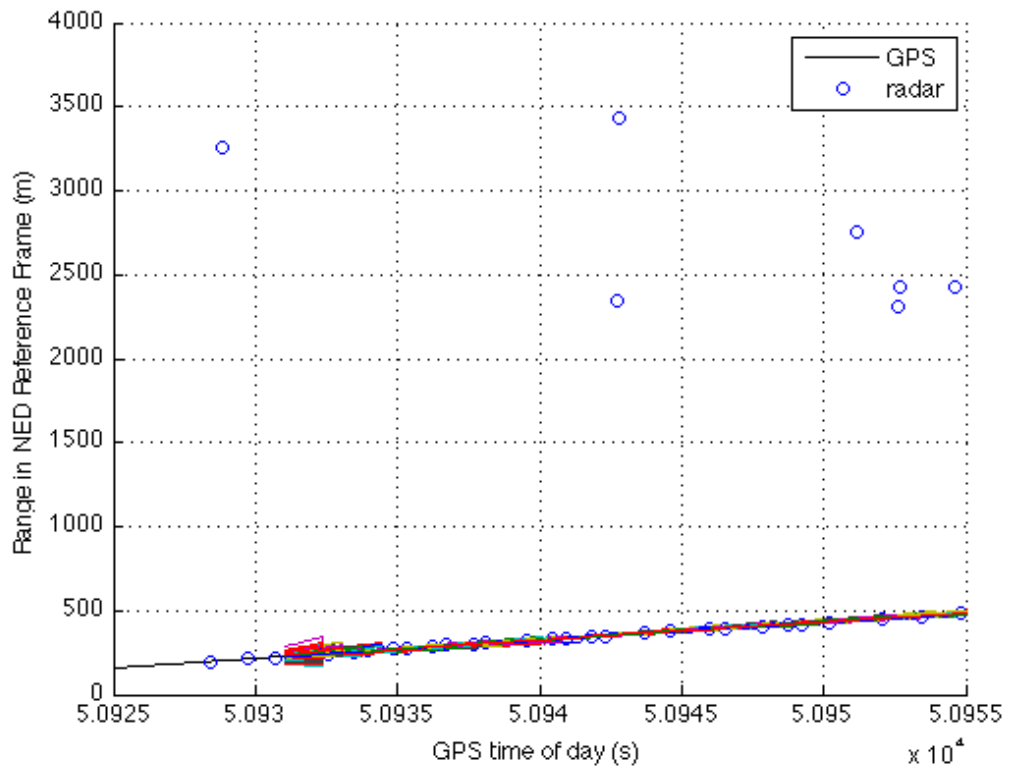
Figure 32. Range as estimated by GPS, by radar, and by radar-only Spherical PF tracker as function of GPS time of the day.
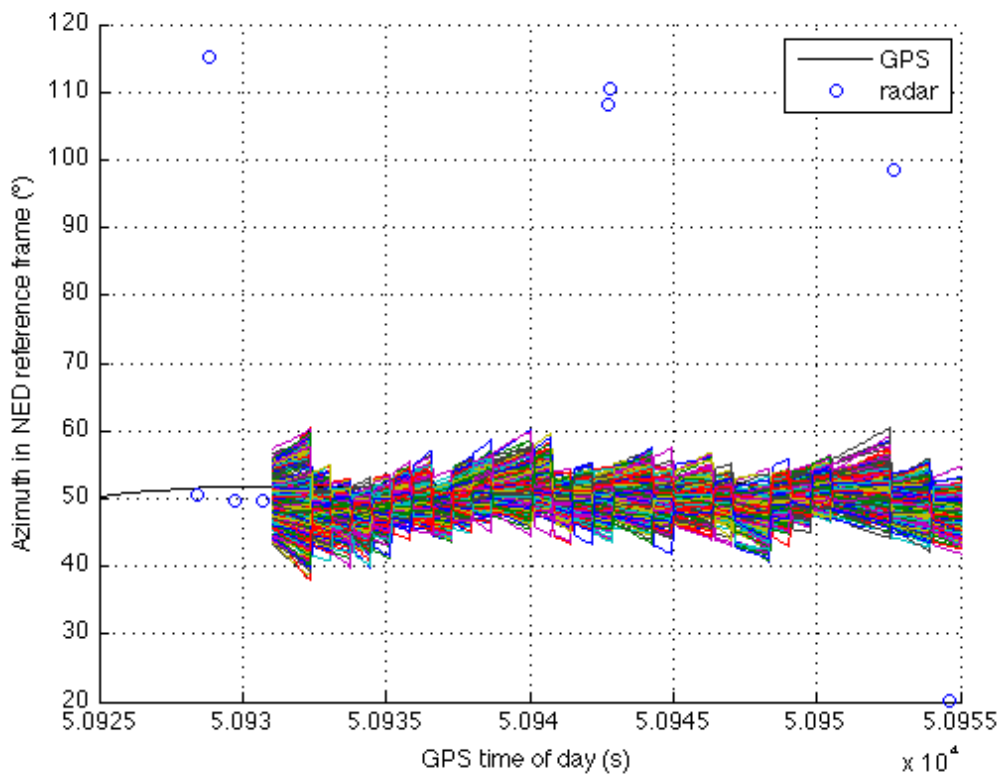
Figure 33. Azimuth in NED reference frame as estimated by GPS, by radar, and by radar-only Spherical PF tracker as function of GPS time of the day.
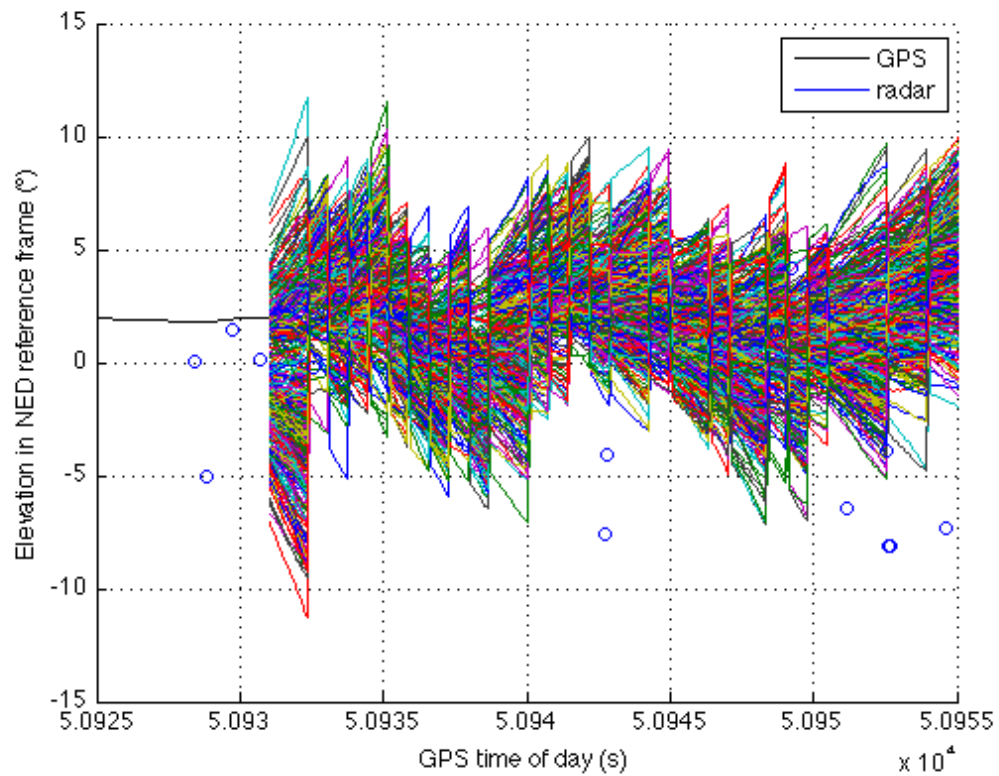
Figure 34. Elevation in NED reference frame as estimated by GPS, by radar, and by radar-only Spherical PF tracker as function of GPS time of the day.
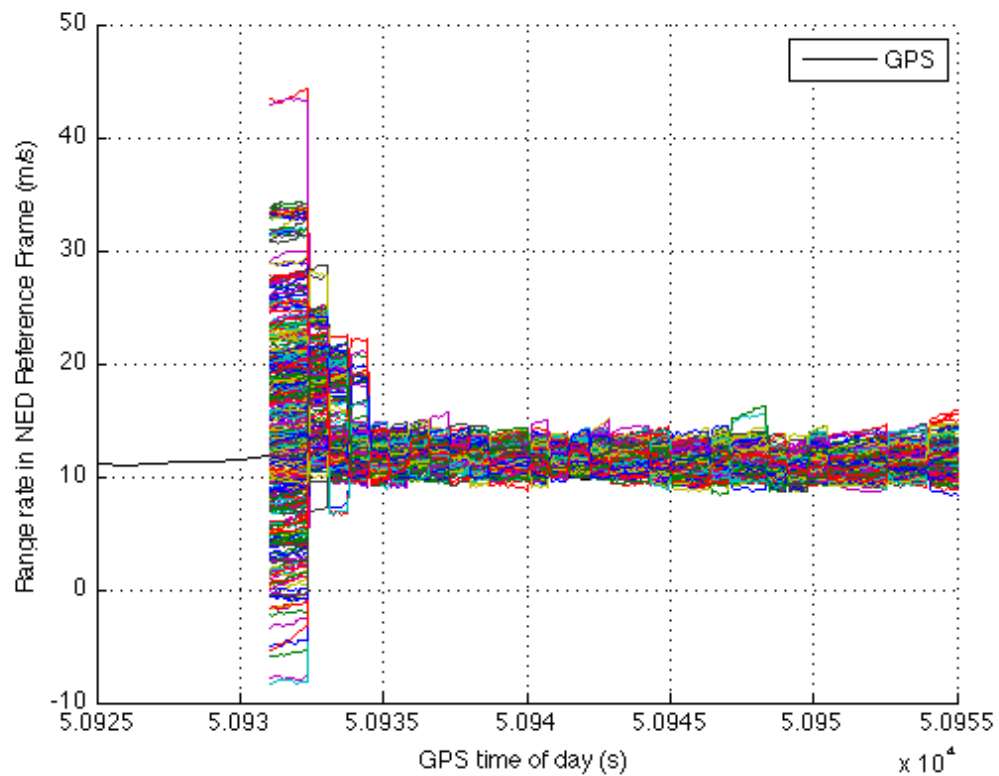
Figure 35. Range rate in NED reference frame as estimated by GPS, and by radar-only Spherical PF tracker as function of GPS time of the day.
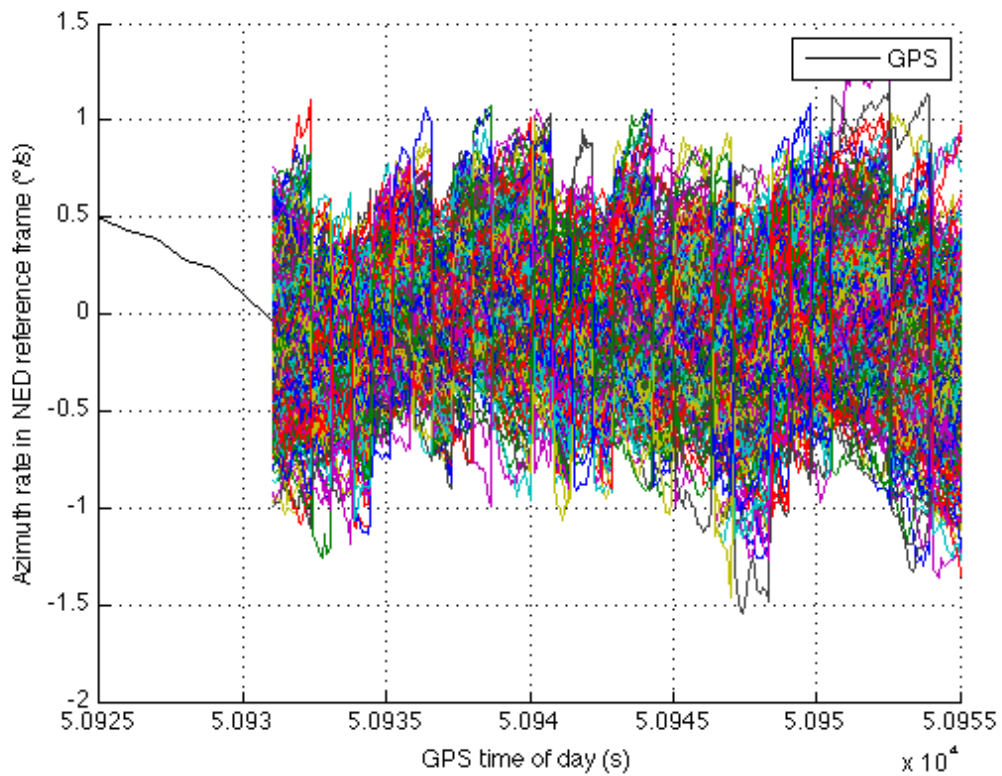
Figure 36. Azimuth rate in NED reference frame as estimated by GPS, and by radar-only Spherical PF tracker as function of GPS time of the day.
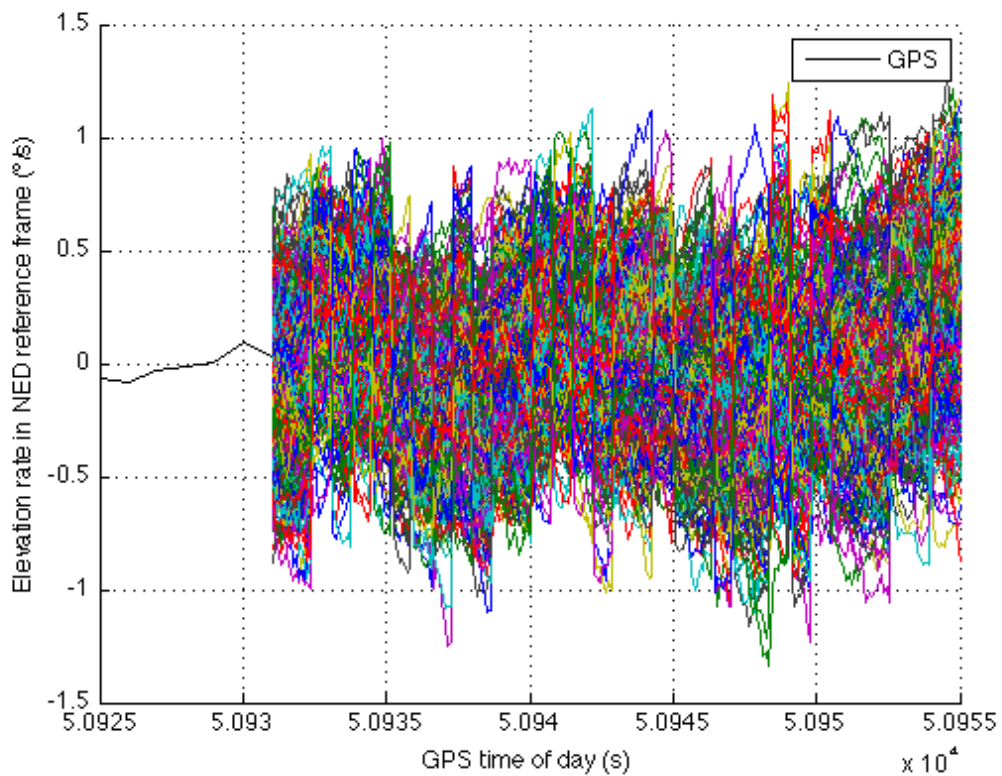
Figure 37. Elevation rate in NED reference frame as estimated by GPS, and by radar-only Spherical PF tracker as function of GPS time of the day.

In Figure 33 and Figure 34, the angular estimates are reported. It can be seen that the initial diversity among the particles is reduced by the arrival of a new measurement and as soon as the resampling procedure is performed.

The Figure 35, Figure 36, and Figure 37 represent the range rate, the azimuth rate and elevation rate, respectively. These estimates are accurate and well modelled by particle filters.

Frontal encounter geometry

The flight segment has a duration of about 15 s with an initial range of about 1800 m. The software outputs are in terms of range, azimuth, elevation and their first time derivatives.

In Figure 38, obstacle range as estimated by radar, by radar-only tracking, and by GPS (reference) together with error estimate with respect to GPS measurements are reported.

The plot shows that after a track is generated on the basis of radar measurements, the tracker is able to follow the obstacle trajectory.
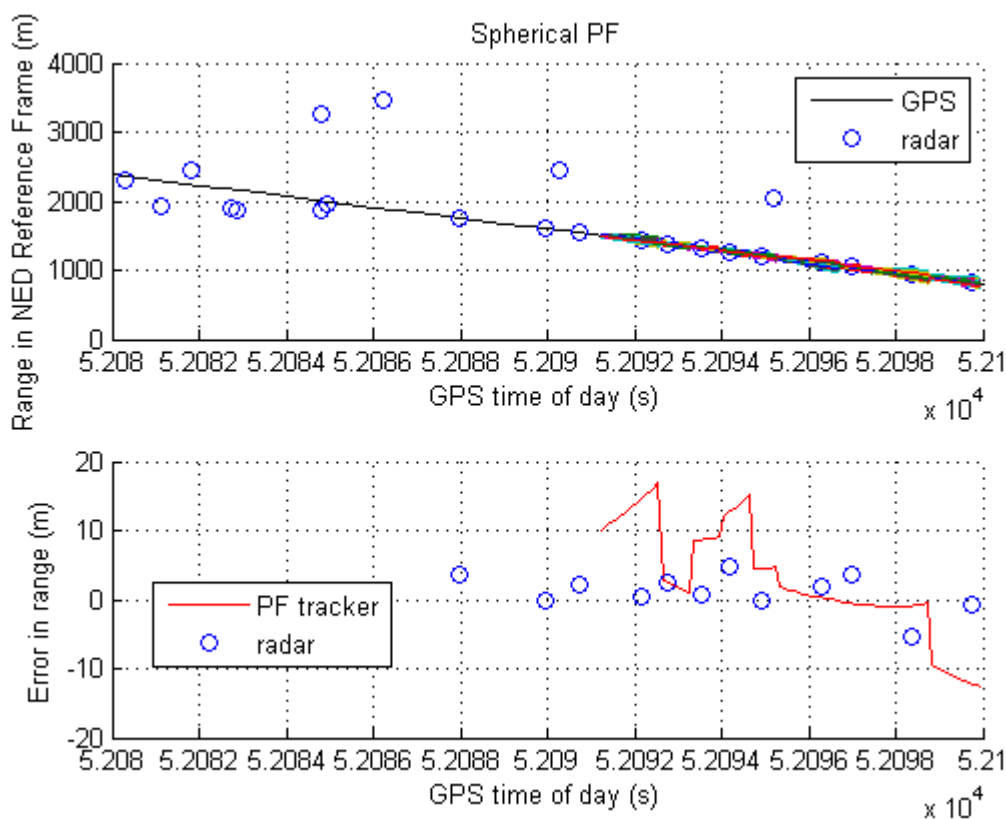
Figure 38. Range as estimated by GPS, by radar, and by radar-only tracker, and estimation error as function of GPS time of the day.

Figure 39 and Figure 40 report the obstacle angular dynamic in terms of azimuth and elevation. These estimates are based only on radar measurements with an update frequency

of 1 Hz as it can be seen in the figures; in this case the tracker is accurate in estimating these variables, in fact the estimation uncertainty in terms of root mean square is of about 2.6 ° for azimuth and 1.5 ° for elevation.

The range and angular rates as estimated by GPS (reference) and Particle Filter tracker are reported in Figure 41, Figure 42 and Figure 43. These variables are very important information sources for collision detection assessment even though they are not directly provided by the radar sensor. The plots show that the tracker estimates are very accurate with a very small value in terms of standard deviation.
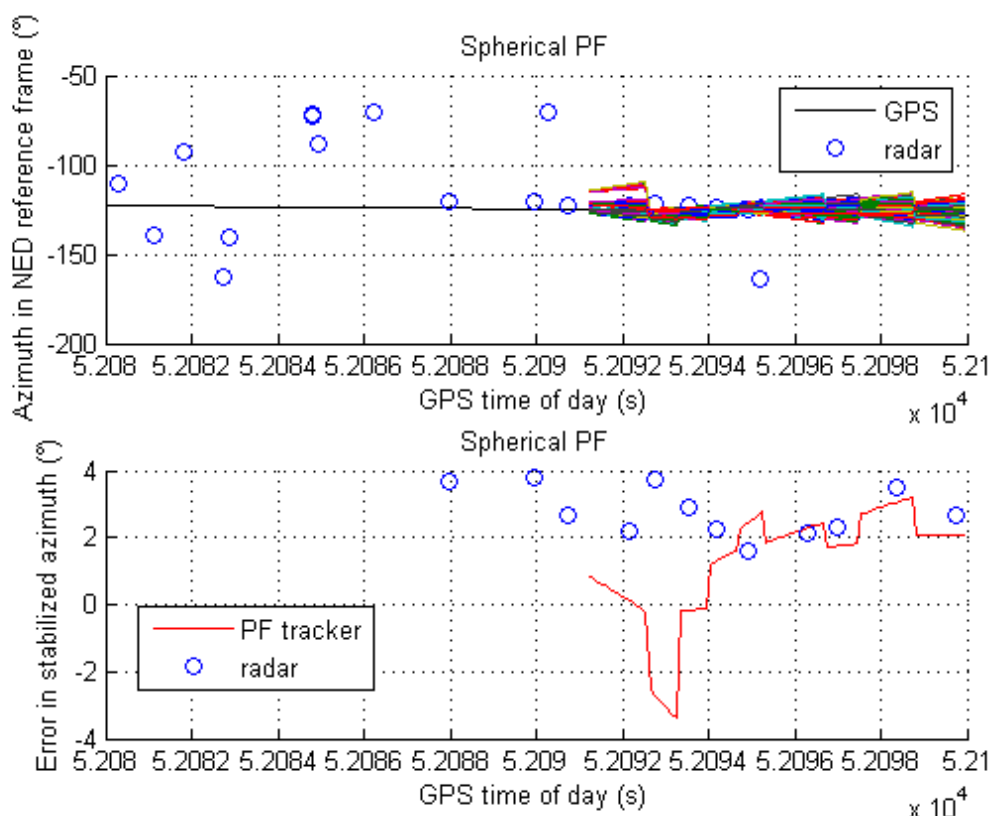
Figure 39. Azimuth in NED reference frame as estimated by GPS, by radar, and by radar-only tracker, and estimation error as function of GPS time of the day.
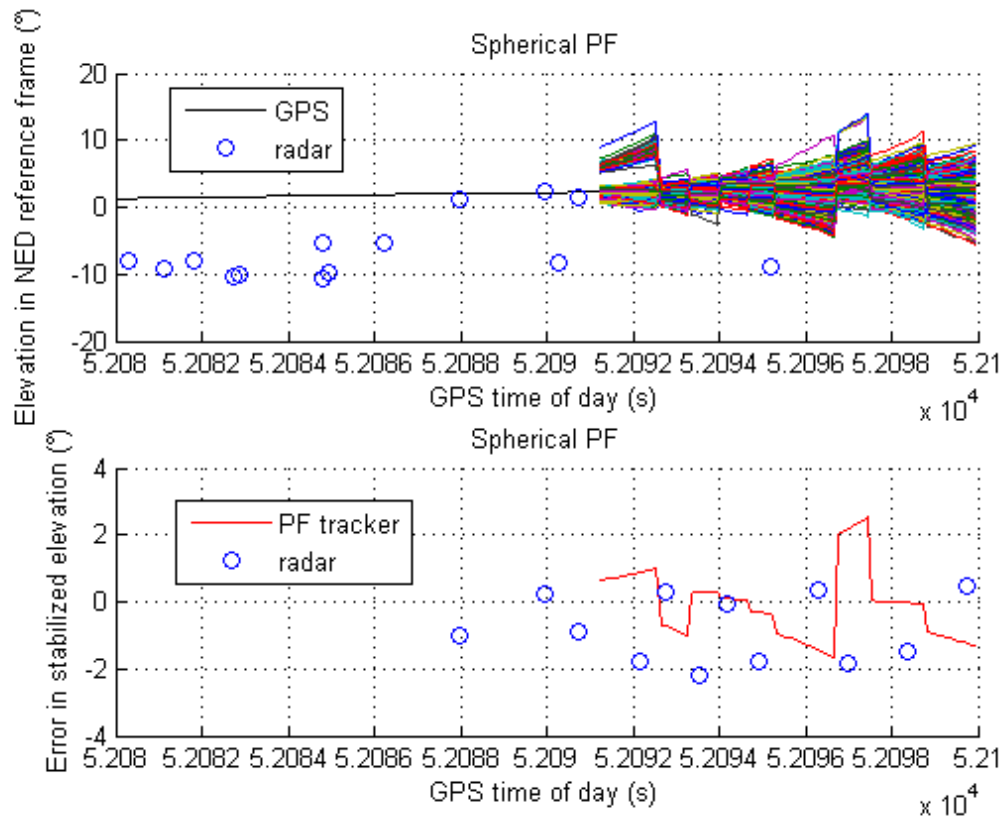
Figure 40. Elevation in NED reference frame as estimated by GPS, by radar, and by radar-only tracker, and estimation error as function of GPS time of the day.
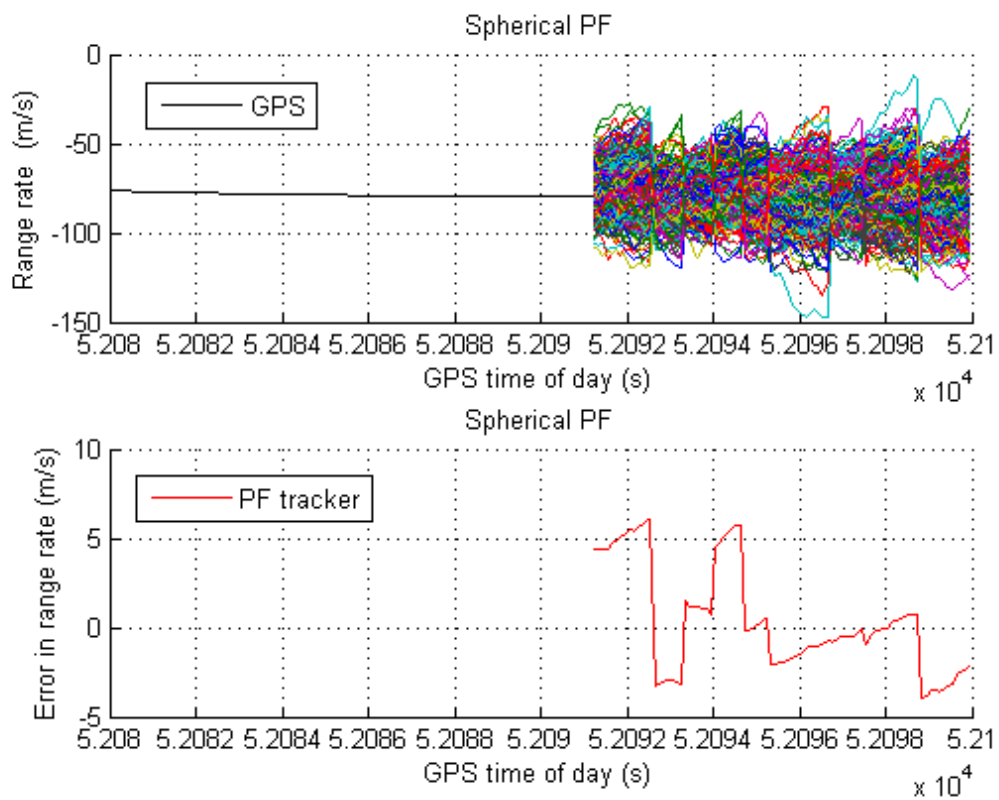
Figure 41. Range rate in NED reference frame as estimated by GPS and by radar-only tracker, and estimation error as function of GPS time of the day.
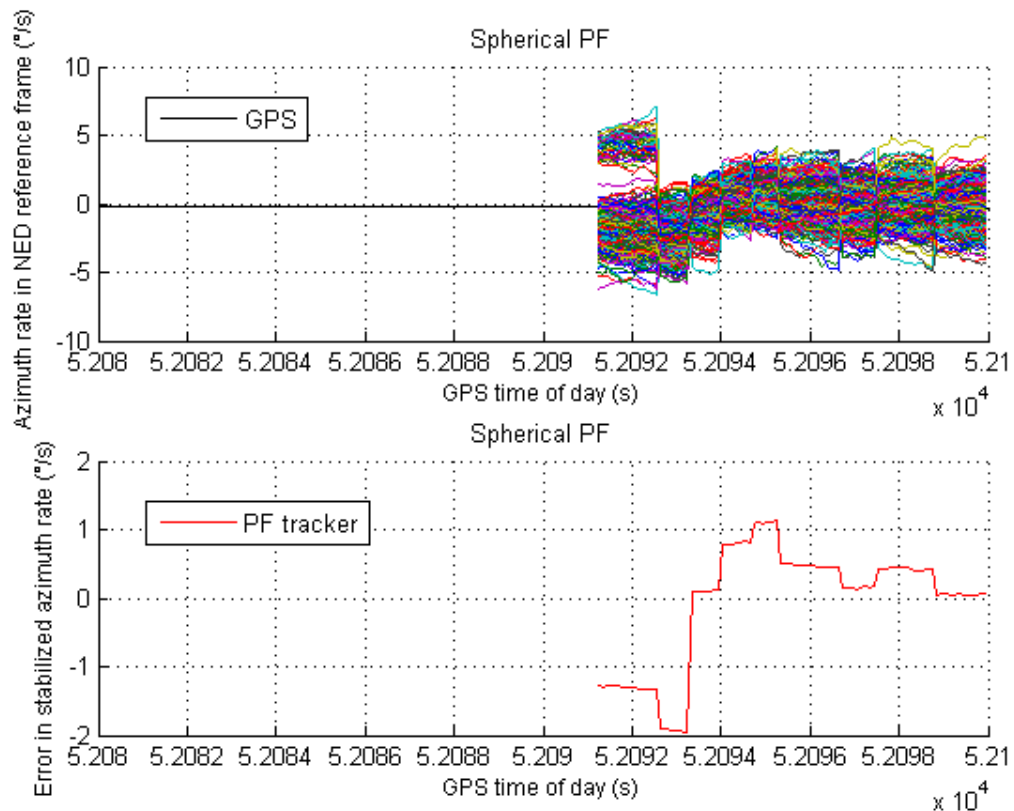
Figure 42. Azimuth rate in NED reference frame as estimated by GPS and by radar-only tracker, and estimation error as function of GPS time of the day.
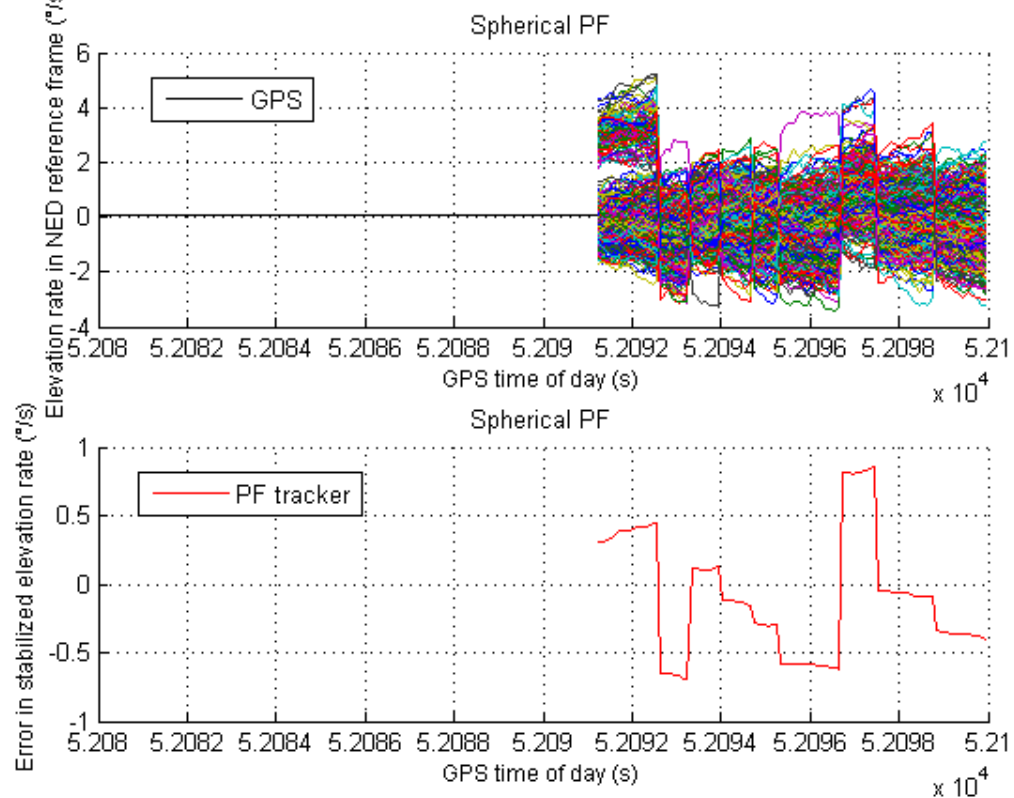
Figure 43. Elevation rate in NED reference frame as estimated by GPS and by radar-only tracker, and estimation error as function of GPS time of the day.

In all figures the effect of the resampling procedure is clearly evident in the particle pattern; this procedure has an important influence on the filter outputs, in fact it enables a great quantity of particles to survive to the prediction step, thus avoiding the degeneracy phenomenon.

5.2.3 Nearly constant velocity model

In this section the tracking algorithm results based on a nearly constant velocity dynamic model are presented and discussed. The target state is comprised of seven variables including obstacle position, velocity and DCPA in spherical coordinates. In this case, different flight scenarios have been analysed including chasing flight and frontal-encounter geometries in order to compare the dynamic models behaviour and to demonstrate the improvements obtained in terms of DCPA with a less sophisticated model. In the following figures, at first the chasing flight results are shown. Then, the frontal encounter flight results are reported since the main objective relies on the assessment of collision risk.

Chasing flight

The analyzed flight is based on a chasing geometry between FLARE and the intruder; the flight segment has a duration of about 30 s with an initial range of about 200 m.

The software outputs are in terms of range, azimuth, elevation and their first time derivatives.

In Figure 44, obstacle range as estimated by radar, by radar-only tracking, and by GPS (reference) together with error estimate with respect to GPS measurements are reported. As it will be shown later on the chapter, the filter algorithm is very accurate to estimate the range variable, in fact the residual error is in the order of 6.4 m; this value is smaller than the same one obtained from the previous model. Figure 45 and Figure 46 report the obstacle angular dynamic in terms of azimuth and elevation.

Figure 47, Figure 48 and Figure 49 report the obstacle range rate and angular rates. These variables are accurately estimated by the PF software; the accuracies are very small and they reach values of about 1.8 m/s in case of range rate and of about 0.17°/s and 0.07°/s for azimuth rate and elevation rate, respectively.
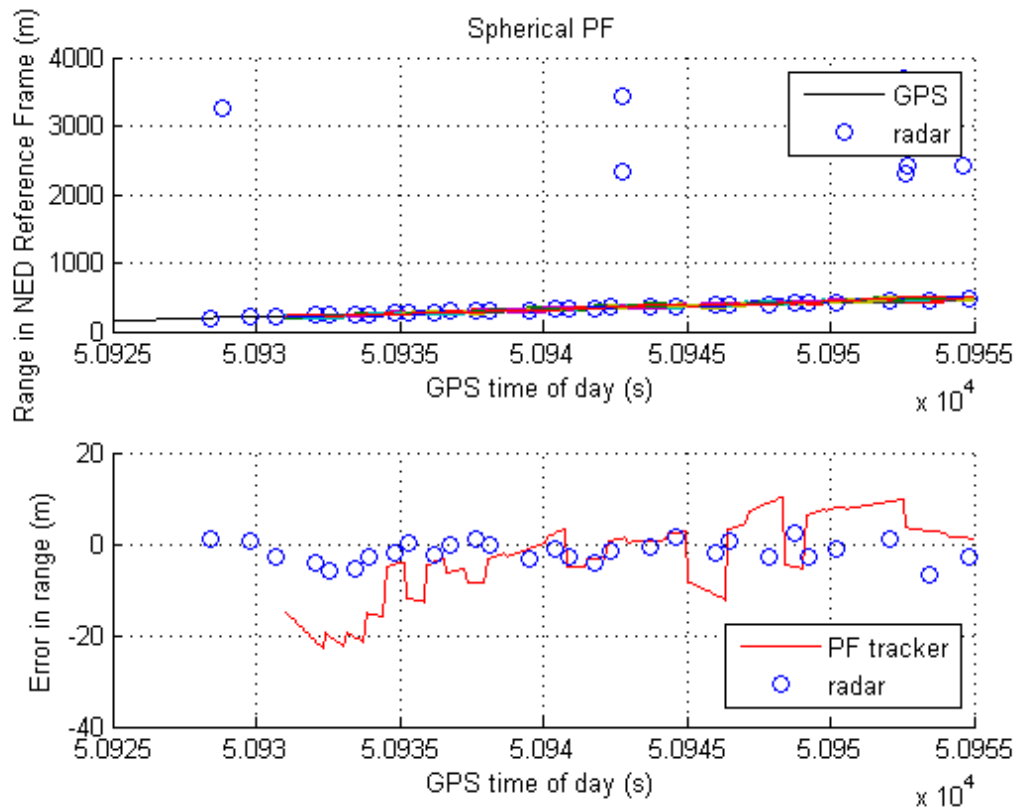
Figure 44. Range as estimated by GPS, by radar, and by radar-only tracker, and estimation error as a function of GPS time of day.
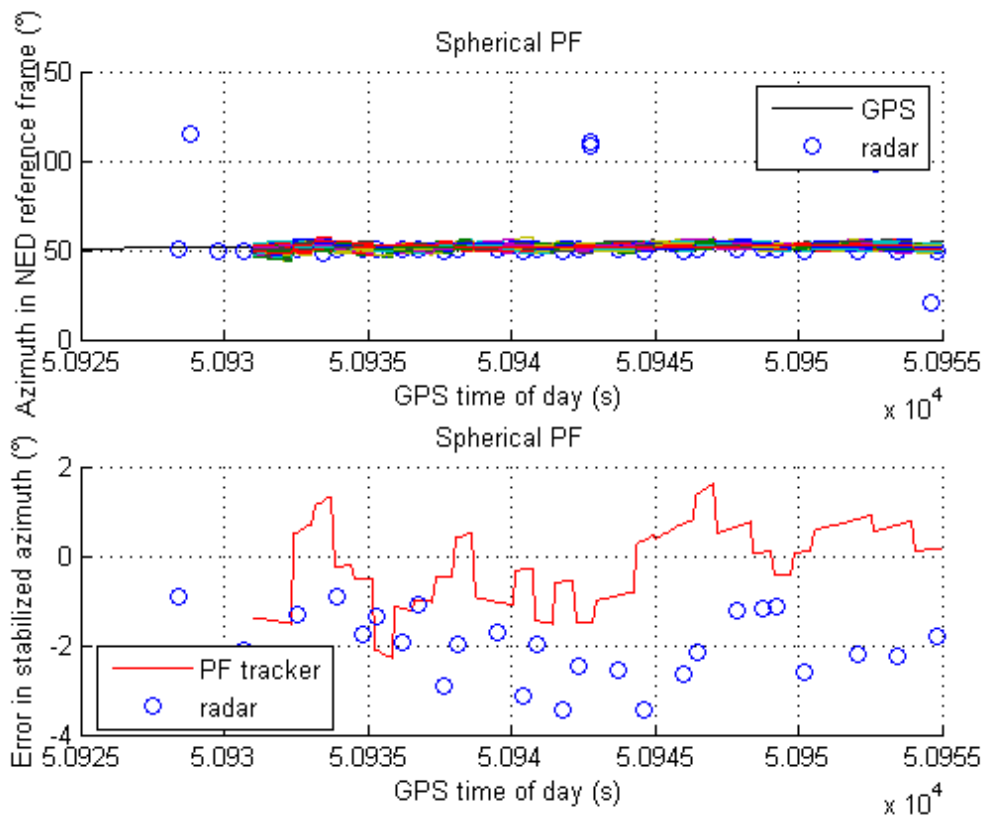
Figure 45. Azimuth in NED reference frame as estimated by GPS, by radar, and by radar-only tracker, and estimation error as a function of GPS time of day.
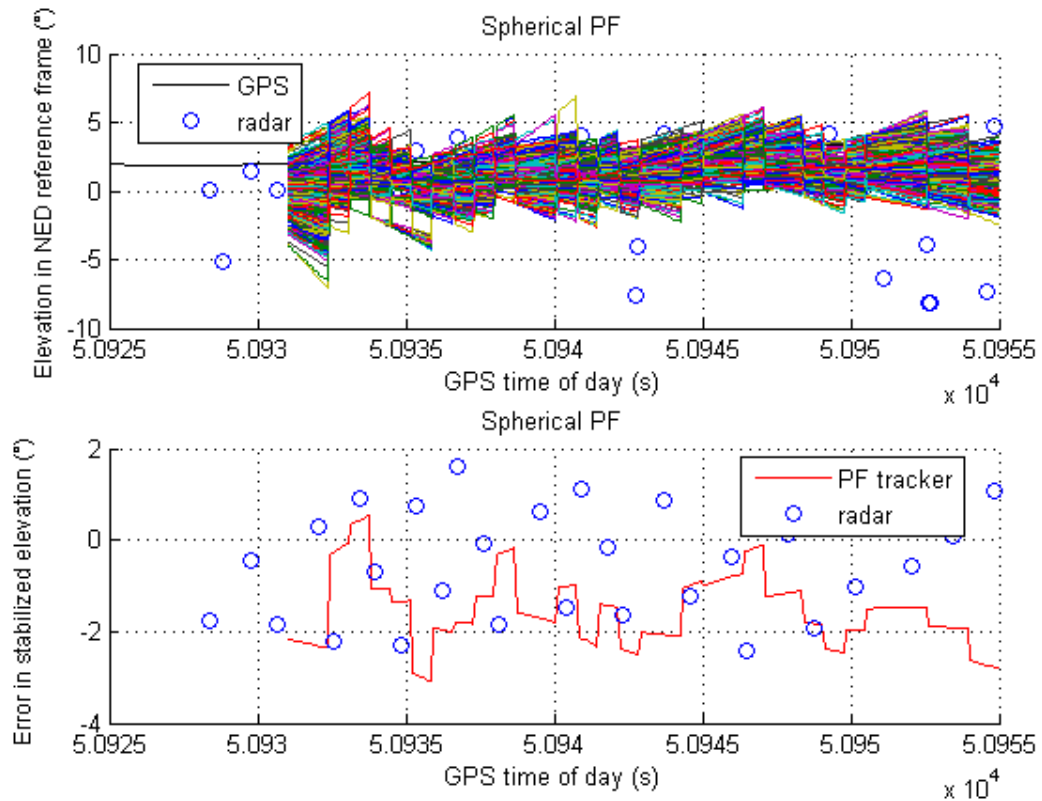
Figure 46. Elevation in NED reference frame as estimated by GPS, by radar, and by radar-only tracker, and estimation error as a function of GPS time of day.
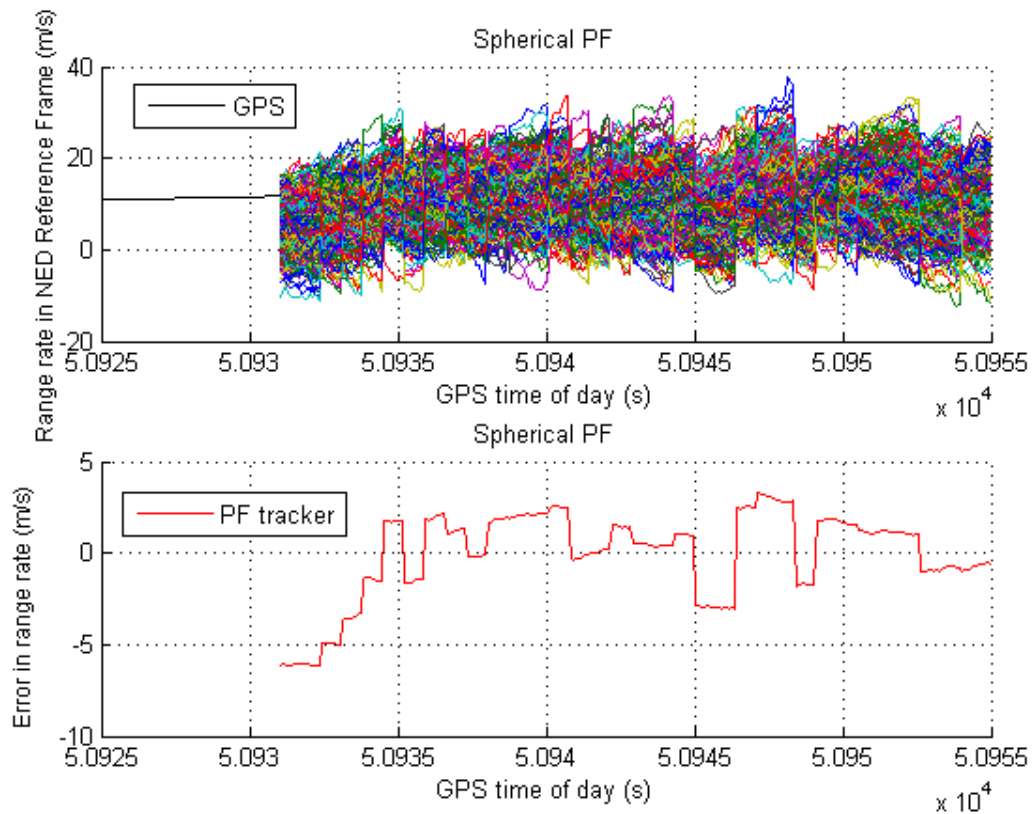
Figure 47. Range rate in NED reference frame as estimated by GPS and by radar-only tracker, and estimation error as a function of GPS time of day.
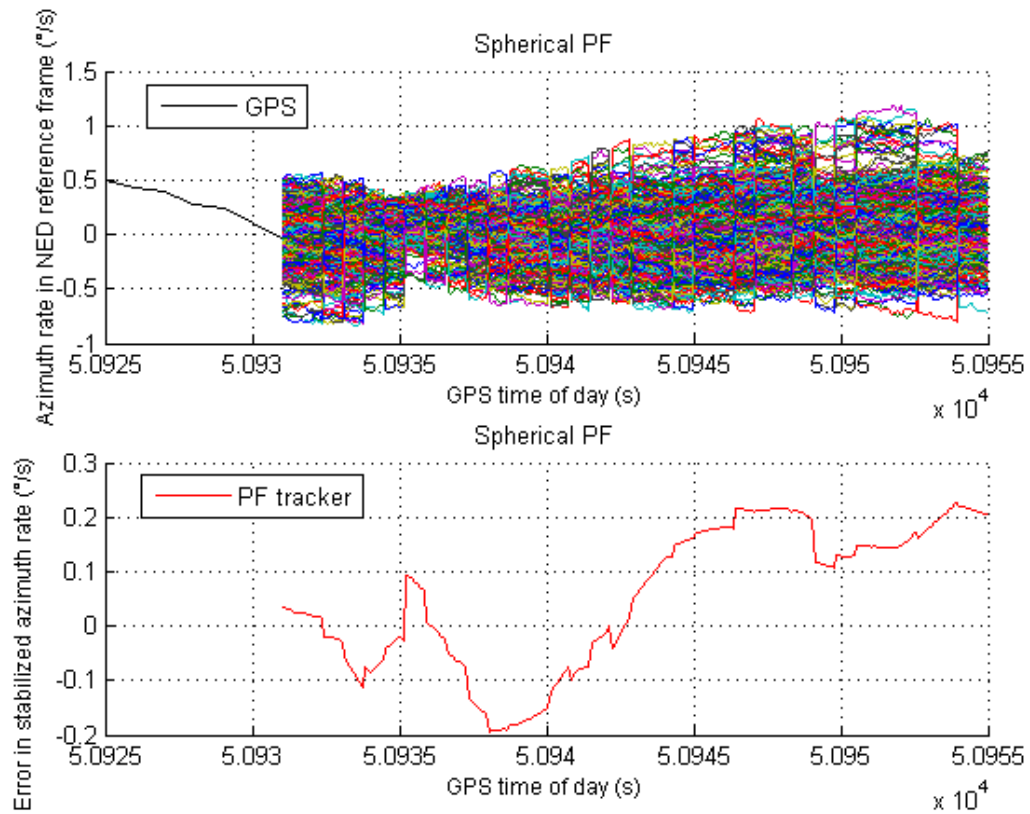
Figure 48. Azimuth rate in NED reference frame as estimated by GPS and by radar-only tracker, and estimation error as a function of GPS time of day.
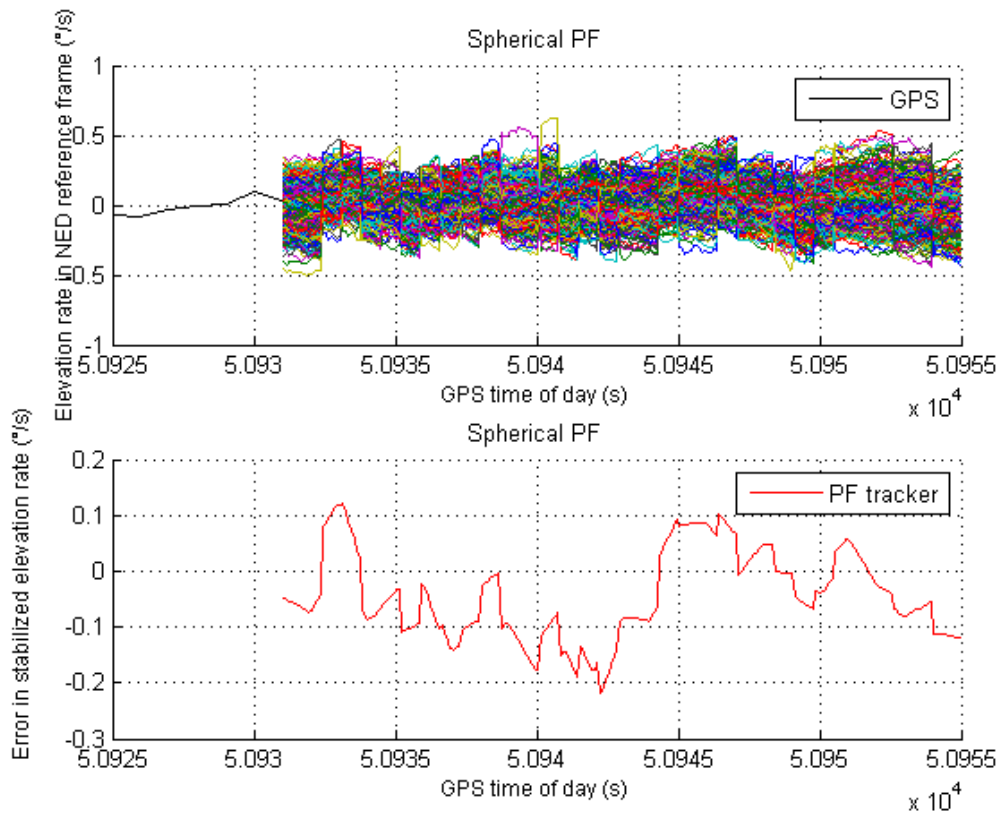
Figure 49. Elevation rate in NED reference frame as estimated by GPS and by radar-only tracker, and estimation error as a function of GPS time of day.

Frontal encounter geometry

The algorithm outputs are based on obstacle position and velocity in terms of range, azimuth and elevation and DCPA in a stabilized North-East-Down reference frame with origin in FLARE centre of mass. The considered flight segment has duration of about 20 s with an initial range of about 2200 m. In Figure 50, obstacle range as estimated by radar, radar-based tracker, and GPS (reference) together with error estimate with respect to GPS measurements are reported. After a firm track has been generated on the basis of radar measurements, the tracker is able to characterize the obstacle trajectory. The radar-only tracker provides a range estimate with an accuracy of the order of few meters that derives from the good radar range accuracy and the absence of intruder manoeuvres. In Figure 50, the coloured lines represent the particles trajectories.
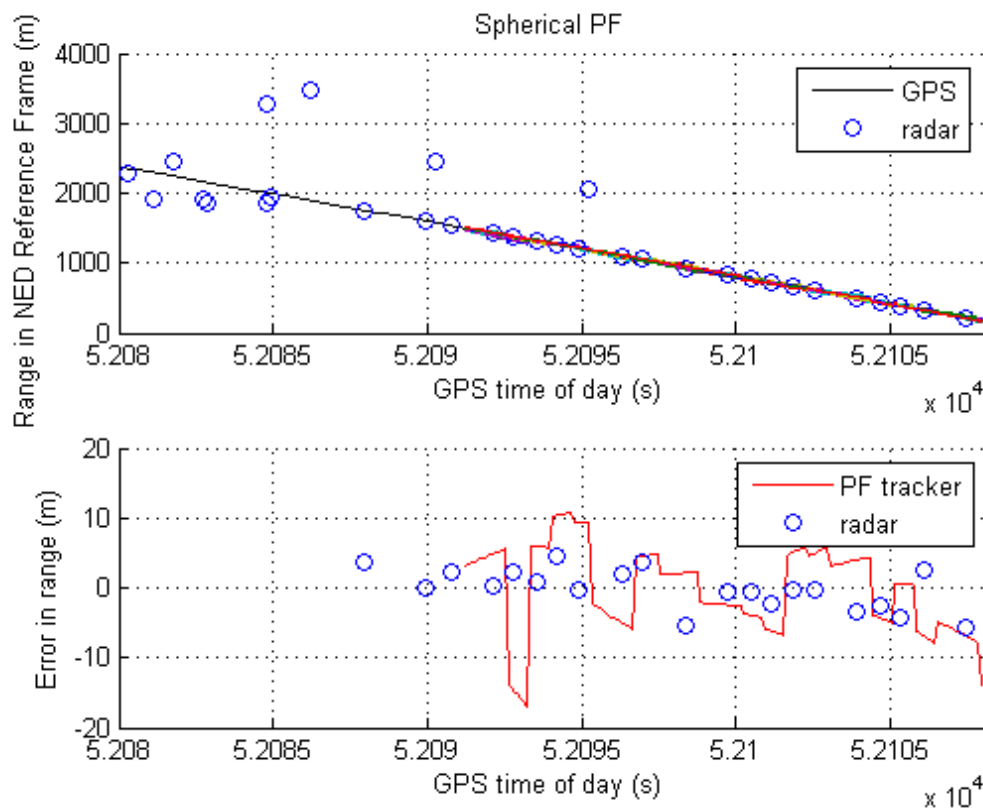
Figure 50. **Range as estimated by GPS, by radar, and by radar-only tracker, and estimation error as a function of GPS time of day.**

Figure 51 and Figure 52 report the obstacle angular dynamics in terms of azimuth and elevation. As expected the order of magnitude of these errors is comparable to the radar accuracy. Being computed in NED, the rms errors include attitude measurement error biases. In fact, error biases in the estimation of magnetic heading are the main reason of the larger

error in azimuth. It is worth noting that these biases have a little effect on the estimation of angular rates and of distance at closest point of approach.

The range and angular rates as estimated by GPS (reference) and Particle Filter tracker are reported in Figure 53, Figure 54, and Figure 55. These variables are very important information sources for collision detection assessment even though they are not directly provided by the radar sensor. The plots show that the tracker estimates are very accurate with a very small value in terms of standard deviation.

Simulation results confirm how the resampling procedure is a key factor for tracking performance, avoiding the degeneracy phenomenon and thus enabling a great quantity of particles to survive to the prediction step, as stated above.
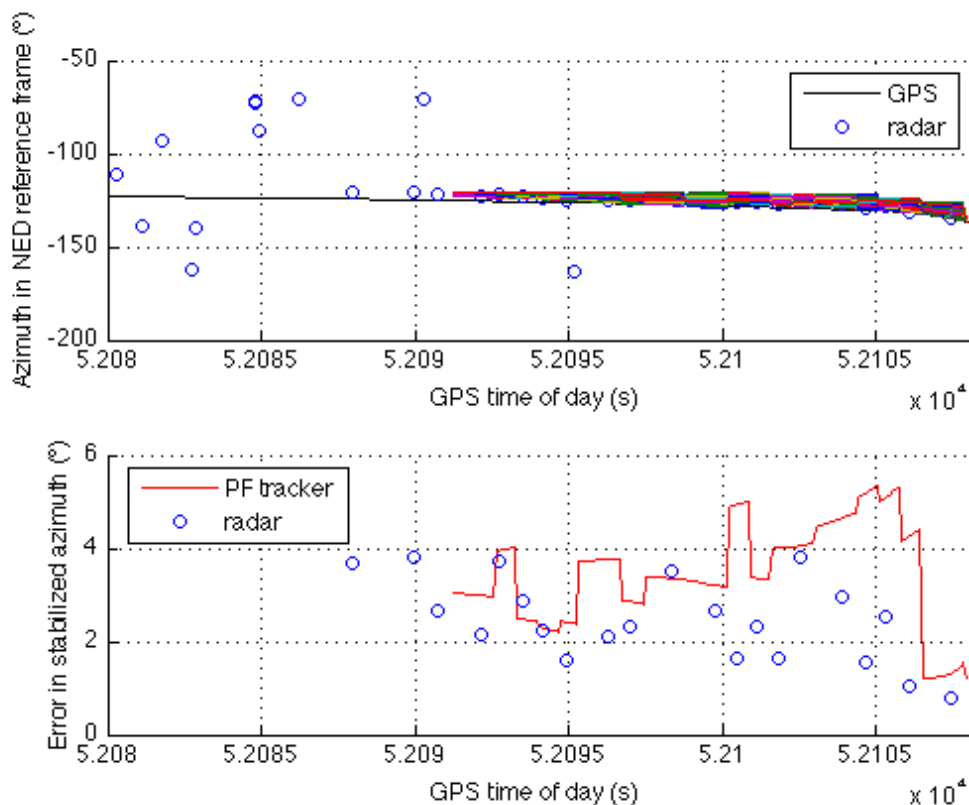
Figure 51. Azimuth in NED reference frame as estimated by GPS, by radar, and by radar-only tracker, and estimation error as a function of GPS time of day.
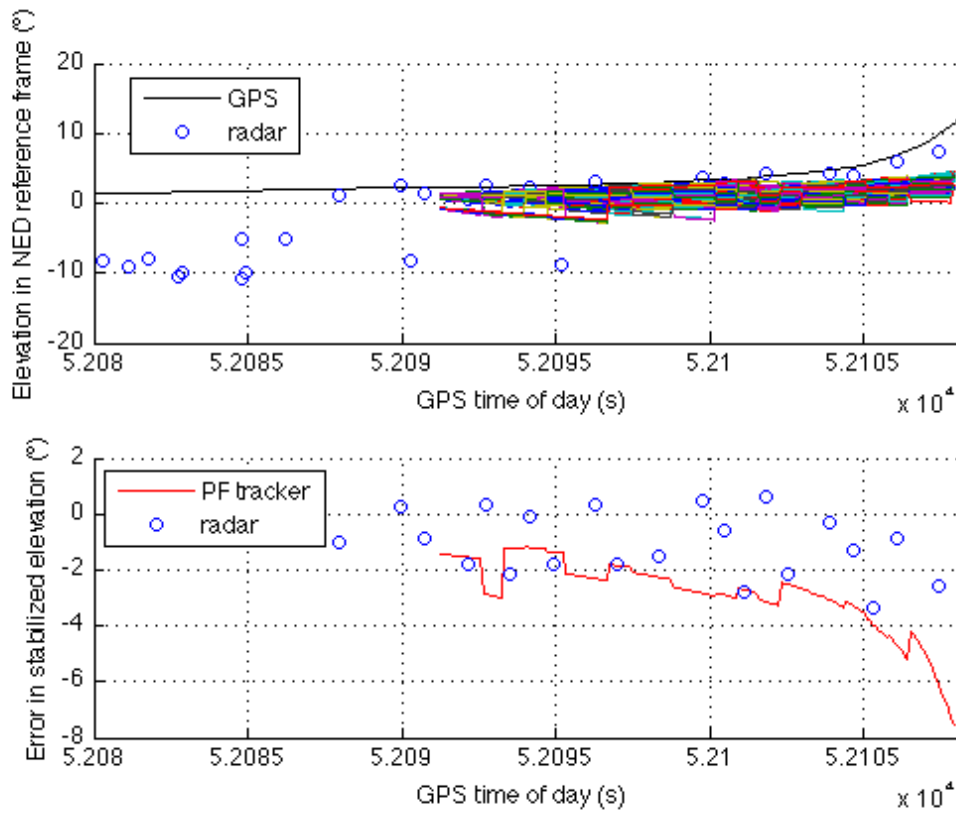
Figure 52. Elevation in NED reference frame as estimated by GPS, by radar, and by radar-only tracker, and estimation error as a function of GPS time of day.
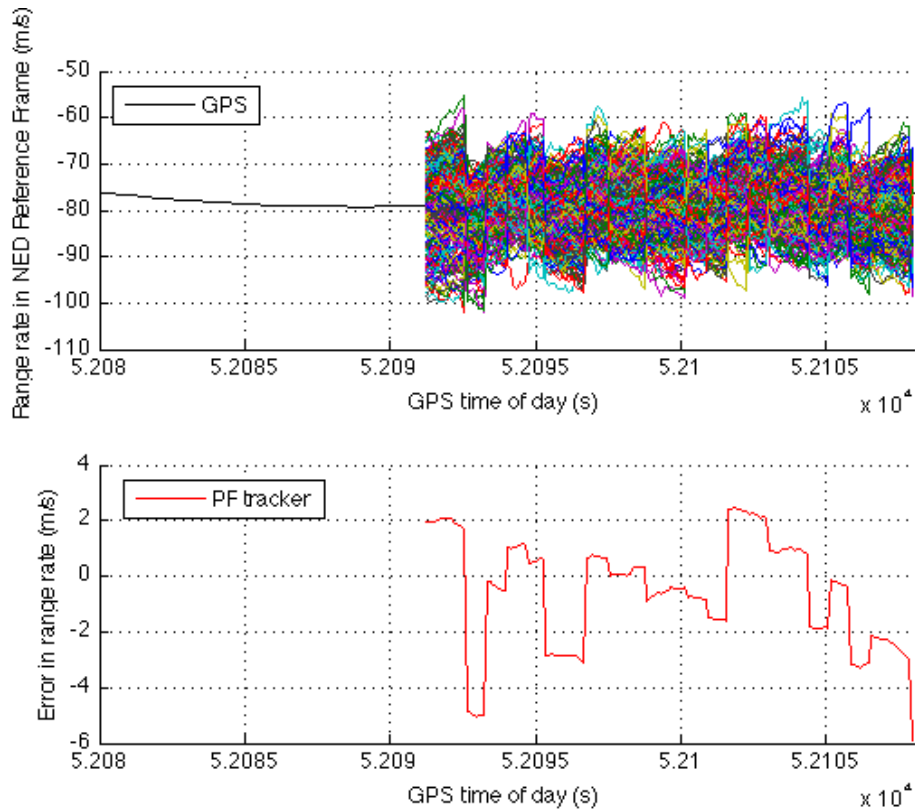
Figure 53. Range rate in NED reference frame as estimated by GPS and by radar-only tracker, and estimation error as a function of GPS time of day.
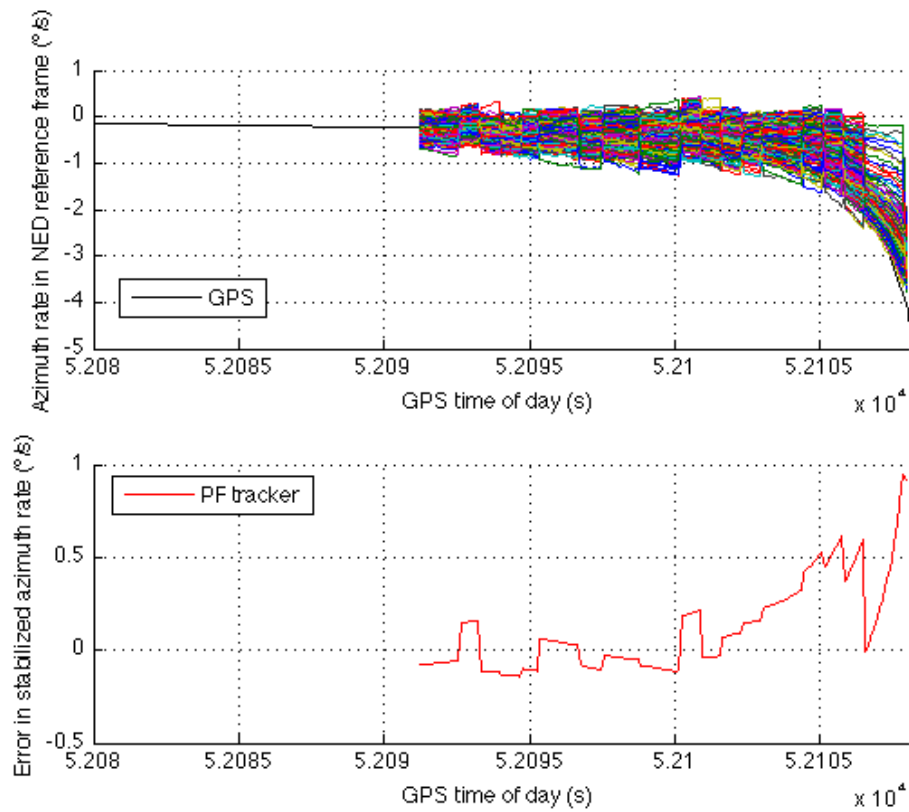
Figure 54. Azimuth rate in NED reference frame as estimated by GPS and by radar-only tracker, and estimation error as a function of GPS time of day.
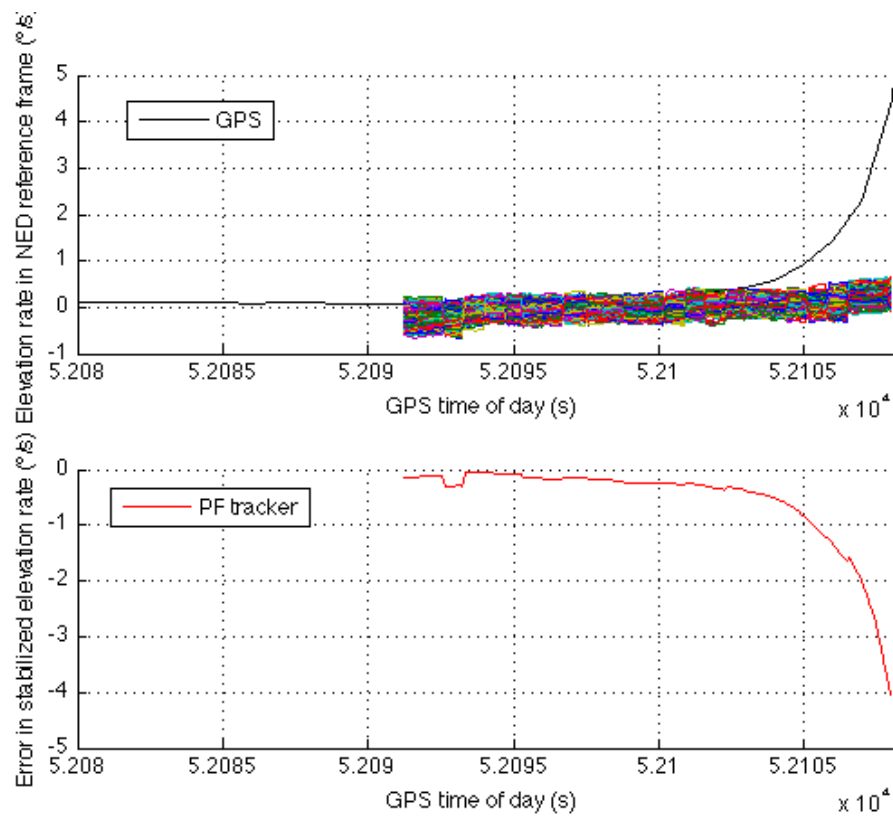
Figure 55. Elevation rate in NED reference frame as estimated by GPS and by radar-only tracker, and estimation error as a function of GPS time of day.

5.3   Obstacle Dynamic models comparison

In the previous section, the results obtained from the developed obstacle detection and tracking software based on Particle Filter have been shown for each of the dynamic model described before. Since the variables plotted in the figures above showed a very similar pattern, in order to justify the choice of the selected coordinates and dynamic model, a comparative analysis will be conducted on the accuracy of the algorithms in terms of root mean square.

In Table 4, the particle filter performance estimated implementing the Singer dynamic model in Cartesian coordinates is reported. In the table, the EKF performance have also been inserted to compare the results and to underline the necessity to make some changes in the coordinates systems and/or dynamic model to enhance the algorithm outputs.

Rms	EKF	Cartesian PF
Range (m)	3.10	12.0
Range Rate (m/s)	0.70	2.30
Azimuth (°)	1.40	1.80
Azimuth Rate (°/s)	0.10	0.30
Elevation (°)	0.80	1.40
Elevation Rate (°/s)	0.04	0.30

Table 4. Particle Filter and EKF performance for Singer dynamic model in Cartesian coordinates.

Modifying the coordinates systems from Cartesian to Spherical provided some improvements. It is worth pointing out that the performance are more accurate than those obtained in case of Cartesian coordinates; for this reason the research analysis was addressed to the realization of a model able to improve these values taking into account only spherical coordinates.

In particular, in Table 5 the results obtained from particle filter algorithm in spherical coordinates are reported. In particular, the table shows the results obtained implementing a nearly acceleration model and considering a chasing flight.

Rms	Spherical PF
Range (m)	7.6
Range Rate (m/s)	1.2
Azimuth (°)	2.1
Azimuth Rate (°/s)	0.15
Elevation (°)	1.65
Elevation Rate (°/s)	0.15

Table 5. Particle Filter performance for nearly constant acceleration dynamic model in Spherical coordinates (chasing flight).

The same model was also applied to evaluate the filter performance in a near quasi-frontal encounter geometry since this configuration is the most important for collision risk assessment. The results in terms of rms are reported in Table 6.

Rms	Spherical PF
Range (m)	8.3
Range Rate (m/s)	3.0
Azimuth (°)	2.1
Azimuth Rate (°/s)	0.8
Elevation (°)	1.0
Elevation Rate (°/s)	0.45

Table 6. Particle Filter performance for nearly constant acceleration dynamic model in Spherical coordinates (frontal encounter flight).

In order to identify an optimal configuration able to provide some improvements with respect to EKF and to the previous model, first of all in terms of distance at closest point of approach, a simplified model has also been developed and tested. In Table 8, the performance obtained by the developed software in Spherical coordinates based on a nearly constant velocity model are reported for both a chasing flight and frontal encounter geometry.

Rms	Spherical PF
Range (m)	6.4
Range Rate (m/s)	1.8
Azimuth (°)	0.75
Azimuth Rate (°/s)	0.17
Elevation (°)	1.7
Elevation Rate (°/s)	0.07

Table 7. Particle Filter performance for nearly constant velocity dynamic model in Spherical coordinates (chasing flight).

Rms	Spherical PF
Range (m)	5.9
Range Rate (m/s)	1.8
Azimuth (°)	3.7
Azimuth Rate (°/s)	0.2
Elevation (°)	2.5
Elevation Rate (°/s)	0.4

Table 8. Particle Filter performance for nearly constant velocity dynamic model in Spherical coordinates (frontal encounter flight).

Comparing the errors in Table 5, Table 6, Table 7 and Table 8 in case of both chasing and frontal encounter, it can be noticed that the nearly constant velocity model allows obtaining estimates errors slightly smaller than those obtained in case of nearly constant acceleration model, thus justifying the choice of the adoption of a less sophisticated model. Of course the introduction of Electro-Optical data can improve angular accuracy since these sensors have a faster update rate than radar. Moreover, the results show that PF tracker performance is comparable to EKF. The most important result is obtained in the angular dynamics; in fact, obstacle velocities provided by PF algorithm are slightly more accurate than EKF in the considered scenario. These variables are very important information sources for collision detection assessment even though they are not directly provided by the radar. This significant outcome immediately reflects on the estimation of DCPA as it will be shown in the following section.

5.4 Collision risk assessment: DCPA estimation

Besides comparing the accuracy of the different outputs of the algorithms, the main objective of the research activity is the evaluation of the DCPA, defined in equation (77) and reported here for the sake of clarification:

$$\overline{DCPA} = \frac{\overline{r} \cdot \overline{V}}{\left\| \overline{V} \right\|^2} \overline{V} - \overline{r}$$

where $\overline{r}$ and $\overline{V}$ are the position and velocity vectors between the own aircraft and the intruder, respectively.

It is clearly evident that a good estimation of the obstacle dynamics plays an important role for an accurate evaluation of this parameter. From the analysis on the state estimates errors presented in the above section, the nearly constant velocity model has shown better performance than those provided by the other investigated models.

For this reason, the results in terms of DCPA in different test conditions based only on a nearly constant velocity model will be presented and discussed.

Figure 56 shows the DCPA as estimated by EKF in frontal encounter geometry during real flight tests. The plot highlights a delay to determine the Near Mid Collision threat that is verified since the reference GPS system measures a DCPA value shorter than 170 m during all the encounter phase.

In general, EKF is a well-assessed technique suitable for real time implementation; however nonlinearities in obstacle dynamics and/or in the measurement equation can cause some loss of accuracy in obstacle tracking performance. On the other hand, innovative filtering techniques developed for non linear systems, such as Particle Filters are expected to provide more accurate estimates of obstacle dynamics than EKF, thus improving the accuracy of the DCPA estimate and potentially reducing the delay in collision detection, since non-linear dynamics should be faster than linear ones to converge to the exact solution [75].

In order to have an assessment of the implemented model, the distance at CPA computed on the basis of GPS measurements can be used as a reference.

In Figure 57, the DCPA as estimated GPS, by EKF tracker, and by Particle Filter radar-only tracker as function of GPS time of the day is plotted. The flight scenario is a frontal encounter geometry with a duration of about 20 s (this flight segment is the same reported in the section above in case of nearly constant velocity model).
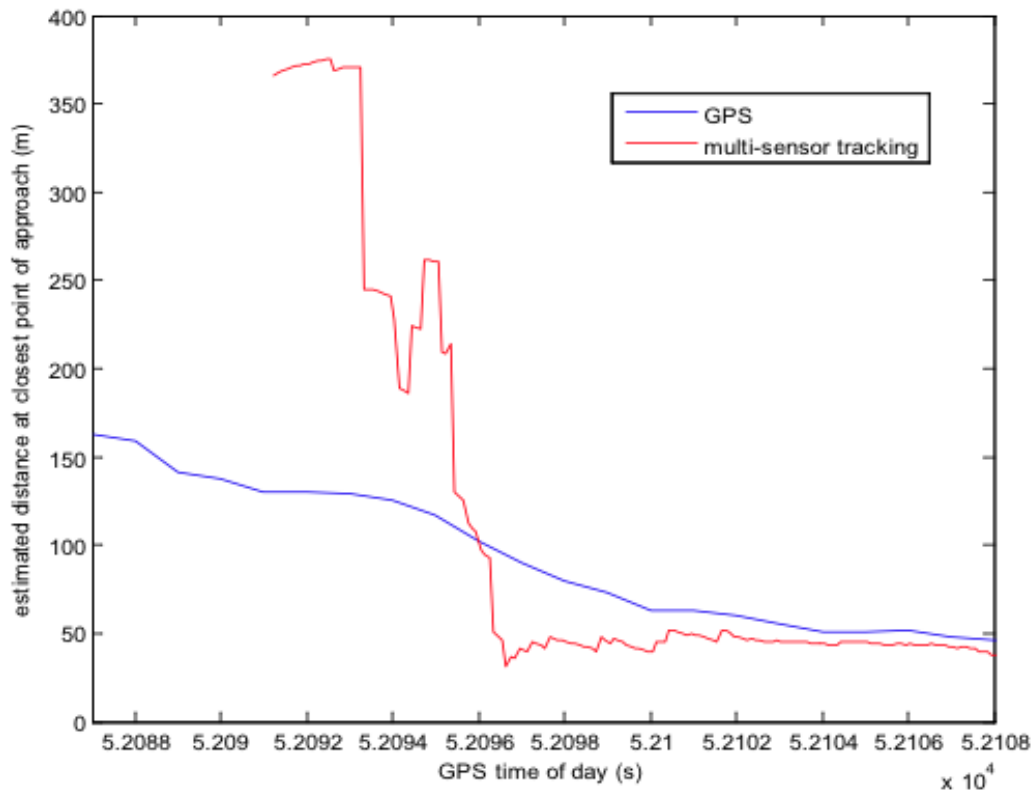
**Figure 56. Distance at closest Point of Approach as estimated by multi-sensor tracker
and by GPS as function of the GPS time of the day.**

Figure 57 shows that the PF algorithm is more accurate than EKF for the estimation of the DCPA in the initial stage of firm tracking, thus providing an improvement in collision risk assessment. In fact, considering the same conditions in the simulation environment for both PF and EKF, the collision threat is detected by PF in advance with respect to the EKF. The Near Mid Air Collision threat is verified since the reference GPS system measures a DCPA value shorter than 150 m in almost the entire time range.

In order to exploit the capabilities of the developed Obstacle Detection and Tracking software and to assess the performance of the particle filter algorithm, tests on different single-quasi frontal encounter configurations have been performed. In particular, two scenarios will be shown below. It is worth pointing out that only the Distance at Closest Point of Approach will be reported since the trajectories of the particles of the estimated variables (range, azimuth, elevation and their first time derivatives) are very similar to those reported before.
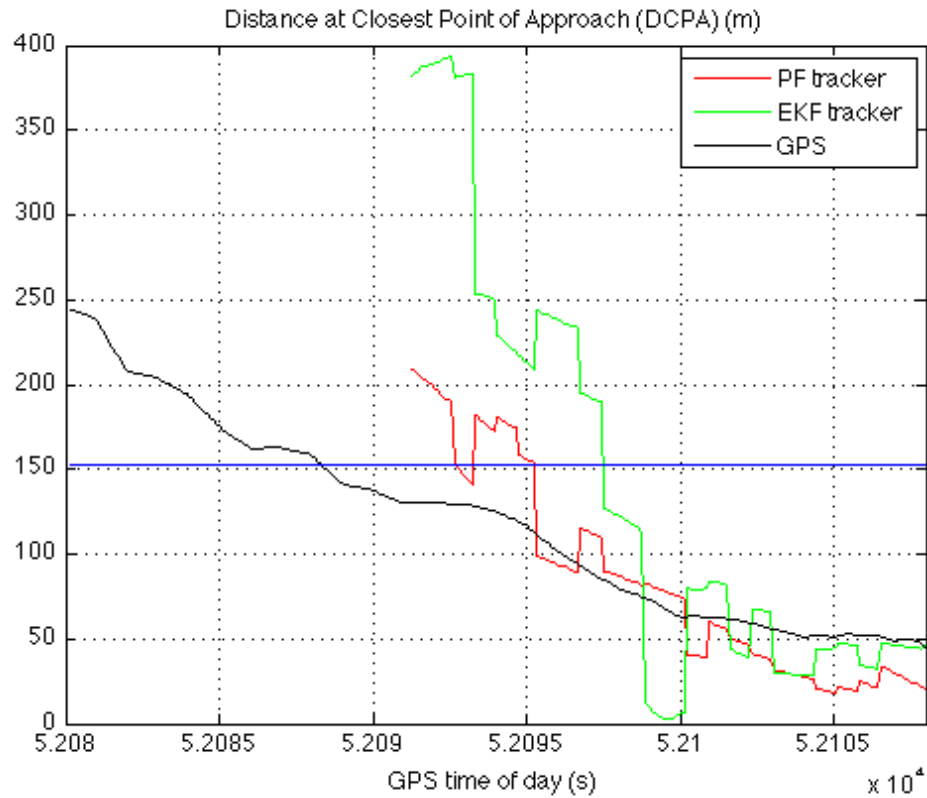
Figure 57. Distance at Closest Point of Approach as estimated by GPS (reference), by EKF tracker, and by PF radar-only tracker as function of GPS time of the day.
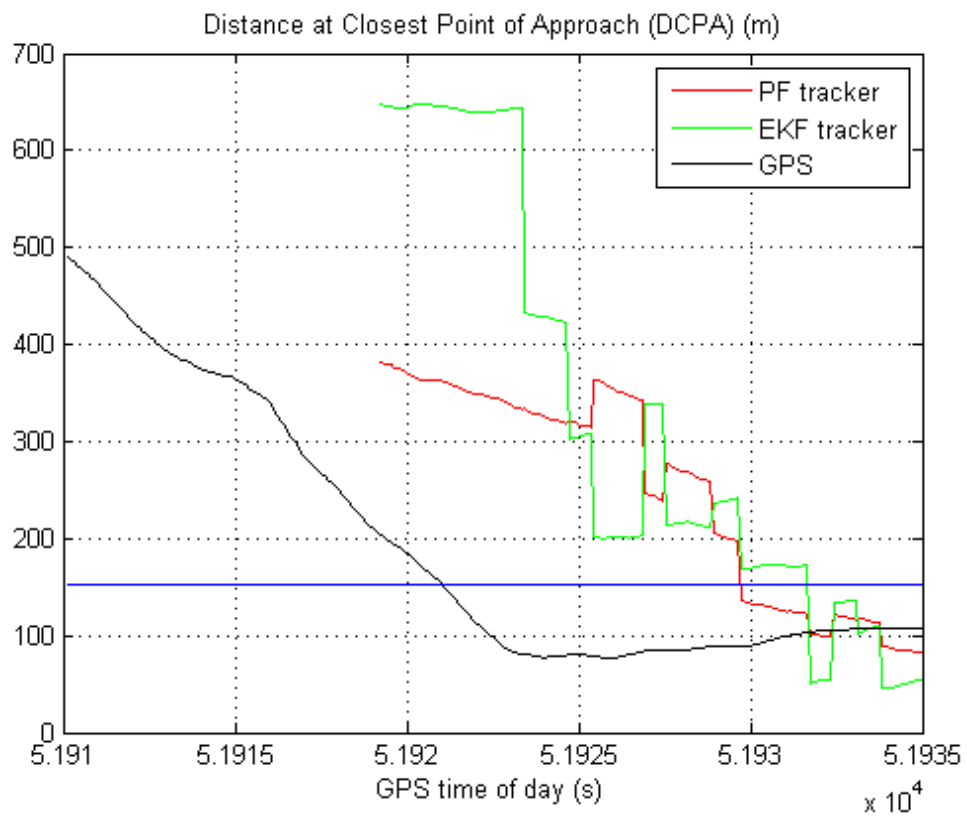
Figure 58. Distance at Closest Point of Approach as estimated by GPS, by EKF, and by PF radar-only tracker as function of GPS time of the day.

In the first case, the flight segment has a duration of about 25 s with an initial range of about 2300 m. In Figure 58, the DCPA as estimated by PF radar-only tracker, by EKF radar-only tracker and by GPS (reference) as function of GPS time of the day is reported.

The plot shows that the PF tracker identifies the collision threat (the blue line is the threshold value) in advance with respect to the EKF. In particular, the PF takes fewer seconds with respect to the EKF to settle to the nominal filtering functioning for the tracking phase. Moreover, comparing the estimated errors of the PF and EKF (calculated considering GPS as reference values), it can be noticed that the PF errors are smaller than EKF ones, thus allowing to obtain some improvements in the accuracy of the DCPA estimate.

The same behaviour occurs in Figure 59. In this case, the flight segment has a duration of about 20 s with an initial range of 1400 m. While the EKF tracker takes few seconds to declare the collision threat due to an initial large error with respect to the reference value (that is the time needed by the filter to start the properly functioning), the PF tracker reduce this delay, in fact its performance is very close to the GPS values.
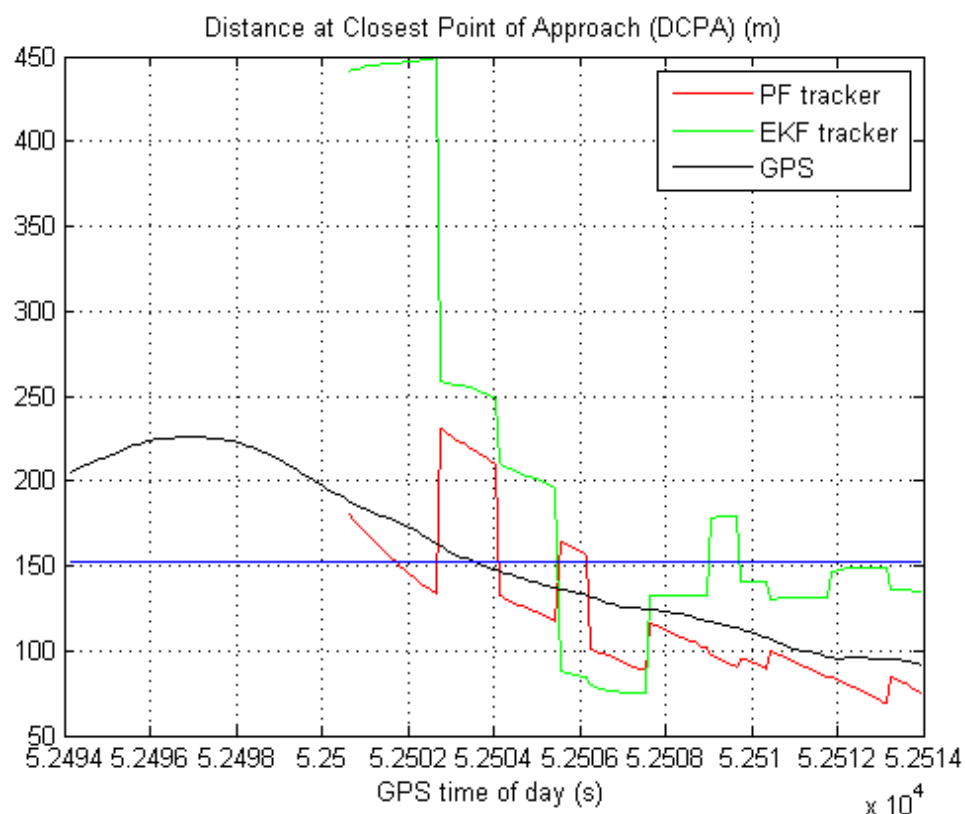
Figure 59. Distance at Closest Point of Approach as estimated by GPS, by EKF, and by PF radar-only tracker as function of GPS time of the day.

Conclusions and further research

This thesis was focused on the exploitation of innovative filtering methodologies for Sense and Avoid units to be installed onboard Unmanned Aerial systems. In particular, it aimed at demonstrating the impact of advanced filtering techniques on an Obstacle Detection and Tracking software performance with respect to assessed methodologies such as Extended Kalman filter. The activities were conducted covering all the aspects starting from pointing out the necessity of a Sense and Avoid system for the introduction of unmanned vehicles into Civil Airspace to the definition of an assessed filtering algorithm for airborne tracking software.

The first approach of this analysis was the investigation of all the possible sensing solutions able to satisfy the requirements imposed for the realization of a suitable and reliable DS&A system. In particular, a multi-sensor architecture constituted by a Ka-band radar and electro-optical sensors (two visible cameras and two infra-red cameras) demonstrated to be a viable solution for an airborne anti-collision system stated the all-time all-weather requirement together with the need of a faster data rate. These sensors were coupled in a hierarchical architecture with radar as main sensor and EO as auxiliary sensor. This choice was very strategic from the application point of view; it takes advantage of the performance of both sensors in terms of accuracy and data rate. The hardware architecture so composed was installed onboard a Very Light Aircraft for the evaluation of its performance in real time environment.

The developed logical architecture was described in more details; it was based on a processing unit dedicate to the elaboration of radar measurements and intruder tracking and on a second unit dedicated to the image processing. These units were connected by means of an Ethernet link; a CAN bus was also present for communications with flight control computer.

The data fusion algorithm for real time tests was based on an Extended Kalman Filter; models and algorithms were developed for the evaluation of its performance in an airborne multi-sensor tracking system. In particular, outputs in terms of Distance at Closest Point of Approach were obtained and analyzed pointing out that the adopted filtering technique showed a delay for the declaration of a potential collision threat whose presence was indicated by the system used as reference.

Thus, the main part of this thesis was dedicated to the analysis of the different filtering innovative techniques able to overcome the drawbacks and limitations of the EKF. The study was carried out identifying several methodologies; the Particle Filter resulted to be the most appropriate for the considered application among them.

A tracking algorithm based on a Sampling Importance Resampling Particle Filter was then developed. Extensive off-line simulations based on data gathered during flight tests were performed to evaluate the system accuracy taking into account several aspects. In fact, the resampling procedure, the choice of coordinate system and the obstacle dynamic model can produce some effects on the final performance such as the loss of track as well as loss of accuracy.

A great effort was dedicated to the identification of the obstacle dynamic model that had to be able to accurately describe the target trajectory. A survey of all the possible models was conducted and some of them were implemented and analyzed, such as: Singer model, Nearly Constant Acceleration model and Nearly Constant Velocity model.

In parallel, the effect of tracking coordinates on Particle Filter performance was evaluated. As first approach, a Particle filter algorithm based on a Singer model in Cartesian coordinates was implemented in which a Systematic resampling procedure had been considered. Simulation results confirmed how the resampling procedure is a key factor for tracking performance, avoiding the degeneracy phenomenon and thus enabling a great quantity of particles to survive to the prediction step.

A residual rms error of about 12 m in range and 1.8° and 1.40° for azimuth and elevation respectively in NED reference frame resulted for intruder detection performed by radar only.

However, the introduction of Spherical coordinates provided an improvement of radar-only tracker performance; in this case errors were slightly smaller than the previous case.

This is in line with the characteristics of Bayesian estimators that have fewer limitations than EKF and can resolve non-linear process and measurement models and can be used with any type of system noise statistical distribution.

Once the tracking coordinates were established, off-line simulations were dedicated to an analysis of the other dynamic models in order to improve the performance of the software trying to reach values comparable to the EKF. This analysis was primarily aimed at identify a configuration able to reduce the delay in the assessment of collision threat.

The algorithm was modified firstly with a nearly constant acceleration model in spherical coordinates and then implementing a less sophisticated model.

The study has demonstrated that a simplified model was able to describe the particles trajectories with an accuracy comparable to EKF. In particular, the most accurate estimates were in terms of angular rates variables where values of 0.2° in azimuth and 0.4° in elevation were obtained. Thus, the obstacle velocities provided by PF were slightly more accurate than EKF; moreover they are very important parameters for the estimation of distance at closest point of approach. In fact, the improvements obtained in the variables accuracy were directly reflected in the DCPA estimate.

Summarizing, the study conducted in this thesis has demonstrated a very important result for anti-collision systems. The most important outcome is based on the improvements obtained with the PF with respect to EKF for the estimation of DCPA, thus providing an improvement in collision risk assessment.

The developed system was tested for several frontal-encounter geometries. In almost all cases, DCPA estimate by PF was more accurate than EKF.

Further studies could involve the introduction of electro-optical data in the developed DS&A system prototype. In this case, the results could take advantages of EO benefits, such as more accurate measurements in angular data and a faster data rate.

REFERENCES

[1].   CARE Innovation Action preliminary study on Integration of Unmanned Aerial Vehicles into Future Air Traffic Management, EURONTROL, v.1.1, December 2001, pp. 12-14, 21-22, 27-31, 34-39, 40-46, 49, 103-105.

[2].   European Union (UAVNET, CAPECON & USICO), European civil Unmanned Air Vehicle Roadmap, Vol.3, March 2005.

[3].   International Civil Aviation Organization (ICAO), Unmanned Aircraft Systems (UAS) Circular, Cir328 AN/190, 2011 available from www.icao.int.

[4].   Guidelines for Approval of the Provision and Use of Air Traffic Services Supported By Data Communications, DO-264, RTCA, Inc., December 2000.

[5].   National Aeronautics and Space Administration, Unmanned Aircraft Systems (UAS) Integration in the National Airspace System (NAS) Project, ICAO Regional Unmanned Aircraft Seminar Lima, Peru April 18-20, 2012.

[6].   Sense and Avoid (SAA) for Unmanned Aircraft Systems (UAS), Federal Aviation Administration, October 2009.

[7].   Federal Aviation Administration Airworthiness certification of unmanned aircraft systems. FAA Order 8130.34, Washington, D.C., Mar. 27, 2008.

[8].   EUROCONTROL, Specifications for The Use of Military Unmanned Aerial Vehicles as Operational Air Traffic Outside Segregated Airspace, version 1.0, 2007, doc no. EUROCONTROL-SPEC-0102.

[9].   Fasano, G., Accardo, D., Moccia, A., Carbone, C., Ciniglio, U., Corraro, F., and Luongo, S., "Multi-Sensor-Based Fully Autonomous Non-Cooperative Collision Avoidance System for Unmanned Air Vehicles", AIAA Journal of Aerospace

Computing, Information, and Communication, vol. 5, pp.338-360, October 2008, DOI: 10.2514/1.35145.

[10].   MTSI, "Non-Cooperative Detect, See, & Avoid (DSA) Sensor Study", July 2002, NASA ERAST technical report.

[11].   Shakernia, O., Chen, W.Z., Graham, S., Zvanya, J., White, A., Weingarten, N., Raska, V.M., May 2007, "Sense and Avoid (DS&A) Flight Test and Lessons Learned", 2nd AIAA Infotech@Aerospace Conference and Exhibit, Paper AIAA 2007-3003, Rohnert Park, CA, pp.1-12.

[12].   Federal Aviation Administration, Integration of Civil Unmanned Aircraft Systems (UAS) in the National Airspace System (NAS) Roadmap, First Edition-2013, available from www.faa.gov.

[13].   Wickens, C. D., Mavor, M., Parasuraman, R., & McGee, J., The future of air traffic control: Human operators and automation. Washington, DC: National Academy of Science, 1998.

[14].   FAA, Introduction to TCAS II version7, Washington, DC: US Department of Transportation 2000.

[15].   RTCA, "Minimum Aviation System Performance Standards For Automatic Dependent Surveillance Broadcast (ADS-B)", RTCA/DO-242A, Washington DC, 2002.

[16].   Klein, L.A., Sensor and Data Fusion – A Tool for Information Assessment and Decision Making, Spie Press, Bellingham WA, USA, 2004.

[17].   Smith, N.E., Cobb, R.G., Pierce, S.J., Raska, V.M., "Optimal Collision Avoidance Trajectories for Unmanned/Remotely Piloted Aircraft", AIAA Guidance, Navigation, and Control (GNC) Conference, August 19-22, 2013, Boston, MA, AIAA 2013-4619.

[18].   Yazdi I. Jenie, Erik-Jan Van Kampen, Coen C. de Visser, and Q Ping Chu, "Selective Velocity Obstacle Method for Cooperative Autonomous Collision Avoidance System for Unmanned Aerial Vehicles," AIAA Guidance, Navigation, and Control (GNC) Conference, August 19-22, 2013, Boston, MA, AIAA 2013-4619.

[19].   Jared Garvey, Benjamin Kehoe, Brandon Basso, Mark Godwin, Jared Wood, Joshua Love, Shih-Yuan Liu, Zu Kim, Stephen Jackson, Yaser Fallah, Tony Fu, Raja Sengupta, and Karl Hedrick, "An Autonomous Unmanned Aerial Vehicle System for Sensing and Tracking," Infotech@Aerospace 2011, 29-31 March 2011, AIAA 2011-1509.

[20].   Jovan Boskovic, Joseph A. Jackson, and Raman Mehra," Sensor and Tracker Requirements Development for Sense and Avoid Systems for Unmanned Aerial

Vehicles", AIAA Modeling and Simulation Technologies (MST) Conference, August 19-22, DOI: 10.2514/6.2013-4971.

[21].   Laith Sahawneh, Randal W. Beard, Sharath Avadhanam, and He Bai, "Chain-based Collision Avoidance for UAS Sense-and-Avoid Systems," AIAA Guidance, Navigation, and Control (GNC) Conference, August 19-22, DOI: 10.2514/6.2013-4995.

[22].   Andrew Zeitlin, "Trade-Offs for Achieving a Sense & Avoid Capability for Unmanned Aircraft Systems," AIAA Infotech@Aerospace 2010, April 20-22, DOI: 10.2514/6.2010-3440.

[23].   Stephen Cook, Andrew Lacher, David Maroney, and Andrew Zeitlin, " UAS Sense and Avoid Development - the Challenges of Technology, Standards, and Certification," 50th AIAA Aerospace Sciences Meeting including the New Horizons Forum and Aerospace Exposition, January 09-12, AIAA 2012-0959.

[24].   Anurag Ganguli, Sharath Avadhanam, He Bai, Joseph Yadegar, James Utt, and John McCalmont, "Multiple intruder tracking using a laser enhanced EO/IR Sense and Avoid system," Infotech@Aerospace 2011, March 29-31, AIAA 2011-1478.

[25].   Scott Graham, Jan De Luca, Won-zon Chen, Jacob Kay, Michael Deschenes, Norman Weingarten, Vince Raska, and Xiaogong Lee, "Multiple Intruder Autonomous Avoidance Flight Test," Infotech@Aerospace 2011, March 29-31, AIAA 2011-1420.

[26].   MITRE, "Unmanned Aircraft System Airspace Integration: Sense and Avoid," CAASD Fact Sheet, available from www.mitre.org.

[27].   Code of Federal Regulations - Title 14 Aeronautics and Space; Part 91 General operating and flight rules; Section 113, "Right-of-way rules: Except water operations".

[28].   US Federal Aviation Administration (FAA), "Investigate a Near Mid Air Collision", FAA Order 8900.1, vol. 7, Chapter 4, Washington DC, USA, 2007.

[29].   ICAO International Standards, Rules of the Air, Annex 2, Section 3.2, July 1990.

[30].   US Federal Aviation Administration (FAA), 1987, "How to Avoid a Mid Air Collision", FAA-P-8740-51, FAA Accident Prevention Program. Washington DC, USA.

[31].   NASA, Sense and avoid Equivalent Level of Safety Definition for Unmanned Aerial Systems, Cover Sheet Access 5 Project Deliverables, Edwards, CA, USA, 2005.

[32].   Doehler, H-U, Löving, K., Oyzel, A., Roviaro, E., See & Avoid Technologies, Unmanned Aerial Vehicle Safety Issues for Civil Applications, project USICO - final report, 2004.

[33]. Lerro, D., and Bar-Shalom, Y., "Tracking with Debiased Consistent Converted Measurements Versus EKF," IEEE Transaction on Aerospace and Electronic Systems, Vol. 29, No. 3, July 1993, pp. 1015–1022.

[34]. Blackman, S.S., Popoli, R., Design and Analysis of Modern Tracking Systems, 1999, Artech House.

[35]. Bar-Shalom, Y., Fortmann, T., E., Tracking and Data Association, Academic Press, 1998.

[36]. Bar-Shalom, Y., Multitarget-Multisensor Tracking: Advanced Applications, Vol. I, 1990, Artech House, YBS Publishing.

[37]. Bar-Shalom, Y., Multitarget-Multisensor Tracking: Applications and Advances, Vol. II, 1992, Artech House, YBS Publishing.

[38]. Blackman, S., S., Multiple Hypothesis Tracking for Multiple Target Tracking, IEEE A&E systems Magazine, vol. 19, No. 1, Part 2: Tutorials, 2004.Li, X., R., Bar-Shalom, Y., Tracking in Clutter with Nearest Neighbor Filter: Analysis and Performance, IEEE Transaction on Aerospace and Electronic Systems, vol.32, No. 3, pp. 995-1010, doi: 10.1109/7.532259, 1996.

[39]. Houles, A., Bar-Shalom, Y., Multisensor tracking of a maneuvering target in clutter, IEEE Transactions on Aerospace and Electronic Systems, vol. 25, No. 2, pp. 176—189, 1989.

[40]. Li, X., R., Vesselin, P., J., A Survey of Maneuvering Target Tracking: Dynamic Models, Proceedings of SPIE Conference on Signal and Data Processing of Small Targets, Orlando, FL, USA, 2000.

[41]. S. Julier and J. K. Uhlmann, A general method for approximating non-linear transformations of probability distributions, Robotics Research Group, Department of Engineering Science, University of Oxford, Tech. Rep., 1996.

[42]. Julier, S.J., Uhlmann, J.K., Durrant-Whyte, H.F., A new approach for filtering nonlinear systems, American Control Conference, Proceedings of the 1995 , vol.3, no., pp.1628,1632 vol.3, 21-23 Jun 1995, doi: 10.1109/ACC.1995.529783.

[43]. Maybeck, P. S., Stochastic Models, Estimation, and Control, volume 2. Academic Press, 1982.

[44]. Gelb A., Applied Optimal Estimation, MIT Press, Massachusetts, 1974.

[45]. Grewal M.S., Andrews A.P., Kalman Filtering: Theory and Practice Using Matlab, Second Edition, John Wiley and Sons, 2001.

[46]. Haykin S., Kalman Filtering and Neural Networks, John Wiley and Sons, 2001.

[47].   Brookner, E., Tracking and Kalman Filtering Made Easy, John Wiley and Sons, New York NY, USA, 1998.

[48].   Kalman, R. E., ''A New Approach to Linear Filtering and Prediction Problems'', Journal of Basic Engineering, Trans. of ASME, Ser. D, Vol. 82, No. 1, March 1960, pp. 35–45.

[49].   Kalman, R. E. and R. S. Bucy, ''New Results in Linear Filtering and Prediction Theory'', Transactions of the ASME, Journal of Basic Engineering, Vol. 83, No. 3, December 1961, pp. 95–107.

[50].   Van der Merwe, R., Wan, E. A., The Unscented Kalman Filter for Nonlinear Estimation, Adaptive Systems for Signal Processing, Communications, and Control Symposium, IEEE, Doi: 10.1109/ASSPCC.2000.882463, pp. 153-158, 2000.

[51].   Soares, G.L., Arnold-Bos, A., Jaulin, L., Maia, C.A., Vasconcelos, J.A, An Interval-Based Target Tracking Approach for Range-Only Multistatic Radar, IEEE Transaction on Magnetics, Vol. 44, No. 6, pp. 1350-1353, Doi: 10.1109/TMAG.2007.916286, May 2008.

[52].   Simon, D., From Here to Infinity, Embedded Systems Programming, 2001.

[53].   Ristic, B., Arulempalam, S., Gordon, N., Beyond the Kalman Filter: Particle Filters for tracking applications, Artech House, 2004.

[54].   Leven, F.L., Lanterman, A.D., Unscented Kalman Filters for Multiple Target Tracking with Symmetric Measurement Equations, Massachusetts Institute of Technology, Cambridge, USA, 2005.

[55].   Ashokaraj, I., Tsourdos, A., Sislson, P., White, B., Sensor Based Robot Localisation and Navigation: Using Interval Analysis and Extended Kalman Filter, 5th Asian Control Conference, vol.2, pp.1086 – 1093, 2004.

[56].   Jaulin, L., Kieffer, M., Didrit, O., Walter, E., Applied Interval Analysis, Springer, 2001.

[57].   Zhang, W., Chen, B.S., Tseng, C.S., Robust H∝ filtering for nonlinear stochastic systems, IEEE Trans. Signal Processing, vol. 53, pp. 589-598, Feb. 2005.

[58].   Nagpaland, K.M., Khargonekar, P.P., Filtering and smoothing in an H∝ setting, IEEE Trans. Automat. Contr., vol. 36, pp. 152-166, Feb. 1991.

[59].   James, M.R., Petersen, I.R., Nonlinear state estimation for uncertain system with an integral constraint, IEEE Trans. Signal Processing, vol. 46, pp. 2926-2937, Nov. 1998.

[60]. Jaewon, S., Myeong-Jong, Y., Chan Gook, P., Jang, G.L., An Extended Robust H Infinity Filter for Nonlinear Uncertain Systems with Constraints, 44th IEEE Conference on Decision and Control, Doi: 10.1109/CDC.2005.1582443, pp. 1935-1940, 2006.

[61]. Shen, X., Deng, L., Game Theory Approach to Discrete H∝ filter design, IEEE Transaction on Signal Processing, 45(4), 1997.

[62]. Hassibi, B., Sayed, A., Kailath, T., Indefinite Quadratic Estimation and Control-A Unified Approach to H2 and H-Infinite Theories, Society for Industrial and Applied Mathematics, Philadelphia, 1999.

[63]. Gustafsson, F., Gunnarsson, F., Bergman, N., Forssell, U., et alii, Particle Filter for Positioning, Navigation and Tracking, IEEE Transaction on Signal Processing, vol. 50, No. 2, pp. 425‐437, Doi: 10.1109/78.978396, 2002.

[64]. Hwang, R.R., Huber, M., A Particle Filter Approach for Multi‐Target Tracking, IEEE/RSJ International Conference on Intelligent Robots and Systems, 2007. IROS 2007, pp. 2753‐2760, Doi: 10.1109/IROS.2007.4399632, 2007.

[65]. Doucet, A., On Sequential Monte Carlo Methods for Bayesian Filtering, Technical Report, University of Cambridge, UK, 1998.

[66]. A. Kong, J. S. Liu, and W. H. Wong, Sequential imputations and Bayesian missing data problems, J. Amer. Statist. Assoc., vol. 89, pp. 278–288, 1994.

[67]. Liu, J.S., Chen, R., Sequential Monte Carlo methods for dynamical systems, J. Amer. Statist. Assoc., vol. 93, pp. 1032–1044, 1998.

[68]. Bergman, N., Recursive Bayesian Estimation: Navigation and Tracking Applications, PhD thesis, 1999.

[69]. Singer, R.A., Sea, R.G., and Housewright, K.B., Derivation and Evaluation of Improved Tracking Filter for Use in Dense Multitarget Environments, IEEE Transactions on Information Theory, vol. 20, no. 4, IEEE, 1974.

[70]. Bar Shalom, Y., and Li, X.-R., Estimation and Tracking: Principles, Techniques and Software, Artech House, 1993.

[71]. Zollo, S., Ristic, B., On the Choice of the Coordinate System and Tracking Filter for the Track-while-scan Mode of an Airborne Pulse Doppler Radar, DSTO-TR-0926, December 1999.

[72]. Haug, A., Williams, L., A spherical constant velocity model for target tracking in three dimensions, Aerospace Conference, 2012 IEEE, vol., no., pp.1-15, 3-10 March 2012, DOI: 10.1109/AERO.2012.6187209.

[73]. Fasano, G., Accardo, D., Moccia, A., and Rispoli, A., 2010, An Innovative Procedure for Calibration of Strapdown Electro-Optical Sensors Onboard Unmanned Air Vehicles, Sensors, 10, 1, pp.639-654.

[74]. G. Fasano, A. Moccia, D. Accardo, A. Rispoli, Development and test of an Integrated Sensor System for Autonomous Collision Avoidance, 26th International Congress of the Aeronautical Sciences, Anchorage, AL, 2008.

[75]. Smith, N.E., Cobb, R.G., Pierce, S.J., Raska, V.M., Optimal Collision Avoidance Trajectories for Unmanned/Remotely Piloted Aircraft, AIAA Guidance, Navigation, and Control (GNC) Conference, August 19-22, 2013, Boston, MA, AIAA 2013-4619.